



THESIS APPROVAL
GRADUATE SCHOOL, KASETSART UNIVERSITY

Doctor of Philosophy (Food Science)

DEGREE

Food Science

Food Science and Technology

FIELD

DEPARTMENT

TITLE: Biopolymer Particle to Inhibit Acrylamide Formation and to Stabilize Pickering Emulsion as Template for Oleogelation

NAME: Miss Ornicha Champrasert

THIS THESIS HAS BEEN ACCEPTED BY

THESES ADVISOR

(Associate Professor Prisana Suwannaporn, Ph.D.)

THESES CO-ADVISOR

(Assistant Professor Kanithaporn Vangnai, Ph.D.)

THESES CO-ADVISOR

(Associate Professor Leonard M.C. Sagis, Ph.D.)

DEPARTMENT HEAD

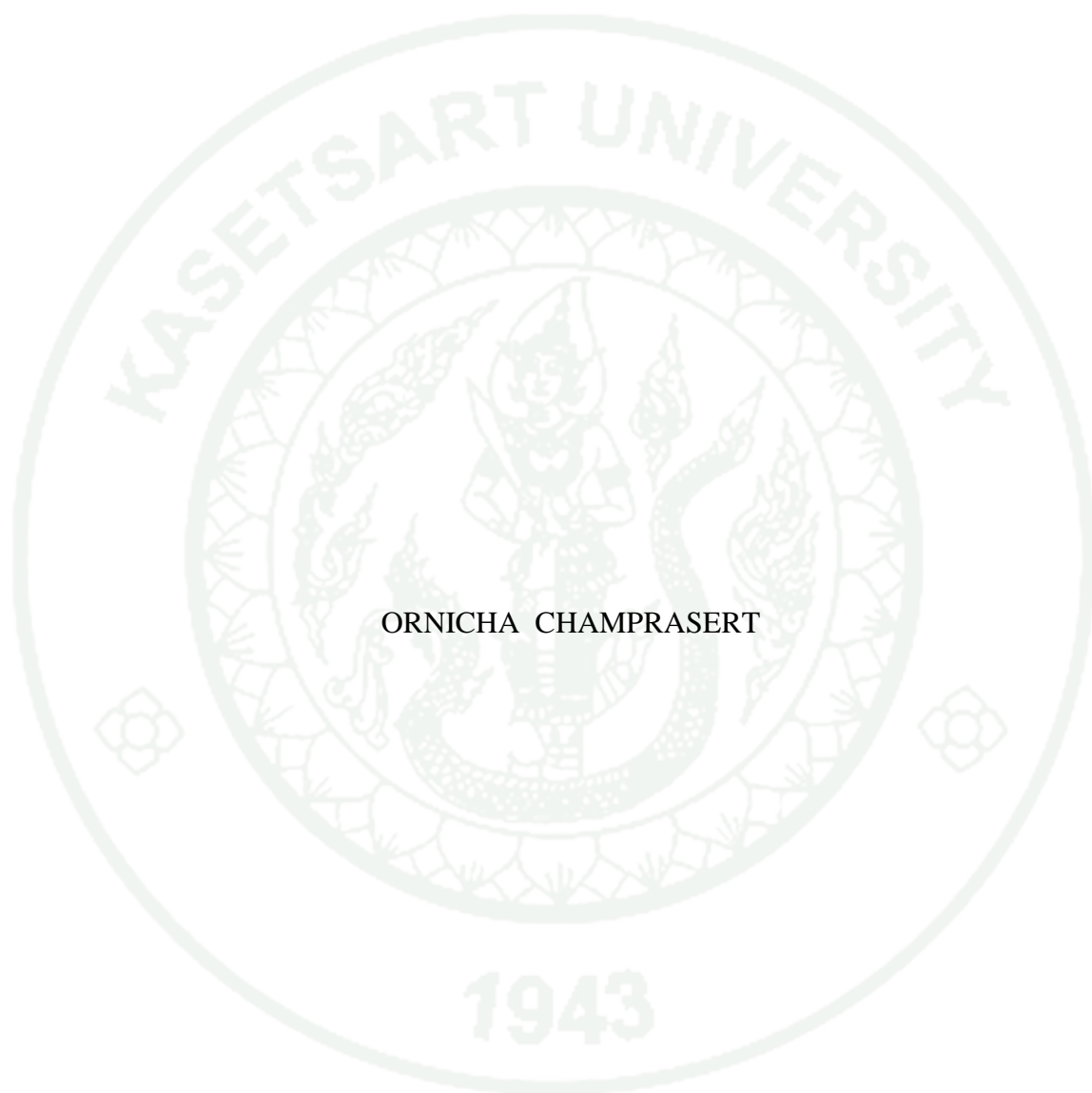
(Assistant Professor Kullanart Tongkhao, Ph.D.)

DEAN

(Associate Professor Srijidtra Charoenlarnnoppa, Ph.D.)

THESIS

BIOPOLYMER PARTICLE TO INHIBIT ACRYLAMIDE
FORMATION AND TO STABILIZE PICKERING EMULSION AS
TEMPLATE FOR OLEOGELATION



ORNICHA CHAMPRASERT

A Thesis Submitted in Partial Fulfillment of
the Requirements for the Degree of
Doctor of Philosophy (Food Science)
Graduate School, Kasetsart University

2022

Ornicha Champrasert 2022: Biopolymer particle to Inhibit Acrylamide Formation and to Stabilize Pickering Emulsion as Template for Oleogelation. Doctor of Philosophy (Food Science), Major Field: Food Science, Department of Food Science and Technology. Thesis Advisor: Associate Professor Prisana Suwannaporn, Ph.D. 125 pages.

Biopolymer particles could be used for various acrylamide mitigation and stabilize Pickering emulsion and produced high internal phase Pickering emulsion. The inhibitory effect of polysaccharides (alginate, pectin and chitosan) on acrylamide formation was investigated in chemical and fried potato food model systems, under two heating regimes (heating block and microwave). Acrylamide formation followed a second order reaction kinetic behavior. Coating potatoes with polysaccharide solutions (1% w/v) prior frying dramatically inhibited acrylamide formation around 41-54%. Furthermore, protein-polysaccharide biopolymer particles composed of potential acrylamide inhibitors, including zein, chitosan, alginate, and pectin were used for acrylamide mitigation. The synergistic effect of zein and polysaccharides in complex particles was hypothesized to inhibit acrylamide formation. These complex particles successfully reduced acrylamide concentration in a heating block and food model compared to the mixture of zein and polysaccharide (non-complex particles) was less effective in terms of acrylamide mitigation. Octenyl succinic anhydride (OSA) modification starch is introduced to native starch so it can stabilize high internal phase Pickering emulsion and use as template for oleogelation. Granular cold water swelling starch (GCWS) modification followed by OSA modification had the highest degree of OSA substitution. OSA starch with and without polysaccharides (pectin, gum arabic and xanthan gum) stabilized Pickering emulsion behaved as soft viscoelastic solids ($G' > G''$). All oleogels had solid-like behavior which applied as fat mimetic. In food model, no significant difference in texture profile analysis of GCWS-OSA oleogel substituted sausage (75%) comparing with control (100% lard).

Student's signature

Thesis Advisor's signature

ACKNOWLEDGEMENTS

I would like to give a grateful thank to my advisor Assoc. Prof. Prisana Suwannaporn for the support and valuable suggestion to completely writing this thesis. Additionally, I am also would like to thank Prof. Caroline Orfila, University of Leeds, UK and Assoc. Prof. Leonard M.C. Sagis, Wageningen University and Research, the Netherlands for supports, encouragements, and suggestions throughout my study.

Finally, thanks to the Royal Golden Jubilee PhD program, Thailand Research Fund for provide funding support to complete my thesis work.

Ornicha Champrasert
July 2022

TABLE OF CONTENTS

	Page
TABLE OF CONTENTS	i
LIST OF TABLES	ii
LIST OF FIGURES	iii
LIST OF ABBREVIATIONS	vi
INTRODUCTION	1
OBJECTIVES	3
LITERATURE REVIEW	4
MATERIALS AND METHODS	26
Materials	26
Methods	28
RESULTS AND DISCUSSION	47
CONCLUSION	95
LITERATURE CITED	96
APPENDIX	117
CURRICULUM VITAE	120

LIST OF TABLES

Table	Page
1 Acrylamide levels ($\mu\text{g}/\text{kg}$) in different food commodities	10
2 Acrylamide mitigation strategies	12
3 Kinetic parameters of acrylamide formation in the chemical model under different heating conditions	49
4 Average particle size, polydispersity index (PDI), and zeta potential of zein, polysaccharides, zein-polysaccharide complex particles, and zein and polysaccharides non particles	59
5 Contact angle, degree of substitution, and particle size of native and OSA starch	67
6 Particle size distribution of Pickering emulsion stabilized by starch particles w/wo polysaccharides	81
 Appendix Table	
1 Benchmark level of acrylamide	121
2 The various composition in chemical model system	121
3 The series of different acrylamide concentrations ($\mu\text{g}/\text{mL}$) prepared from the stock solution ($10 \mu\text{g}/\text{mL}$) through dilution in water.	122
4 The series of different acrylamide concentrations ($\mu\text{g}/\text{mL}$) prepared from the stock solution ($100 \mu\text{g}/\text{mL}$) through dilution in water	122

LIST OF FIGURES

Figure	Page
1 Schematic representation of the process whereby liquid oil is first used to prepare O/W emulsion, followed by the removal of water through drying	21
2 Acrylamide formation in the chemical model system during heating mainly by conduction in a heating block (conventional) and microwave	48
3 Acrylamide formation in conventional heating and microwave in the chemical model in the presence of various inhibitors.	51
4 Acrylamide formation in the food model in the presence of various inhibitors relative to control (frying with no inhibitors).	53
5 (A) The dose-dependent inhibitory effects of zein solutions heated in a heating block at 150 °C, 160 °C, 170 °C, and 180 °C for 30 min on acrylamide; (B) browning formation at various concentrations of zein heated in a heating block at 170 °C for 30 min; (C) structure of glutamine and asparagine	56
6 Confocal laser scanning microscope (CLSM) images (63x) of zein-chitosan, zein-alginate, and zein-pectin complex particles.	61
7 (A) Acrylamide formation after using protein-polysaccharide complexes as inhibitors in a heating block. (B) Effect of zein-polysaccharide complex particles and non-complex particles (1:0.50) on browning formation at 170 °C for 30 min in a heating block	63
8 Schematic image of the potential mechanism by which zein-polysaccharide complex particles inhibit acrylamide formation	64
9 Inhibition of acrylamide (%) in potato strips soaked in various zein-polysaccharides complex particles (1:0.5) for 30 min and deep fried at 170 °C for 3 min	65

LIST OF FIGURES (Continued)

Figure	Page
10 Particle size distribution of Pickering emulsion stabilized by starch-based particles	68
11 Microstructure images under light microscope(40x) and confocal laser scanning microscope of Pickering emulsion stabilized by starch-based particles	68
12 Small amplitude oscillatory shear test at 20°C for frequency sweep test and amplitude sweep test of Pickering emulsion stabilized by starch-based particles	70
13 Normalized Lissajous curves of shear stress versus shear strain and shear stress versus shear rate of Pickering emulsion stabilized by starch-based particles	72
14 The shear thickening (T factor) and shear stiffening (S factor) of Pickering emulsion stabilized by starch-based particles	74
15 Dissipation ratio of oleogel using Pickering emulsion stabilized by starch-based particles	75
16 The frequency sweep test and amplitude sweep test of oleogel using Pickering emulsion stabilized by starch-based particles	76
17 Normalized Lissajous curves of shear stress versus shear strain and shear stress versus shear rate of oleogel using Pickering emulsion stabilized by starch-based particles	78
18 The shear thickening (T factor) and shear stiffening (S factor) of oleogels using Pickering emulsion stabilized by starch-based particles	79
19 Dissipation ratio of oleogel using Pickering emulsion stabilized by starch-based particles	80
20 Amplitude sweep test showing storage modulus and loss modulus of Pickering emulsion stabilized by starch-based particles w/wo polysaccharides	83

LIST OF FIGURES (Continued)

Figure	Page
21 Frequency sweep test showing storage modulus and loss modulus of Pickering emulsion stabilized by starch-based particles w/wo polysaccharides	84
22 Normalized Lissajous plot of shear stress versus shear strain and shear stress versus shear rate of starch-based Pickering emulsion w/wo polysaccharides	86
23 The S factor or ratio of shear stiffening and T factor or ratio of shear thickening of starch-based Pickering emulsion (60% oil), w/wo hydrocolloids	87
24 The amplitude sweep test of oleogel from starch-based oleogel w/wo polysaccharide showing storage modulus (G') and loss modulus (G'')	89
25 The frequency sweep test of oleogel from starch-based oleogel w/wo polysaccharide showing storage modulus (G') and loss modulus (G'')	90
26 Normalized Lissajous plot of shear stress versus shear strain and shear stress versus shear rate (1/s) of starch-based oleogel	92
27 The S factor or shear stiffening and T factor or shear thickening of starch-based oleogel (60% oil), w/wo polysaccharides	93
28 Texture profile analysis of emulsion type sausage from various types of oleogel (75% substitution) comparing with positive control (100% lard) and negative control (100% liquid oil)	94
29 Emulsion-type sausage made from 100% liquid oil and oleogel (75% substitution)	95

Appendix Figure

1 Acrylamide standard curve at concentration from 1 $\mu\text{g/mL}$ to 100 $\mu\text{g/mL}$	121
--	-----

LIST OF ABBREVIATIONS

AA	=	Acrylamide
Alg	=	Sodium alginate
AO	=	Acridine orange
DD	=	Deacetylation degree
DS	=	Degree of substitution
CLSM	=	Confocal Laser Scanning Microscopy
CS	=	Chitosan
Ea	=	Activation energy
Fit C	=	Fluorescein
GCWS	=	Granular Cold Water Swelling Starch
HS	=	High amylose rice starch
LAOS	=	Large amplitude oscillatory shear
OSA	=	Octenyl Succinic Anhydride
pI	=	Isoelectric point
PDI	=	Polydispersity index
RhB	=	Rhodamine B
RR	=	Ruthenium red
SAOS	=	Small amplitude oscillatory shear
TPA	=	Texture profile analysis
WS	=	Waxy rice starch

BIOPOLYMER PARTICLE TO INHIBIT ACRYLAMIDE FORMATION AND TO STABILIZE PICKERING EMULSION AS TEMPLATE FOR OLEOGELATION

INTRODUCTION

Recently, biopolymer-based particle has been receiving an increased interest account for its biocompatibility, biodegradability, and low-toxicity. AA is found in heat treated starchy foods such as fries, baking products, and roasted coffee. Conventional heating such as boiling, frying is known to facilitate Maillard reaction which is the intermediate for AA formation. However, contradictory and nonconclusive results have been published on the impact of microwave heating on AA formation (Maskan, 2001; Oliveira and Franca, 2002). In this study, the intermediates of Maillard reaction that effect AA formation was investigated in two systems, conventional heating using heating block and microwave heating under controlled temperature and time. In contrast to previous research, a Microwave Accelerated Reaction System was used to carefully monitor temperature changes. Later, the effect of polysaccharides on AA mitigation was investigated in chemical and food model systems under heating block and microwave heating.

Use of polysaccharide was ever reported to reduce AA formation. The protein-polysaccharide complex particles were composed of potential AA inhibitors such as chitosan, alginate, and pectin. It was then hypothesized that the synergistic effect of protein-polysaccharide complexes could enhance AA mitigation at high temperature more effectively than only polysaccharides. Zein-polysaccharide complex particle was stabilized by electrostatic interaction between charged zein and anionic polysaccharides. The zein-polysaccharide complex particles were then obtained via antisolvent precipitation. The zein-polysaccharide complex particle was then investigated for its AA mitigation in a chemical and food model system comparing to zein, polysaccharides, and non-complex particles (the mixture of zein and polysaccharides).

In the second part, granular cold water-swelling (GCWS) rice starch was proposed to modify with octenyl succinic anhydride (OSA) (GCWS-OSA) to stabilize Pickering emulsion and use as a template for oleogelation. Rice starch is highly hydrophilic so it cannot form emulsion by nature. GCWS starch is a pregelatinized starch which the intact starch granules still existed. GCWS has loose structure and gelatinizes at room temperature hence the hydroxyl group was hypothesized to be able to highly expose to OSA during modification. Moreover, unlike other pregelatinized starch, the GCWS still keeping its strong intact starch granules with high wettability that acted as solid particle to stabilize Pickering emulsion. The GCWS-OSA was then used to stabilize (60% oil) O/W Pickering emulsion. After eliminated the water phase, the densely packed oil gel structure or oleogel was obtained. In this section, oleogel prepared from GCWS-OSA based Pickering emulsion with and without hydrocolloids were proposed to use as a template for oleogelation. The Pickering emulsion and fat mimetic oleogel with high oil content (60%) was investigated for its rheological properties using oscillatory test (small and large amplitude sweep test). The prepared oleogel was then applied in a food model to investigate for its possibility to use in a low trans-fat or saturated fat foods.

OBJECTIVES

1. To investigate the inhibitory effect of three polysaccharides (citrus pectin, sodium alginate and chitosan) tested at various concentrations, on acrylamide formation in chemical and food model systems.

2. Two models (chemical and food) were used to compare the mitigation effects of zein-polysaccharide complex particles, zein, polysaccharides, and the mixture of zein and polysaccharides (non-complex particles) on acrylamide formation.

3. To prepare Pickering emulsion and used these as a template to structure edible liquid oils into solid-like fats or oleogels and compare functionality of various starch type and characterize the rheology of both template and oleogels in SAOS and LAOS.

4. The prepared oleogel was then applied in a food model to investigate its possibility to use in a low trans-fat or saturated fat foods.

LITERATURE REVIEW

1. Biopolymer particle

Food industry tried to develop innovative products through the rational design of functional structures based on the fundamental physicochemical principle (McClements *et al.*, 2009; Ubbink and Krüger, 2006). There are many potential applications for particles constructed from edible biopolymers in foods, cosmetic, health care and pharmaceutical products. These particles can be used for encapsulation, protection, and delivery of bioactive or functional compounds (Chen *et al.*, 2006; Emerich and Thanos, 2007; Goldberg *et al.*, 2007; Kulkarni *et al.*, 2005). Biopolymer would precipitate around a core as active encapsulating ingredients or cross-linked as shell by covalent bond to maintain its integrity. However, to control particle size and prevent particle agglomeration had limited stability in different aqueous matrices which depended mostly on the type of biopolymer used (Zielinska *et al.*, 2020).

1.1. Protein-polysaccharide complexes

Protein-polysaccharide complexation is one of the major research focuses in colloidal delivery system due to its superior physical and chemical properties over other delivery systems (Jones and McClements, 2011; Turgeon *et al.*, 2007). The nano- and micro-biopolymer particle fabricated from either protein and/or polysaccharide was used to modulate physicochemical and sensory characteristics of foods (Jones and McClements, 2010). Spherical biopolymer particle was used to imitate textural and optical characteristics of lipid droplets as fat replacers (Liu *et al.*, 2007; Tamime *et al.*, 2007).

1.1.1 Formation of electrostatic protein-polysaccharide complexes

Biopolymer particles can be constructed through a controlled association of protein and polysaccharide. Protein and polysaccharide interact with

each other by electrostatic attraction between opposing electrical charge. Protein possesses a net negative charge above its isoelectric point (pI) and a net positive charge below this pH. For anionic polysaccharide, when protein possesses a high net negative charge ($\text{pH} > \text{pI}$) there is a repulsive force between protein and polysaccharide. The negative charge on the anionic polysaccharide molecules remain relatively constant until the pKa value of its charged groups is reached then it will start to decrease (Jones and McClements, 2008). For cationic polysaccharides, complex formation is achieved by mixing the biopolymers at pH below pI of protein in which protein and polysaccharide are both positive charges (Norton and Frith, 2001; Tolstoguzov, 2003). Protein attains a net-positive charge when pH is reduced below their pI. At pH sufficiently far above this point, the strong negative charges on the two biopolymers result in electrostatic repulsion.

Protein/polysaccharide complexes occur from the electrostatic interactions between oppositely charged macromolecules. Attractive interaction and complexation begin at pH slightly above pI of protein, due to the anionic groups on the polysaccharide and cationic patches on a protein surface (Gao *et al.*, 1997). When the solution is adjusted to around pI of protein ($\text{pH} \sim \text{pI}$), cationic segments of protein interact with anionic groups of polysaccharides leading to weak electrostatic complexation and formation of soluble complexes (Gao *et al.*, 1997). Further pH reduction induces greater interaction between protein and polysaccharide, results in phase-separation or coacervation of the fully neutralized complex (de Kruif and Tuinier, 2001). Zein/polysaccharide complex particle is prepared in the same way by simply dispersing zein in ethanol solution into polysaccharide aqueous solution under mild stirring at ambient temperature. Zein can form complexes with various polysaccharides such as caseinate, chitosan (Luo *et al.*, 2012; Luo *et al.*, 2011) pectin (Hu *et al.*, 2015) and gum arabic (Chen and Zhong, 2015) with improved functionality and stability of resultant zein complex particles.

Biopolymer particle is recently being used to formulate colloidal complex particles for encapsulation such as eugenol (Veneranda *et al.*, 2018) and α -tocopherol (Luo *et al.*, 2011). This method is performed without the need of special

equipment or synthetic surfactants. Polysaccharide is emulsified with protein and hydrophobic ligands using sodium caseinate as a natural emulsifier. Protein forms complexes when adjusting pH but some protein likes zein can easily form particles when dissolve in aqueous alcohol solution and hydrophobic ligands are trapped by hydrophobic interaction with protein. After that, the charges on protein's surface are adsorbed the opposite charged of polysaccharide by electrostatic interaction and heat treatment, leading to the formation of biopolymer particles with core-shell structure. So, protein-polysaccharide complexes can be used as coating material.

1.1.2 Factors affecting electrostatic protein-polysaccharide complexation

a) pH and ionic strength

As ever mentioned, protein-polysaccharide complexes formed when polysaccharide is mixed with protein at pH below and slightly above pI of protein. The driving force for complexation is attributed primarily to electrostatic forces between the different charge of polysaccharide and protein surface. In case of pectin, hydrophobic forces are also thought to play a role for pectin molecules with higher degree of methoxylation (Girard *et al.*, 2003). The nature of the complexes formed depend on the linear charge density and hydrophobicity of the pectin molecules, as well as pH and ionic strength of the solution (Cooper *et al.*, 2005; Seyrek *et al.*, 2003). When pectin and β -lactoglobulin are mixed at neutral pH, and then reduce the pH, the soluble complex formation is firstly observed, then coacervate formation, and finally precipitation, as the strength and number of electrostatic bonds increase. Thus, it is possible to form complexes with different properties by controlling solution pH.

The formation of the electrostatic protein-polysaccharide complexes is carried out at ambient temperature. Under this condition, the biopolymer particles formed are highly unstable to changes pH or ionic strength of the solution. The coacervation will dissociate when the pH or ionic strength of the solution is adjusted to weaken the electrostatic interactions (Alonso-Sande *et al.*, 2006; Cooper *et al.*, 2005; Schatz *et al.*, 2004).

b) Heating process

Heating process was used to reinforce the protein-polysaccharide complex formation, due to the heat induced self-aggregation of protein core and harder adsorption of polysaccharide onto protein layer (Doublier *et al.*, 2000). Heating at optimum pH induces strong complexation among polymers and thus achieve desirable structure for encapsulation and delivery application (Chang *et al.*, 2017). Moreover, heating process decreased biopolymer particle size with increasing temperature. This event based on a nucleation and growth mechanism. At high temperature, protein unfolding, and aggregation occur rapidly leading to the formation of a large number of nuclei. These nuclei grow into relatively small particles before all available protein is depleted (Jones and McClements, 2010).

c) Protein-polysaccharide ratio

Protein concentration has an effect on complex formation. The higher protein concentration, the more complexes will lose their compact structure and become heterogeneous. The loose compact structure happens because of polysaccharide concentration is not sufficiently stabilize a high protein concentration in the core. Furthermore, at high protein concentration, complexes become more opaque owing to the larger particle size. It is noticeable that at the same protein concentration, the turbidity increases slightly after heating process although particle size reduces drastically. The heating process induces partial protein denaturation which result in the formation of more solid particles (Dissanayake *et al.*, 2009).

1.1.3 Characterization of protein-polysaccharide complexes

a) Particle size

Particle size is measured by either light scattering or microscopy methods. Static light scattering (SLS) relies on measurement of the intensity of scattered light waves as a function of scattering angle. An appropriate mathematical

model (usually Mie theory) is used to convert scattering pattern into particle size distribution. Sample preparation often requires dilution and stirring, which alter the integrity or aggregation state of biopolymer particles. Consequently, the result of SLS shall be treated with caution. Another popular method for measuring size of biopolymer particles is dynamic light scattering (DLS), which depends on the measurement of the direction and speed of particle movement due to Brownian motion. This method must be carefully interpreting the result owing to the problem with sample preparation and signal interpretation. For example, large particles (>3000 nm) may not be observed by DLS since their movement is too slow.

b) Particle charge

The electrical properties of biopolymer particles are performed by their ζ -potential. ζ -potential analysis is used in predicting the stability of particle suspension to aggregation as it provides an indication of the electrostatic forces acting between particles. This analysis can also be used to assess the location of bioactive components within biopolymer particles. However, ζ -potential measurements are highly sensitive to pH and ionic strength, and therefore dilution of samples must be carried out carefully. In addition, in systems consisting of a mixture of different biopolymer particles it may be difficult to interpret the data since they will all contribute to the overall signal.

c) Particle morphology

The morphology of particles is studied by using microscopy techniques. Typically, optical microscope can be used to study the overall microstructure, provided that the structures are sufficiently large (>1000 nm). Dyes or fluorescent probes can be used to visualize specific components within biopolymer systems. Confocal microscopy is also used on fluorescent samples and provides a better spatial 3D image. However, the resolution of confocal scanning laser microscopy is comparable to that of conventional optical microscopy, which is inadequate to study the morphology of nanoparticles. Spherical particles are commonly produced when

fabricating biopolymer particles, but other shapes have also been reported. For example, particles produced using fluid gels typically have irregular shapes and can even have tail like structures.

2. Thermal process contaminants

Thermal-process foods could induce chemical conformation alteration during high temperature condition which cause toxic compound formation known as thermal process contaminants. The International Agency for Research on Cancer (IARC) classified mixtures and exposures of carcinogenicity into five categories as followings:

Group 1: Carcinogenic to humans: There is enough evidence to conclude that it can cause cancer in humans.

Group 2A: Probably carcinogenic to humans: There is strong evidence that it can cause cancer in humans, but at present it is not conclusive.

Group 2B: Possibly carcinogenic to humans: There is some evidence that it can cause cancer in humans but at present it is far from conclusive.

Group 3: Not classifiable as carcinogenicity in humans: There is no evidence at present that it causes cancer in humans.

Group 4: Probably not carcinogenic to humans: There is strong evidence that it does not cause cancer in humans. Only one substance – caprolactam – has been assessed for carcinogenicity by the IARC and placed in this category.

The classification is based on the strength of evidence for carcinogenicity, not on the relative increase of cancer risk due to exposure, or the amount of exposure necessary to cause cancer. According to the categories, acrylamide is classified in group 2A while hydroxymethylfurfural in group 2B.

2.1 Acrylamide formation

AA does not naturally present in foods but can be formed during thermal food processing (at temperature higher than 120°C). AA is detected in heat processed starchy foods such as potato chips and fries, bakery products and roasted coffee

(Krishnakumar and Visvanathan, 2014). The major pathway for AA formation is the Maillard reaction between the α -amino group of free asparagine (Asn) and carbonyl group of reducing sugar (Mottram *et al.*, 2002). These carbonyl compounds, amino acids, and the degraded derivatives produce the desired flavored compounds and melanoidin pigments in foods (Claeys *et al.*, 2005; Mottram *et al.*, 2002). Under heat, the Schiff base decarboxylates are forming products that can hydrolyze to form 3-aminopropionamide, which further degrade via the elimination of ammonia to form AA. They can also decompose directly to form AA via the elimination of imine. A minor route is from the degradation of acrolein (Gertz and Klostermann, 2002).

2.2 Acrylamide in food products

AA is formed during thermal processing such as frying, roasting and baking, whereas boiled or microwaved foods do not have acrylamide. The highest levels of AA have been found in fried potato, bread and bakery, and roasted coffee. AA level in different food commodities was shown in Table 1. AA (2-propenamide) is a white crystalline solid with a MW of 71.08 kDa (Keramat *et al.*, 2011). Some toxicological studies suggested that AA vapor irritates the eyes and skin and cause paralysis of the cerebrospinal system (Zhang *et al.*, 2005). AA is transferred to all parts of the body through the blood stream. It is found in many tissues and parts of the body such as liver, kidney, brain, heart and even breast milk (Hogervorst *et al.*, 2007). Daily intake of AA through diet in adult is about 0.3–0.6 $\mu\text{g kg}^{-1}$, and in children and adolescents, is 0.4–0.6 $\mu\text{g kg}^{-1}$ (Tardiff *et al.*, 2010). The concentration of AA can vary enormously in the same food item, depending on factors such as temperature, cooking time, and the amount of reducing sugars and free amino acids like asparagine (Kim *et al.*, 2005). Cereals (cookies, breads, and tostadas etc.), coffee, and fried potatoes are among food types that present significant amounts of AA (Granda *et al.*, 2004; Takatsuki *et al.*, 2003).

Table 1 Acrylamide levels in different food commodities.

Food commodities	N	Acrylamide levels ($\mu\text{g}/\text{kg}$)		
		Minimum	Mean	Maximum
Potato Crips	216	490	628	4180
French fried	529	253	350	2668
Home cook potatoes	121	150	319	2175
Biscuits	227	169	317	4200
Coffee	208	188	253	1158
Breakfast cereals	128	100	156	1600
Bread	272	50	136	2430
Cereal-based baby foods	76	42	74	353
Jar baby foods	84	31	44	162

Note: N = Number of individual data analyzed for each food category

Source: European Food Safety Authority (EFSA) (2009)

2.3 The effect of acrylamide on human health

Many studies indicate that AA is neurotoxic in animals and humans and a reproductive toxicant, germ-cell mutagen, and carcinogen in rodents. Several studies in rodents support the evidence that AA is a multi-organ carcinogen, being able to cause tumors to many organs such as lung, uterus, skin, mammalian gland, brain etc. (Rice, 2005). Thermal process contaminants are taken place during heating amino acid especially asparagine and reducing sugar (Maillard reaction) in food components, (Dybing and Sanner, 2003; Mottram *et al.*, 2002; Parzefall, 2008). AA is obtained highly interested because it causes DNA adducts, gene mutations and chromosome abnormalities in animal tests by IRAC of the WHO (Vainio, 2003). AA is considerably concerns as it could be formed in foods during cooking (Tareke *et al.*, 2002), particular the heat-induced contaminants occur in bakery and fried products (Capuano and Fogliano, 2011).

2.4 The potential strategies to reduce acrylamide

Even though there was no regulation to limit AA content in thermal-processing foods, there have been various attempts to reduce AA formation during thermal food processing. The potential strategies to reduce AA are summarized in Table 2. The modification of thermal conditions, including heating time, temperature, and cooking method, altogether with the application of chemical agents, vitamins, natural extracts, and hydrocolloids are applied to reduce of AA formation in thermally processed foods. The oxidation and/or thermal degradation of lipids in fried foods are reported to be the possible mechanistic route contributing to AA formation via acrylic acid intermediate (Yasuhara *et al.*, 2003).

a) Chemical agents

Mono- and divalent cations such as Na^+ and Ca^{2+} could prevent AA formation, whereas monovalent cations almost halved the AA formation. The presence of cations in the reaction mixture influenced the rate of decomposition of AA precursors significantly. Adding cations into the reaction mixture increased the rate of glucose decomposition while most asparagine remained unreacted. The potatoes were dipping into calcium chloride solution was reported to inhibit AA formation up to 95% during frying. The sensory quality of fried potato strips, such as golden yellow color and crispy texture, was not adversely affected by this treatment (Gökmen and Şenyuva, 2007). A glucose-asparagine reaction model system was used to test the effect of ferulic acid, catechin, CaCl_2 , NaHSO_3 , and L-cysteine on acrylamide formation inhibition altogether with the immersion of fresh potato in different concentration of these agents. Result showed a greatly inhibited effect on AA formation, and the efficiency increased with concentration. L-cysteine is the most efficient agent with little effect on the texture of crisps. But CaCl_2 is regarded as the suitable choice because of its low price and the acceptable mouth feel with increased in brittleness (Ou *et al.*, 2008).

Table 2 Acrylamide mitigation strategies

AA reduction	Effect	Results	Ref.
Variety selection	-	Select potato varieties with low acrylamide precursors	Capuano and Fogliano, 2011
Ingredient addition			
- Na ⁺ and Ca ²⁺ cation	-	Prevent formation of schiff base of asparagine	Gökmen and Şenyuva, 2007
- Phenolic compound	-	Contradictory and nonconclusive results. Naringenin, phenol in virgin olive oil can reduce AA content	(Cheng <i>et al.</i> , 2009; Morales, <i>et al.</i> , 2014)
	+	Some phenolic compounds can increase AA content such as BHT, soluble vitamin, curcumin	
	0	Some phenolic compounds have no effect on AA such as ascorbyl palmitate and sodium ascorbate	
- Amino acid or protein based ingredient	-	Amino acid (e.g. sodium caseinate, lysine and cysteine) competed with asparagine for sugar	Anese <i>et al.</i> , 2009
Hydrocolloids	-	Alginic acid and pectin inhibited AA formation in chemical and food model	Zeng <i>et al.</i> , 2010
Cooking method	-	High temperature and prolonged heating times reduced AA level due to elimination / degradation reactions	Biedermann <i>et al.</i> , 2002; Rydberg <i>et al.</i> , 2003
	-	A microwave precooking effectively minimize AA formation. Controlling microwave power could decrease AA formation during food processing	Yuan <i>et al.</i> , 2007

Table 2 (Continued)

AA reduction	Effect	Results	Ref.
	+	Microwave heating facilitated Maillard reaction similarly to conventional heating	Maskan <i>et al.</i> , 2001; Oliveira <i>et al.</i> , 2002

Note: + Increase acrylamide, - Decrease acrylamide, 0 no effect on acrylamide

b) Hydrocolloids

Chemical and food model (fried snack, fried potato strips) were used to study the potential of hydrocolloids on AA formation inhibition. It was noted that among different model of the same pattern, the relative inhibitory activities were dissimilar. In chemical model, alginic acid and pectin (2%, w/w) could significantly inhibited AA formation by over 50% comparing with control. But only a mild inhibition of around 20% was found in the snack model (2.5%, w/w). However, most hydrocolloids showed effective AA inhibition (around 30%) when the concentrations were increased to 5% (w/w) in the snack model (Zeng *et al.*, 2010). Chitosan was used to limit AA generation in chemical model and fried batter system (Chang *et al.*, 2016; Sansano *et al.*, 2017). The addition of small amounts of chitosan (~0.5%) could reduce AA generation in chemical system and batter model by 58% and 61%, respectively. The action mechanism was based on the free amino groups present in chitosan which compete with asparagine in binding to the reducing sugars, hence reduce AA formation.

2.5 Acrylamide detection

AA is a highly water-soluble organic molecule with low volatility. Thus, the analytical methods that have been developed were either based on derivatization of the molecule to increase its volatility to employ in a liquid chromatography. There are many methods that have been developed for the analysis of AA but not all these methods are suitable for use in foods.

a) Gas chromatography (GC)

Acrylamide in the extracted sample is derivatized with bromine (mixture of potassium bromide and hydrobromic acid) to give 2, 3-dibromopropionamide derivative. It is measured by GC using an electron capture detector (ECD). It can also be measured by a flame ionization detector (FID) but this is less sensitive. GC methods without derivatization of AA are in development.

b) Gas chromatography/Mass spectroscopy (GC/MS)

The food sample is blended with water, the solid is removed by centrifugation and the supernatant is brominated. The brominated derivative is extracted into ethyl acetate. The sample was clean up or the extracts can be analyzed directly by GC/MS. This method has been modified by the addition of a water immiscible organic solvent as the food is blended with water to assist lipids removal. Extraction from processed foods exploits the high aqueous solubility of acrylamide. A sample is homogenized and extracted with hot water. (Methacrylamide, $\text{CH}_2=\text{C}(\text{CH}_3)_2\text{CONH}_2$, is frequently used as an internal standard). Acrylamide can be determined directly or converted to the 2,3-dibromopropionamide by treatment with a brominating solution. An option is to further treat this derivative to form a more stable analyte, the 2-bromopropenamide.

c) Liquid chromatography/Mass spectroscopy (LC/MS/MS, LC/MS)

Liquid chromatography-based separation methods avoid the necessity of preparing a derivative. Current methods are severely inconvenient, expensive and time consuming. Several methods have been shown to be sufficient in acrylamide detection such as liquid chromatography with tandem mass spectrometry (LC-MS/MS). These methods are currently mostly used for acrylamide detection. For the purpose of validation, recovery correction and matrix effect reduction during the analysis, regardless of the type of method, the internal standard $^{13}\text{C}_3$ -acrylamide is used.

Analyses performed by LC-MS and LC-MS/MS, usually the ions with m/z 72 and m/z 55 for acrylamide, or m/z 75 and m/z 58 for $^{13}\text{C}_3$ -acrylamide were monitored. The most popular ionization techniques used in these methods are electrospray ionization (ESI) and chemical ionization under atmospheric pressure (APCI), which are considered to be gentle ionization techniques that enable the detection of very polar substances such as acrylamide (Jozinović *et al.*, 2019).

2.6 Acrylamide regulation

The Commission of the European Union (EU) has issued new requirements to control acrylamide levels in certain food products. Because it is defined as a contaminant under EU law, acrylamide represents a potential hazard in foods. The EU's Regulation on the management of acrylamide in food takes effect in April 2018 and will be applicable to those who produce or place on the market, potato fries and crisps, snacks, crackers and other products made from potato dough, bread, most breakfast cereals, cookies, biscuits and other fine bakery wares, coffee and coffee substitutes, and baby food and other cereal-based foods intended for infants and young children. The benchmark level of acrylamide in food was shown in appendix (Table 1).

3. Granular cold water swelling starch (GCWS)

Native starch has a complex granular structure. Within the granule, amylopectin molecules are arranged radially and the branch chains form double helical crystalline clusters. Amylose molecules are interspersed among the amylopectin molecules. Because of the complex semi-crystalline structure of the starch granules, energy is required to melt (gelatinize) the starch crystallites. Physical modifications of the starch can be applied alone or with chemical reactions to change the granular structure and convert native starch into cold-water soluble starch or into small-crystallite starch. GCWS is a modified pregelatinized starch with the intact starch granules are still existed. GCWS as a pregelatinized starch is an important ingredient used in instant and microwave foods. Moreover, starches with submicron (less than 1 μm in diameter) crystallites have been applied for use as fat substitutes, to provide a fat-like texture and

mouthfeel. Most commercial pregelatinized starches are manufactured by drum drying, extrusion, or cooking followed by spray drying. The products are cold-water-dispersible but the quality of the dispersion does not match that of the freshly cooked pastes. The pregelatinized starch pastes are usually graininess, less sheen, and less flexibility to processing conditions.

3.1 Granular cold water swelling starch formation

GCWS starches have been produced by a heating starch slurry (12-20%, w/w) in aqueous alcohol solution (18-26%, w/w) under elevated pressure to about 160-170°C for about 2-5 min (Eastman and Moore, 1984). Eastman (1987) patented another process using a combination of starches, an amylose free starch (such as waxy maize starch) and a 20-28% amylose starch and 72% to 80% amylopectin to evaluate the effect of various ratios of waxy starch to common starch on the properties of the starch material. The slurry of the combined starches in an aqueous alcohol is heated to about 155-178°C for about 1-10 min. The slurry was then cooled, washed with alcohol, and dried. The resulting GCWS starches display 50-90% of cold-water solubility.

Rajagopalan and Seib (1991, 1992) proposed a process for preparing GCWS under atmospheric pressure. Starch slurry in a mixture of water-polyhydric alcohol such as ethylene glycol, glycerol, 1,2- or 1,3-propanediol was heating at about 80-130°C for 3-30 min. Polyhydric alcohols has many hydroxyl groups, leading to high boiling points such as boiling point of ethylene glycol 197°C. However, this method cannot be applied on high-amylose or waxy starch alone. GCWS starches made from amylose-containing starches, using 1,2- or 1,3-propanediol and 1,3-butanediol, gave strong V-type X-ray patterns, which was attributed to V-complex formation between amylose and ethanol during solvent exchange.

Chen and Jane (1994) proposed an alcoholic-alkaline modification without heat treatment which could effectively apply in a wider range of starches. Treatment with a higher concentration of NaOH increased the swelling of the granules. However,

high concentration of ethanol in the reaction mixture restricted starch granule swelling and retarded destruction of the double helical crystalline structure.

GCWS starch could also be prepared using a spray-dryer fitted with two fluid nozzles. The starch slurry (35-45%, w/w in water) was atomized into an enclosed chamber from an atomization aperture within the nozzle, and steam was injected into the chamber from the second aperture in the nozzle at the same time to cook or gelatinize the starch. The gelatinized starch granules were moving rapidly and exited the chamber to a subsequent spray-drying process (Pitchon *et al.*, 1981).

4. Biopolymer particle to stabilize Pickering emulsion

Pickering emulsion refer to emulsion that does not stabilize by any emulsifier but instead by solid colloidal particles. These solid particles are partly wetted by oil and water and acted as emulsifiers. Previously, several inorganic solid particles such as silica or clay have been used to stabilize Pickering emulsion. Silica-based particles are interested, such particles are commercially available, with various and well-defined particle sizes (from a few nanometers to microns), surface areas, and hydrophobicity. Apart from being non-food grade, these solid particles could increase droplet aggregation or precipitation caused by noncovalent interaction including hydrophobic and electrostatic interaction (Berton-Carabin and Schroen, 2015). Therefore, a safer food-grade solid particle that could adsorb at the oil-water interface and stabilize Pickering emulsion was interested such as starch, protein, and polysaccharide (Liu *et al.*, 2018).

Conventional Pickering emulsion was stabilized by solid particles such as polysaccharides and/or protein and/or low MW emulsifiers to form a steric elastic film or reduce the interfacial tension (Bos and van Vliet, 2001; Dai *et al.*, 2018). Unlike emulsifiers, biopolymer particles can be adsorbed at the interface to form a rigid thick layer shell with reduced mobility, hence enhanced emulsion stability. Pickering emulsion had potential uses for texture modification, calorie reduction, encapsulation,

and delivery. The focus of Pickering emulsion is shifting from inorganic particles to food grade biological particles such as polysaccharides and/or protein particles.

4.1. Starch based Pickering emulsion

Starch is largely used in fabrication of Pickering emulsion due to its non-allergic, cheap, and abundant source (Zhu, 2019). However, starch is highly hydrophilic so it cannot form emulsion by nature. Starch modification by octenyl succinic anhydride (OSA, e-number 1450) is commercially used to make starch more hydrophobic. With this method, the hydroxyl groups of starch react with OSA and the hydrophobicity was increased from the hydrophobic octenyl group of OSA. However, less than 3% of OSA is allowed in food application (Modig *et al.*, 2006). As so, much research has focused on how to increase degree of OSA-substitution to accelerate emulsifying property. The emulsifying property of solid emulsifier depended mostly on surface characteristic especially the balance between hydrophobicity and hydrophilicity (Linke and Drusch, 2017). One attempt to increase surface characteristic of starch is to increase the degree of OSA substitution either by using different types of starch (such as quinoa, waxy maize, or arrow root) (Park *et al.*, 2020) or applying different modification process (such as non-solvent precipitation or dissolved starch etc.) (Saari *et al.*, 2019).

GCWS was proposed to use in this study as it had loose structure which allowed more hydroxyl groups to expose to OSA during modification. Moreover, unlike other pregelatinized starch, the GCWS still keeping its strong intact starch granules with high wettability that acted as solid particle to stabilize Pickering emulsion. The GCWS was then modified by OSA to stabilize O/W emulsion, followed by the elimination of water phase to obtain tightly packed oil gel structure.

4.2. Protein based Pickering emulsion

Zein was often used as a potent food grade colloidal nanoparticle to stabilize Pickering emulsion (de Folter *et al.*, 2012; Gao *et al.*, 2014). However, zein emulsion faced stability problem due to the creaming and coalescence that occur at pH

close to its isoelectric point (pI) and the poor wettability of zein colloidal particles. To improve the feasibility of zein, surface modification with sodium stearate has been done (Gao *et al.*, 2014). Colloidal particles with equilibrium contact angle (around 90°) at oil/water interface could promote effective packing of particles and form a steric barrier, thus preventing the droplet coalescence (Gao *et al.*, 2014).

The toxicity of a surfactant such as sodium stearate was still a problem when applying in foods. Food grade sodium caseinate was used as an alternative emulsifier to improve stability and dispersibility of zein colloidal particle. The surface-active casein contains hydrophilic and hydrophobic groups in various sequences and proportions. The mechanism of sodium caseinate to stabilize zein colloidal particle could be both electrostatic repulsion and steric stabilization (Feng and Lee, 2016; Patel *et al.*, 2010). The cationic and anionic polysaccharides were also used together with zein to stabilize Pickering emulsion such as pectin (Soltani and Madadlou, 2016), gum arabic (Dai *et al.*, 2018), chitosan (Wang *et al.*, 2015; Wang *et al.*, 2016), and propylene glycol alginate (Sun *et al.*, 2018). The complex colloidal particles with core-shell structure are fabricated through hydrogen bonding and electrostatic interaction. Polysaccharides and/or sodium caseinate provided intermediate surface wettability for zein colloidal particles (Wang *et al.*, 2016). These zein particles were used to produce surfactant-free O/W Pickering emulsion with droplet size in the range of 10-200 μm and oil fraction from 50% to 80% (Dai *et al.*, 2018; Wang *et al.*, 2016).

5. Oleogel formation

Oleogelation is a transforming process of a high concentration liquid oil into a visco-elastic, gel-like structured oil systems (Jiang *et al.*, 2018). There are two main structure approaches to entrap oil based in the system, a direct and indirect oleogelation. The direct oleogelation is to disperse lipid-based in a gelator such as waxes, fatty acids, fatty alcohols, and mono glycerides etc. These gelators are directly dispersed into oil phase at elevated temperature followed by cooling. The indirect method used emulsions as a template which is a promising method use in foods. This method involves in preparing oil in water Pickering emulsion, follow by the removal of water to obtain

dried products that physically entrapped high oil content. The strategy of structuring liquid oils into solid-like oil gels by freeze-drying the biopolymer particle precursor. Several food polymers such as protein and/or polysaccharide can stabilize oil-in-water emulsion because of their amphiphilic nature. After these polymers were adsorbed onto the oil-water interface and formed a stable emulsion, water can be removed from the system until high level of oil was entrapping in this polymer network. Dehydrated form of Pickering emulsion could be obtained in dried microstructure with entrapped oil phase which transform oil into a range of structured oil systems such as oil powder, oil gel, and soft solid. The fat-structured foods, such as chocolate, ice cream, spreads, and shortening are usually created by colloidal networks of fat crystals or hydrogenated vegetable oils, which composed of saturated and/or trans fatty acids (Patel and Dewettinck, 2016).

Zein-chitosan particle emulsion was reported to have visually solid-like gel without oil leakage via freeze-drying. The oil content entrapped in this matrix was over 92% (Wang *et al.*, 2016) (Figure 1). Biopolymer nanocomplex of zein, sodium caseinate, and propylene glycol alginate can entrap high volume fraction of oil (up to 80%) with more solid-like properties and no free oil indicating the strength of emulsion droplet structures (Sun *et al.*, 2018). Apparently, the Pickering emulsion gels stabilized by zein-gum arabic particles could obtain an elastic gel-like structure using dynamic oscillatory measurements (Dai *et al.*, 2018).

In this study, we are structuring liquid oil into solid-liked oleogel using biopolymer particle Pickering emulsion from GCWS as template. By this strategy, the zero trans-fats and less saturated fats with surfactant-free was obtained using indirect oleogelation. The O/W Pickering emulsion (60% oil) which stabilized by protein and polysaccharides was firstly prepared and freeze-dried to evaporate water phase. Solid like oil gel is obtained and has a potential to use in fatted food formulation that could provide structure and influence textural properties in foods. The schematic representation of the process whereby liquid oil is first used to prepare O/W emulsion, followed by the removal of water through drying to form oleogel was presented in Figure 1. Addition, the association of rheological properties of Pickering emulsion and

its oleogel was investigated comparing with animal fat (lard). It is challenging the food industry to seek healthy fat replacement that do not change the physical and sensory properties of end products.

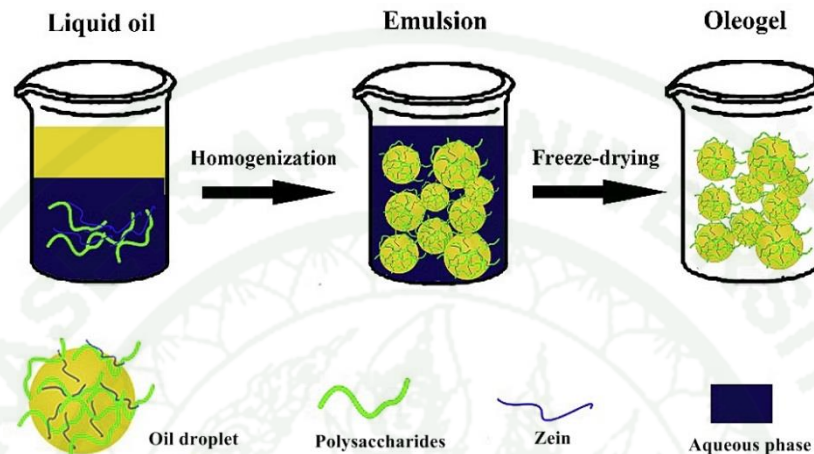


Figure 1 Schematic representation of the process whereby liquid oil is first used to prepare O/W emulsion, followed by the removal of water through drying

Source: Jiang *et al.* (2018)

6. Rheology measurement

The oscillatory shear tests can be used to study the rheology of soft materials. The material is subjected to a sinusoidal deformation and the mechanical response is recorded as a function of time. They can be divided into two types: small amplitudes oscillatory shear (SAOS) and large amplitudes oscillatory shear (LAOS). Oscillatory techniques involve subjecting the test material to strain that is variable in time. As the easiest way to analyze, the signal used is usually sinusoidal in nature and expressed as:

$$\gamma(\omega t) = \gamma_0 \sin(\omega t)$$

where; γ is strain or deformation, ω is angular frequency of oscillation, and t is time.

For linear viscoelastic response, material can be quantified by two measures: the elastic storage modulus G' and the viscous loss modulus G'' . In the linear viscoelastic region, the strain amplitude is small enough so that the elastic and loss moduli are independent to the strain amplitude. Owing to the theoretical foundations, linear viscoelasticity tests (also called SAOS test) is an excellent way to explain the rheological characteristic of complex fluids and soft materials. However, if the amplitude of the applied strain is increased at a constant frequency, a transition between the linear and non-linear regions is observed beyond the SAOS regime (Ptaszek, 2017).

The nonlinear region is characterized by the storage and loss moduli being functions of the strain amplitude, namely $G'(\gamma_0)$ and $G''(\gamma_0)$. At larger strain amplitudes, the nonlinear behavior is more apparent and hence nonlinear dynamic tests are typically referred to as LAOS tests. Even though SAOS tests are efficient tools to comprehend the relationship between microstructure and rheology of complex fluids, it is important to realize that the linear viscoelastic tests have a meaning only when the total deformation is quite small. The deformations can be often large and rapid in processing operations and thus linear viscoelastic tests are not sufficient to characterize the rheology in these nonlinear situations. It is therefore understood that studying the nonlinear viscoelastic response of soft materials is important (Ewoldt *et al.*, 2010).

There are several ways to characterize the nonlinear rheology of soft materials, Fourier Transform rheology is one of the most used methods. It transforms time dependent response to frequency domain which is used to simulate the non-sinusoidal response using higher harmonics. When the elastic (G') and viscous (G'') components of stress are plotted with respect to strain (γ) and strain rate ($\dot{\gamma}_0$), respectively. The stress components deviate from linearity into the non-linear region (Duvarci *et al.*, 2017; Hyun *et al.*, 2011).

Lissajous curves (sometimes called Lissajous-Bowditch curves) provide a useful way of describing the viscoelasticity of a fluid. Lissajous Bowditch curves showed clear changes in both stress response and its elastic and viscous components. The clockwise rotation of the major axis toward the strain-axis was the result of

intracycle strain softening and the upturn of the shear stress was the result of intracycle strain stiffening. For SAOS, Lissajous curves are always ellipses, possibly tilted at the origin. A nonlinear viscoelastic response will distort the elliptical shape of a Lissajous curve. Furthermore, Lissajous curves provide a meaningful way to visualize and interpret viscoelastic nonlinearities in general. Elastic Lissajous projects the oscillatory response curves onto the stress $\sigma(t)$ vs strain $\gamma(t)$ plane, whereas viscous Lissajous curves denote parametric plots of stress $\sigma(t)$ vs strain rate $\dot{\gamma}(t)$. A linear elastic material response appears as a straight line on the elastic Lissajous curve of $\sigma(t)$ vs $\gamma(t)$ or a circle in a suitably scale plot of σ vs $\dot{\gamma}$ (Ewoldt *et al.*, 2010). The area in Lissajous is proportional to the quantity of energy dissipated by the material. To compare the quantity of energy dissipated by the material, a dissipation coefficient (ϕ) is introduced (Ptaszek, 2017).

Rheological properties are important properties for starch-based food and materials. Starch paste is a kind of pseudoplastic fluid with shear thinning behavior, as starch chains undergo disentanglement and orientational arrangement under shear, leading to decreases in flow resistance and viscosity. Dynamic rheology can effectively reflect the processing properties and monitor the movement of molecular chains and the structural evolution of materials during processing (Lee *et al.*, 2019). In case of waxy starch, chains can be considered as rheologically long branched chains. Specifically, the rheological properties of the starch solution are sensitive to the molecular structure especially branched-chain length, and thus rheology can be used for the qualitative and quantitative characterization of starch chain structure (Liu *et al.*, 2019). Precha-Atsawanon *et al.* (2018) reported that the flow behavior of debranched starch gel was significantly different from the native starch. The waxy starch, which contains highly branched amylopectin molecules, exhibited a weak gel behavior in the linear viscoelastic regime, and the moduli had a frequency, concentration and temperature dependence which is similar to a weakly aggregated particle system. The debranched starch, which contains a mixture of short and long linear starch chains, produced much stronger, brittle, and turbid gels, with a concentration and temperature dependence for the moduli characteristic of a gel consisting of dense clusters of rigid polymers. Furthermore, another reason for the growing interest in LAOS tests is their

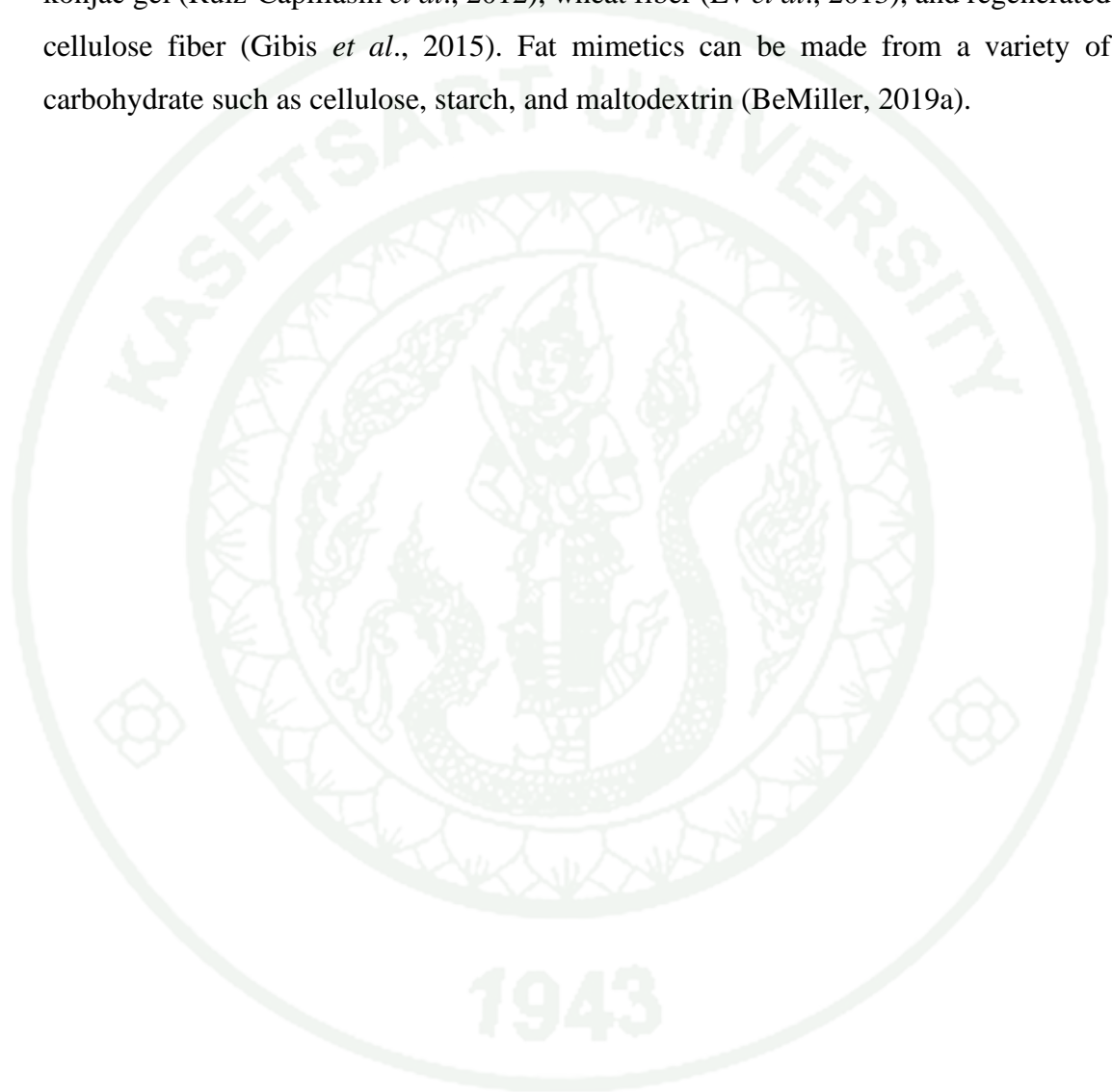
usefulness in describing the elastic and viscous properties of complex fluids at large deformations (outside the linear viscoelastic regime), which are closer to real processing and application conditions. For instance, it has been proved recently that LAOS measurements are related to the sensory and textural properties of food (Melito *et al.*, 2013).

7. Fat mimetics

Solid fat is indispensable ingredient as it plays a role in modifying or improving qualities of foods such as texture (tenderness, flakiness), flavor, leavening, emulsifying, sticking prevention, heat transferring, and satiety (Pehlivanoglu *et al.*, 2018). The excessive intakes of saturated and trans fatty acids could result in negative effects such as obesity, diabetes, and cardiovascular disease (Mozaffarian and Clarke, 2009). The U.S. Food and Drug Administration (FDA) has declared that partially hydrogenated oil, a solid fat that has been widely used in food processing, must be banned from using in human foods. However, most people are reluctant to give up the sensation of fattiness in their food, fat mimetics have been sought. A fat mimetic is a substance that imitates the sensory characteristics of fat. However, solid fat contains large number of saturated and trans fatty acids. Therefore, it has a demand and an emergent technical challenge for researchers and food manufactures to seek a new fat substitute with low saturated fatty acids and trans-fat.

Oleogelation, a physical modification approach to convert a liquid oil into a solid-like gel without modifying the chemical characteristics of oil, is considered a promising oil-structuring technique to prepare healthy fat substitutes (Marangoni and Garti, 2018). The functional properties of lipids that must be mimicked include organoleptic properties (largely rheology and lubricity), the ability to dissolve lipid-soluble flavors and other substances, aeration, aroma, emulsification, flavor, heat stability, and spreadability (Rios *et al.*, 2014). The fatty sensation is primarily dependent on particle or droplet size and rheology. The low-fat sausage (12%-14% fat) was reported to have lower cohesiveness with soft texture (Matulis, *et al.*, 1995; Salcedo-Sandoval *et al.*, 2013). The decrease in hardness of the low-fat formulation is

due to the reduction in fat content and the increase in water content while keeping protein level constant (Pietrasik and Janz, 2010; Atashkar *et al.*, 2018). Hardness was also reported to decrease in the reduced fat sausage with added polysaccharides such as xanthan gum (Rather *et al.*, 2015a; 2015b), tragacanth gum (Abbasi, *et al.*, 2019), konjac gel (Ruiz-Capillasm *et al.*, 2012), wheat fiber (Lv *et al.*, 2013), and regenerated cellulose fiber (Gibis *et al.*, 2015). Fat mimetics can be made from a variety of carbohydrate such as cellulose, starch, and maltodextrin (BeMiller, 2019a).



Hypothesis

1. Zein-polysaccharide complex particles can inhibit acrylamide formation in both chemical and food models because free amino acid from zein compete with asparagine to bind with carbonyl group. Moreover, the highly stable and thickening property of emulsion stabilized by zein-polysaccharide particles could reduce interaction between heat and acrylamide intermediates.

2. GCWS-OSA starch particles are soft and deformable with high diffusability to the outer surface of oil droplets, starch particles are partly wetted by oil and water and acted as emulsifier and steric barrier at the interface

MATERIALS AND METHODS

1. Chemicals

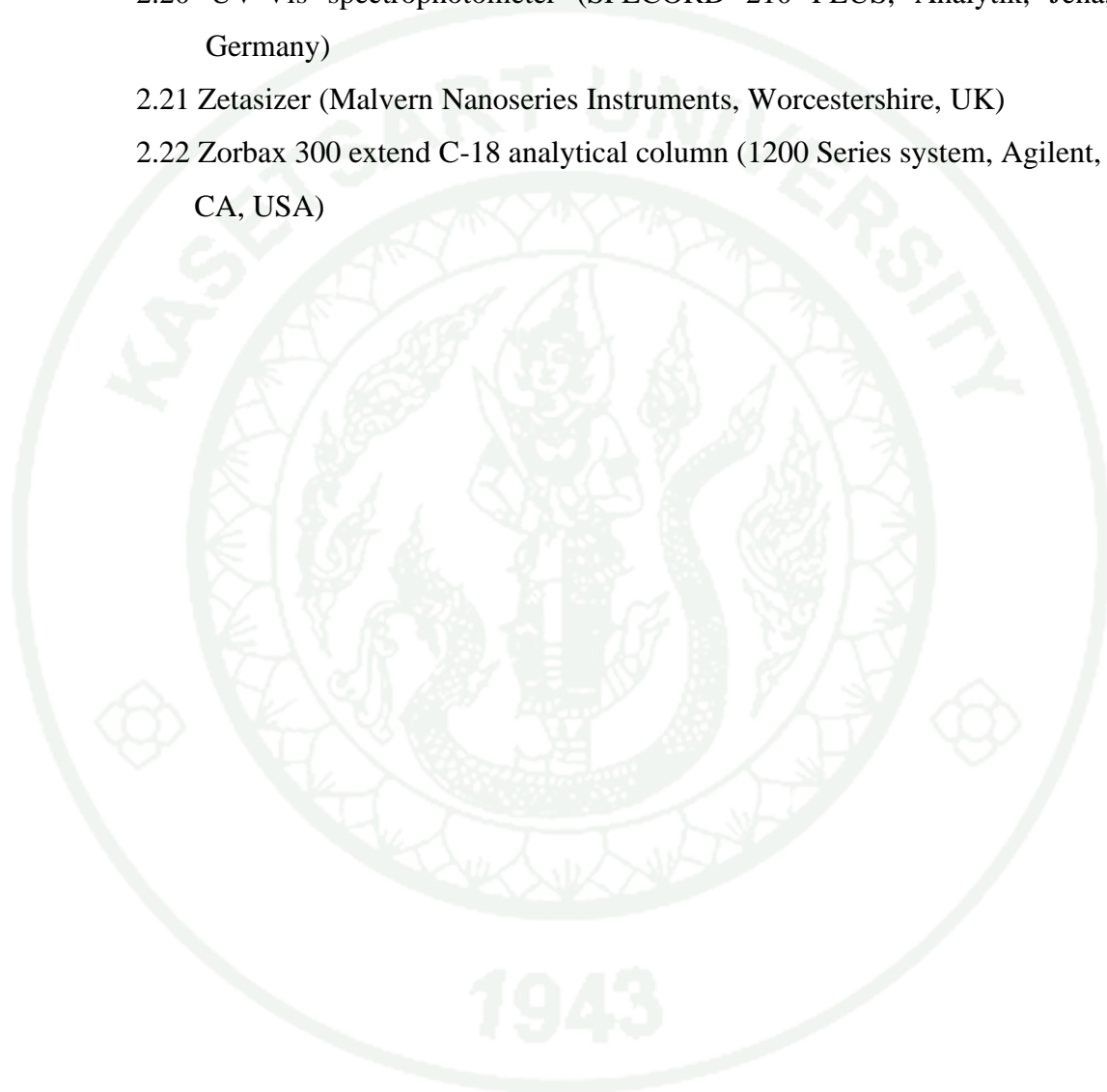
- 1.1 Acetic acid (CH_3COOH ; CAS 64-19-7, Sigma–Aldrich, MI, USA.)
- 1.2 Acridine orange ($\text{C}_{17}\text{H}_{19}\text{N}_3\cdot\text{HCl}$; CAS 65-61-2, Fisher Scientific, MA, USA.)
- 1.3 Acrylamide ($\text{C}_3\text{H}_5\text{NO}$; CAS 79-06-1, Sigma–Aldrich, MI, USA.)
- 1.4 Asparagine ($\text{C}_4\text{H}_8\text{N}_2\text{O}_3$; CAS 70-47-3, ACROS organics (Morris Plains, NJ, USA.)
- 1.5 Citric acid ($\text{C}_6\text{H}_8\text{O}_7$; CAS 77-92-9, Sigma–Aldrich, MI, USA)
- 1.6 Chinart 1 and Kor Khor 6 rice varieties (Watcharawan Green Farm, Payao, Thailand)
- 1.7 Ethanol ($\text{CH}_3\text{CH}_2\text{OH}$; CAS 64-17-5, Fisher Scientific, MA, USA.)
- 1.8 Fluoresceinamine ($\text{C}_{20}\text{H}_{13}\text{NO}_5$; CAS 3326-34-9, Fisher Scientific, MA, USA.)
- 1.9 Formic acid (CH_2O_2 ; CAS 64-18-6, Sigma–Aldrich, MI, USA.)
- 1.10 Glucose ($\text{C}_6\text{H}_{12}\text{O}_6$; CAS 50-99-7, Sigma–Aldrich, MI, USA.)
- 1.11 Hydrochloric acid (HCl ; CAS 7647-01-0, Fisher Scientific, MA, USA.)
- 1.12 Isopropyl alcohol ($(\text{CH}_3)_2\text{CHOH}$; CAS 67-63-0, Fisher Scientific, MA, USA.)
- 1.13 Low molecular weight chitosan (CAS 9012-76-4, Sigma–Aldrich, MI, USA.)
- 1.14 Medium chain triglyceride (MCT) oil
- 1.15 Nile blue ($2\text{C}_{20}\text{H}_{20}\text{N}_3\text{O} \cdot \text{SO}_4$; CAS No.3625-57-8, Sigma–Aldrich, MI, USA)
- 1.16 Nile red ($\text{C}_{20}\text{H}_{18}\text{N}_2\text{O}_2$; CAS No. 7385-67-3, Sigma–Aldrich, MI, USA)
- 1.17 Octenyl Succinic Anhydride (OSA) ($\text{C}_{12}\text{H}_{18}\text{O}_3$; CAS 7757-96-2, Sigma–Aldrich, MI, USA.)
- 1.18 Pectin from citrus peel (CAS 9000-69-5, Sigma–Aldrich, MI, USA.)
- 1.19 Potassium hexacyanoferrate (II) trihydrate ($\text{K}_4\text{Fe}(\text{CN})_6 \cdot 3\text{H}_2\text{O}$; CAS 14459-95-1, Sigma–Aldrich, MI, USA.)

- 1.20 Rhodamine B ($C_{28}H_{31}ClN_2O_3$; CAS 81-88-9, Fisher Scientific, MA, USA.)
- 1.21 Ruthenium red ($[(NH_3)_5RuORu(NH_3)_4ORu(NH_3)_5]Cl_6$; CAS 11103-72-3, Fisher Scientific, MA, USA.)
- 1.22 Sodium alginate (CAS 9005-38-3, Fisher Scientific, MA, USA.)
- 1.23 Sodium hydroxide (NaOH; CAS 1310-73-2, Fisher Scientific, MA, USA.)
- 1.24 Zein (CAS 9010-66-6, Sigma–Aldrich, MI, USA.)
- 1.25 Zinc acetate dihydrate ($Zn(CH_3COO)_2 \cdot 2H_2O$; CAS 5970-45-6, Sigma–Aldrich, MI, USA.)

2. Equipments

- 2.1 Basket centrifuge (Wasino Co., Ltd., Thailand)
- 2.2 Centrifuge (Centrifuge 5424R; Eppendorf, Hamburg, Germany)
- 2.3 Centrifuge (Hettich, Germany)
- 2.4 Commercial microwave (DeLonghi, Treviso, Italy)
- 2.5 Confocal Laser Scanning Microscopy LSM 900 upright with Airyscan 2 device (Carl Zeiss, Oberkochen, Germany)
- 2.6 Confocal laser scanning microscopy (Zeiss 510, Jena, Germany).
- 2.7 Deep Fat fryer r (Cookworks™, Milton Keynes, UK)
- 2.8 Genevac EZ 2 plus (Warminster, PA, USA.)
- 2.9 Heating block (VWR analog Heatblock, Hampton, NH, USA)
- 2.10 High-pressure homogenizer (HU-3.0, Delta Instruments, Taiwan)
- 2.11 High-speed homogenizer (IKA Ultra-Turrax T25, Wiggins, Germany)
- 2.12 HPLC-Diode array detector (Agilent 1200 series, CA, USA)
- 2.13 Light microscope (Zeiss Axioskop 2 plus + Axiocam erc 5s) (Zeiss, Jena, Germany)
- 2.14 Mastersizer (Malvern Nanoseries Instruments, Worcestershire, UK)
- 2.15 Microwave accelerated reaction system (MARS 6®, Matthews, NC, USA)
- 2.16 Rotor mill (Hosokawa Micron Corp, Japan)

- 2.17 Rheometer (Anton Paar, Graz, Austria)
- 2.18 Super mass colloidier (Aerosia Interpac Co., Ltd, Thailand)
- 2.19 Texture analyzer TA-TX Plus (Stable Micro Systems Ltd., Godalming Surrey, UK)
- 2.20 UV-Vis spectrophotometer (SPECORD 210 PLUS, Analytik, Jena, Germany)
- 2.21 Zetasizer (Malvern Nanoseries Instruments, Worcestershire, UK)
- 2.22 Zorbax 300 extend C-18 analytical column (1200 Series system, Agilent, CA, USA)



Part 1

Inhibitory effect of polysaccharides on acrylamide formation in chemical and food model systems

1. Acrylamide formation in a chemical model system

1.1 Conventional heating

The reaction under conventional heating was carried out following the method described by Sansano *et al.* (2017) with minor modifications. In this study heating block was used to generate heat instead of oil bath due to constant temperature. The mixture between asparagine (Asn, Fisher, AC371601000) and glucose (Glc, Sigma-Aldrich, G8644) was heated at equimolar amounts; 5 μ M glucose and 5 μ M asparagine (1.5 ml of each) were mixed in a Pyrex tube fitted with a screw cap. Samples were heated at 150, 160, 170 and 180 °C in heating block (VWR analog Heatblock, Hampton, NH, USA) for 10, 20, 30, 40, 50 and 60 min. Heating block was pre-heated for 2 h. The temperature fluctuation was within 2 °C. The tubes were occasionally swirled manually. The heating block temperature was measured using an infrared thermometer. It was assumed that temperature in the heating block was identical to the temperature inside the tube by neglecting the conductive resistance to heat transfer. At the end of the heating time, the samples were cooled immediately in an ice bath to stop reaction for 5 min.

1.2 Microwave heating

The microwave heating was performed via a Microwave Accelerated Reaction System (Model MARS 6®, Matthews, NC, USA). In the microwave chamber, there were 10 microwave sample vessels in a rotating carousel, which allowed 10 simultaneous sample reactions under identical reaction conditions. The reaction temperature, time, and the control limits were modulated via a digital intelligent control panel. The reaction mixtures were treated at the constant microwave power of 800 W

with even wave administration (no hotspots). All reactions contained the same reactant concentrations as described for the conventional heating reactions and microwaved for 30, 60, 90 and 120 sec. The mixtures were then cooled immediately in an ice bath.

2. Acrylamide formation in food model

2.1 Fried potato chips

Potatoes were washed, peeled and cut into the similar size strips (10 x 10 x 50 mm.) prior frying in deep fat fryer (Cookworks™). Frying was performed using sunflower oil. Potatoes (50g per portion) were soaked in inhibitor solution (50 ml) for 30 min and drained for 2 min before frying at 170 °C, 3 min. Fryer was pre-heated until temperature reaching to 170 °C. Then, fried potato chips were grounded by mini food processor, after all samples were cooled and drained excess oil on sieve.

Acrylamide extraction from food model was adapted from (Gökmen and Şenyuva, 2007). Ground food sample (1 g) was weighted into a 15 ml centrifuge tube. Carrez I and II (500 µL of each) and 9 ml of 1.2% (v/ v) of acetic acid were added. Sample was mixed vigorously for 2 min. After mixing, 1 ml of sample was centrifuged at 10,000 rpm for 10 min at 0 °C (Centrifuge 5424R Eppendorf). Supernatant was collected and diluted with Milli-Q water (1:10) before HPLC analysis.

2.2 Microwaved potato chips

Potatoes were washed, peeled and cut into the similar size strips (10 × 10 × 50 mm) prior to heating in commercial microwave. Our preliminary experiment showed that at 3 min potato chips did not form any brown color, and 5 min would burn the potato chips. Therefore, microwave process was performed at 800 W for 4 min. All samples were cooled before grinding in mini food processor and extracted as previously described.

3. Kinetic parameters

To order of reaction and the reaction rate constant (k) for the formation of acrylamide, it could be calculated from linear regression of concentration, \ln concentration and $1/\text{concentration}$ versus reaction time for zero, first and second order reaction kinetics, respectively. When linear graph was obtained, rate constant (k) was taken natural logarithm and plotted versus $1/T$ (K unit) to calculate activation energy (E_a) from Arrhenius equation ($\ln k = \ln k_0 - E_a/RT$).

4. UV-Vis spectrophotometer measurement

The UV–VIS absorption of reaction solution was measured according to previously described method (Zhou *et al.*, 2016). Appropriate dilution was made (1:50) using Milli Q water and the absorbance was measured at 294 and 420 nm using an SPECORD 210 PLUS spectrophotometer (Analytik Jena, Germany) for determining UV-absorbance of intermediate products and browning products in final stage of Maillard reaction, respectively.

5. Acrylamide determination by HPLC

Acrylamide was analyzed in triplicate following the method by Galani *et al.* (2017) with slight modifications. A HPLC system (Agilent 1200 series, Santa Clara, CA, USA) equipped with an auto sampler and a diode array detector was used. Two microliters of sample were injected by auto sampler and separated using a Zorbax 300 Extend C18 analytical column (2.1 mm \times 100 mm, 3.5 μm) (Santa Clara, California, USA). Formic acid (Sigma-Aldrich, F0507) (0.1% in water) was used as mobile phase with flow rate of 0.1 ml/min. The running time was 5 min and retention time of acrylamide was at 3.4 min. Acrylamide solution (Sigma-Aldrich, A9099) (1 mg/mL) was prepared, then a series of acrylamide concentrations (1–100 $\mu\text{g/mL}$) were prepared from the stock solution. The position of the acrylamide peak in reaction mixtures was confirmed by spiking. All test samples were diluted in Milli-Q water to be within the standard range and filtered with Nylon filter (0.45 μm) (Sigma-Aldrich Co., St. Louis, MO, USA) and transferred to a vial for chromatography analysis.

6. Preparation of polysaccharide solutions

In chemical system, sodium alginate (Sigma-Aldrich, W201502) was dispersed in Milli Q water (1 g in 100 ml) and heated at 70 °C with stirring for 30 min, then cooled down at ambient temperature. Dilutions were made to 0.1% to 0.3% (v/v) (pH = 4). Pectin from citrus peel (Sigma-Aldrich, P9135) was dispersed in Milli Q water (1 g in 100 ml) and stirred overnight at room temperature. Pectin solutions were diluted to 0.1% to 0.3% (v/v) (pH = 4). 1 g of chitosan (Sigma-Aldrich, 448869) which had molecular weight at 50–190 kDa and 75–85% deacetylated degree was solubilized in acetic acid (1% v/v), 100 ml and stirred overnight until completely dissolve. Dilutions were made to 0.1% to 0.3% (v/v) with 1% acetic acid and adjusted pH to 4.0 with 0.1 M and 1 M NaOH. In food system, 1% dilution of sodium alginate, pectin and chitosan were made using same method as describe above.

7. Statistical analysis

The data was subjected to analysis of variance (ANOVA) and least significance difference test to determine difference between means. Duncan's multiple range tests was used to compare means at a significance level of 0.05 using the SPSS software package version 24 (IBM Institute., New York, USA).

Part 2

Acrylamide mitigation using zein-polysaccharide complex particles

1. Solution preparation

1.1 Zein solution

Zein solution Zein concentrations (0.5, 1.0, 2.0, 3.0, 4.0, 5.0% weight/volume [w/ v]) were prepared by dissolving zein in 80% ethanol (100 mL) and stirring for 3 h. Zein solution (1 mL, pH 5.8) was mixed with 0.5 M glucose solution (1 mL) and 0.5 M asparagine solution (1 mL) to obtain final zein concentrations of 0.17, 0.30, 0.67, 1.00, 1.33, and 1.67% (w/ v).

1.2 Chitosan solution

Low molecular weight chitosan 1g was solubilized in acetic acid (1% v/v), 100 ml and stirred overnight to completely dissolve. Chitosan solution was diluted to 0.6% and 0.3% (v/v) with 1% acetic acid and adjusted pH to 4.0 by 0.1M and 1M NaOH.

1.3 Sodium alginate solution

Sodium alginate 1g was dispersed within Milli Q water, 100 ml and heated at 70°C with stirring for 30 min, then cooled down at ambient temperature by tap water. Dilution was made to 0.6% and 0.3% (v/v) and adjusted to pH 4.0, using 0.1M and 1M HCl.

1.4 Pectin solution

Pectin from citrus peel 1g was added into Milli Q water, 100 mL and stirred overnight. Pectin solution was diluted to 0.6% and 0.3% (v/v) with Milli Q water and adjusted pH to 4.0 by 0.1M and 1M NaOH.

2. Formation of zein–polysaccharide complex particles

Zein solution (2%) was prepared as described in section 1.1. Subsequently, the solution was mixed with chitosan, sodium alginate, and pectin in three ratios, namely 1:0.50, 1:0.30, and 1:0.15 (w/w). After vortexing for 1 min, all suspensions were placed in a Genevac-EZ 2 plus (Warminster, PA, USA.) for 2 h so that ethanol could evaporate and were then centrifuged. The temperature was maintained at 40 °C under the low-pressure mode. The complex particles in the supernatant were collected and stored at 4 °C for further analysis. The complexation method was performed using a modified protocol of a previously described method (Li *et al.*, 2018). The mixture of zein and polysaccharides (non-complex particles) was prepared by direct mixing of the zein solution with the polysaccharide solution in three ratios (as previously described) and vortexing for 1 min.

3. Acrylamide inhibition in a chemical model

The reaction in the chemical model was performed according to the method reported by (Gökmen and Şenyuva, 2007). The reaction mixture contained 0.5 M glucose solution (1 mL), 0.5 M asparagine solution (1 mL), and acrylamide inhibitors (1 mL) in a tube with a screw cap. Acrylamide inhibitor contained zein solutions (0.17, 0.30, 0.67, 1.33, 1.67% w/v), zein–polysaccharide complex particle solutions (1:0.15, 1:0.3, 1:0.50), and zein–polysaccharide non-complex particles (1:0.15, 1:0.3, 1:0.50). All samples were heated at 170 °C for 30 min in a heating block (VWR Analog Heat Block; VWR, Radnor, PA, USA). The temperature fluctuation was maintained within ± 2 °C. The heated samples were immediately cooled in an ice bath for 5 min.

4. Acrylamide inhibition in a food model

Potatoes were washed, peeled, and cut into strips (1 cm × 1 cm × 5 cm). These strips (50 g) were soaked in 50 mL of zein solution (2.0% w/v), zein–chitosan (1:0.50), zein–alginate (1:0.50), or zein–pectin (1:0.50) complex particle solutions for 30 min, drained for 2 min, and fried at 170 °C for 3 min using a deep fat fryer (Cookworks™, Milton Keynes, UK). A sample not containing protein–polysaccharide was used as control. After frying, all samples were cooled down and drained using a sieve. The process was performed using the modified method described by Zeng *et al.* (2010) with minor modification. Acrylamide inhibition (%) was calculated using the equation mentioned below.

$$\% \text{ Acrylamide inhibition} = \frac{\text{Acrylamide content control} - \text{Acrylamide content sample}}{\text{Acrylamide content control}} \times 100$$

5. Acrylamide determination

5.1 Preparation of acrylamide standard curve

The stock solution of acrylamide standard (1 mg/mL) was prepared and diluted to a series of concentrations (1–100 µg/mL). A calibration curve was constructed using the peak area of acrylamide eluted from the column against the concentration. Acrylamide concentration was calculated based on the solution concentration and the injection volume. In case an unidentified peak was suspected to be acrylamide, the sample was spiked with acrylamide standard for confirmation. The acrylamide standard equation obtained was as follows: $y = 63.223x + 36.509$, $R^2 = 0.9991$ (Figure 1 appendix).

5.2 Determination of acrylamide in a chemical model

After heating, all sample solutions were diluted (1:10) with Milli-Q water, filtered using a nylon filter (0.45 µm), and transferred to a vial for chromatographic analysis. Acrylamide was analyzed in triplicate using a slightly modified protocol of the method described by Galani *et al.* (2017). Using an auto sampler, sample solution

(2 μ L) was injected in the high-performance liquid chromatography (HPLC) device equipped with a diode array detector and a Zorbax 300 extend-C18 analytical column (2.1 \times 100 mm, 3.5 μ m) (1200 Series system, Agilent, Santa Clara, CA, USA). Formic acid solution (0.1% in water) was used as a mobile phase at a flow rate of 0.1 mL/min, running time of 5 min, and retention time of 3.4 min (for acrylamide). The chromatogram of acrylamide was recorded at 210 nm.

5.3 Determination of acrylamide in a food model

Grounded sample (1 g) was placed in a centrifuge tube. Carrez I, II (500 μ L each) and 1.2% acetic acid (9 mL) were added, and the solution was mixed vigorously for 2 min. Carrez I was prepared by dissolving zinc acetate dihydrate (21.9 g) with acetic acid (3.0 g) in Milli-Q water and adjusting the volume to 100 mL. Carrez II was prepared by dissolving potassium hexacyanoferrate (II) trihydrate (10.6 g) in Milli-Q water and adjusting the volume to 100 mL. After mixing, sample (1 mL) was transferred to an Eppendorf tube using a 1 mL syringe. Centrifugation (Centrifuge 5424R; Eppendorf, Hamburg, Germany) was performed at 10,000 rpm for 10 min at 0 $^{\circ}$ C. The supernatant was collected and diluted (1:10) with Milli-Q water prior to HPLC analysis. Acrylamide extraction was performed using a modified protocol of the method described by Gökmen and Şenyuva (2007).

6. Characterization of zein–polysaccharide complex particles

6.1 Particle size and charge measurement

Measurement of particle size distribution of a suspension with relatively small particles was conducted using Dynamic Light Scattering (Malvern Nanoseries Instruments, Worcestershire, UK). Samples were diluted with Milli-Q water (1:20) prior to analysis. The Z-average diameter and polydispersity index (PDI) were calculated from the measured distributions. The zeta potential of the particles in the suspensions was determined using an Electrophoretic Light Scattering device (Malvern

Nanoseries Instruments). Samples were diluted with pH adjusted water (pH 4.0) prior to measurement to avoid multiple scattering effects.

6.2 Confocal laser scanning microscopy

CLSM was carried out by LSM900 with Airyscan2 (Carl Zeiss, Oberkochen, Germany). Protein-polysaccharide particles were dyed with blended fluorescent colorant solution. Chitosan, pectin, sodium alginate and zein were colored Rhodamine B (RhB), Ruthenium red (RR), Fluorescein (FitC) and Acridine orange (AO), respectively. The dyed particles were placed on slide and lidded by a coverslip before visualized at least 3 hours to prevent particles mobility. Microscopic images were obtained by selectively excitation/ emission at 271/520, 493/517, 495/519 and 543/565 nm for AO, RR, FitC and RhB, respectively.

7. Statistical analysis

The data were analyzed using analysis of variance and the least significance difference test to determine differences between means (significance level: 0.05) using the SPSS software package version 16 (IBM company, Chicago, IL, USA.). All experiments and measurements were performed in triplicate.

Part 3

Granular Cold-Water Swelling-Octenyl Succinic Anhydride Starch to Stabilize Pickering Emulsion and Use as a Template for Oleogelation

1. Rice starch extraction

The milled rice grains (high amylose and waxy rice) were soaked in water at ratio 1:3 for 4 h, ground with a super mass colloidizer (Aerosia Interpac Co., Ltd, Thailand), and centrifuged by basket centrifuge (Wasino Co., Ltd., Thailand). The rice cake was dried at 40°C until moisture content was 10-12%, milled by rotor mill (Hosokawa Micron Corp, Japan), sieved through a 100 mesh (Gilson company Inc, WI., USA.), and kept in a freezer (-18°C).

Rice starch was extracted by dispersing rice flour (100 g) in 5% NaCl (400 mL), stirring with an overhead stirrer for 2 h, and centrifuging at 1520 g (Hettich, Germany) for 15 min. A volume of 95% ethanol (400 mL) was added to the precipitate, and this was stirred for 2h, and centrifuged at 1520 g for 15 min. The precipitate was washed with 0.1 M NaOH under continuous stirring for 15 h, and left to settle for 10 h. The precipitate was washed twice with distilled water, centrifuged at 1520 g for 15 min, and neutralized with 1M HCl. The collected precipitate was centrifuged and dried at 50°C for 2 h. The protein content of rice starch, which was determined by the Kjeldahl method, was 0.15-0.21 %.

2. Granular cold-water swelling starch preparation

Granular cold-water swelling starch (GCWS) was prepared using the alcoholic-alkaline method (Chen and Jane, 1994). Native waxy rice starch (10 g) was suspended in absolute ethanol (70 g) and mixed under water bath until the temperature reached 35°C. Then 3M NaOH (20 g) was slowly added, followed by 80 % ethanol (10 g): this was stirred for 15 min, and filtered using a Büchner filter. The collected starch was mixed with 80% ethanol (10 g), stirred for 10 min, and neutralized with 3M HCl in

absolute ethanol. The starch was rinsed with 95% ethanol, dehydrated with absolute ethanol, and air dried overnight. The starch was sieved on a 100 mesh (149 μm) and stored in a tight plastic bag at room temperature.

3. OSA modification

Starch (100 g) was dispersed in distilled water (200 mL), and the pH was adjusted to 7.4-7.8 using 1M NaOH. Subsequently, 4 portions of 3 % OSA (Trigon Chemie, Germany) were added to the starch suspension at 15 min intervals. OSA starches containing not more than 3% of octenylsuccinyl groups are allowed to use as food additives according to the Commission Regulation (EU) No 1130/2011, E-number 1450. FDA and agencies in many countries have permitted OSA starch in foods at a level of 3%. Automatic titration with 1M NaOH was used to maintain a pH close to 7.6, while stirring. The titration step was terminated once the pH was stable for at least 15 min. The suspension was then centrifuged at 1520 g for 10 min and the supernatant was discarded. The precipitated starch was washed twice with distilled water, washed again with citric acid solution (pH 4.5-5), and distilled water. The starch was dried at 50°C for 2h. The samples prepared in this way were termed: high amylose starch-OSA (HS-OSA), waxy starch-OSA (WS-OSA), and granular cold water swelling starch-OSA (GCWS-OSA) (Saari *et al.*, 2019).

4. Starch particle characterization

4.1 Degree of substitution

The degree of substitution was measured following the method of (Song *et al.*, 2006). Starch samples (2.5g, db) were wetted with a few drops of ethanol prior to the addition of 0.1M HCl (25 mL), stirred for 30 min, and centrifuged at 4000 rpm for 10 min. The precipitate was washed with 95% ethanol (25 mL), and washed twice with distilled water. The precipitate was dispersed in distilled water (150 mL) and heated in a water bath at 90°C for 10 min. The solution was rapidly cooled to 25°C using an ice bath, and the suspension was titrated while stirring with 0.1M NaOH until it reached

pH 8.3. The volume of NaOH used was recorded to calculate the degree of substitution (DS) as:

$$DS = \frac{0.162 \cdot A \cdot M/W}{1 - (0.210 \cdot A \cdot M/W)} \quad \text{Eq (1)}$$

Where A is the titration volume of NaOH, M is the molarity of the NaOH solution, and W is the dry weight of starch

4.2 Particle size distribution of the starch

Starch (0.1g) was suspended in water (10 mL). The particle size distribution and zeta potential of this starch suspension were determined using a Mastersizer 2000 (Malvern Instruments Ltd., Worcestershire, UK) and a Zetasizer Nano ZS (Malvern Instruments, UK), respectively. The refractive index (RI) of starch and water were taken as 1.54 and 1.33, respectively (Saari *et al.*, 2019). All measurements were performed at least in triplicate at 20 °C.

4.3 Contact angle in the oil-water interface

The three-phase contact angle (θ) of starch samples was measured using a sessile drop method (OCA25, Dataphysics Instrument, Germany) (Yan *et al.*, 2019). Starch powder was pressed into a thin tablet (13 mm diameter, 2 mm thickness) and was submerged in an oil bath of the OCA25 platform. Deionized water (2 μ L) was dropped onto the tablet surface using a syringe. The water droplet shape was captured by a high-speed camera, and the contact angle was calculated using the LaPlace-Young equation by the OCA25 software.

5. Emulsion preparation and characterization

HS-OSA, WS-OSA, and GCWS-OSA suspensions were prepared at a concentration of 200 mg/mL(oil). A coarse O/W emulsion was prepared using 60 %

medium-chain triglyceride (MCT) oil, by mixing with a high-speed homogenizer (IKA Ultra-Turrax T25 homogenizer, Wiggins, Germany) at 13500 rpm, for 2 min. The coarse emulsion was then passed through a high-pressure homogenizer (HU-3.0, Delta Instruments lab homogenizer, Taipei, Taiwan) at 100 bar for 10 passes. Sodium azide (0.02 %) was added as a preservative. These emulsions were characterized as followings:

5.1 Droplet size distribution

The droplet size distribution was determined using a Mastersizer 2000 (Malvern Instruments Ltd., Worcestershire, UK). The refractive index (RI) of MCT oil was taken as 1.46.

5.2 Microstructure

The emulsions were visualized using light microscopy (ZeissAxioskop 2 plus, Jena, Germany) at 40 x magnification and confocal laser scanning microscopy (Zeiss 510, Jena, Germany). The samples were dyed with 1 mg/mL Nile Red (CAS No. 7385-67-3, Sigma-Aldrich, St. Louis, MO) dissolved in isopropyl alcohol, and 1 mg/mL Nile Blue (CAS No. 3625-57-8, Sigma-Aldrich, St. Louis, MO) dissolved in MilliQ water, for straining the oil phase and starch granules, respectively. The fluorescent dyes were excited by an argon laser at 488 nm for Nile blue and a helium neon (He/Ne) laser at 633 nm for Nile red (Ge *et al.*, 2017).

5.3 Rheological properties

Rheological properties of the emulsions were investigated using a stress-controlled rheometer (MCR302, Anton Paar, Graz, Austria) with a 50 mm diameter stainless-steel parallel plate geometry, and 1 mm gap size. Emulsions (2 mL) were placed on the lower plate that was fixed on a Peltier element for 15 min at $20\pm 0.1^\circ\text{C}$ before analysis. The method was slightly modified from Precha-Atsawan *et al.* (2018). All samples were measured in triplicate.

5.3.1 Small amplitude oscillatory shear (SAOS)

The linear viscoelastic (LVE) properties were determined using SAOS measurements. Frequency sweep tests were applied with angular frequency (ω) ranging from 0.1-150 rad/s, at a constant shear strain of 1.0 %. This was followed by an amplitude sweep test to determine the extent of the LVE region, using shear strains (γ) ranging from 0.01 to 100 % (ramp logarithmic mode), at a constant angular frequency (ω) at 1 rad/s, at 20°C.

5.3.2 Large amplitude oscillatory shear (LAOS)

The nonlinear viscoelastic properties were determined using LAOS measurements. Amplitude sweep tests were applied with strains ranging from 0.01-100 %, at constant angular frequency (ω) of 1 rad/s, at 20 °C. The intra-cycle nonlinear stress response of the emulsions was evaluated by Lissajous plots. The intra-cycle behavior was quantified by calculating the strain stiffening factor (S) and shear thickening factor (T), as defined in Eq (2) and Eq (3) (Ewoldt *et al.*, 2008).

$$S = \frac{G'_L - G'_M}{G'_L} \quad (2)$$

$$T = \frac{\eta'_L - \eta'_M}{\eta'_L} \quad (3)$$

Here, G'_L is the elastic modulus at maximum intra-cycle strain, G'_M is the elastic modulus at minimum strain (the slope of the Lissajous plot at zero strain), η'_L is the viscosity at maximum shear rate, and η'_M is the viscosity at minimum shear rate

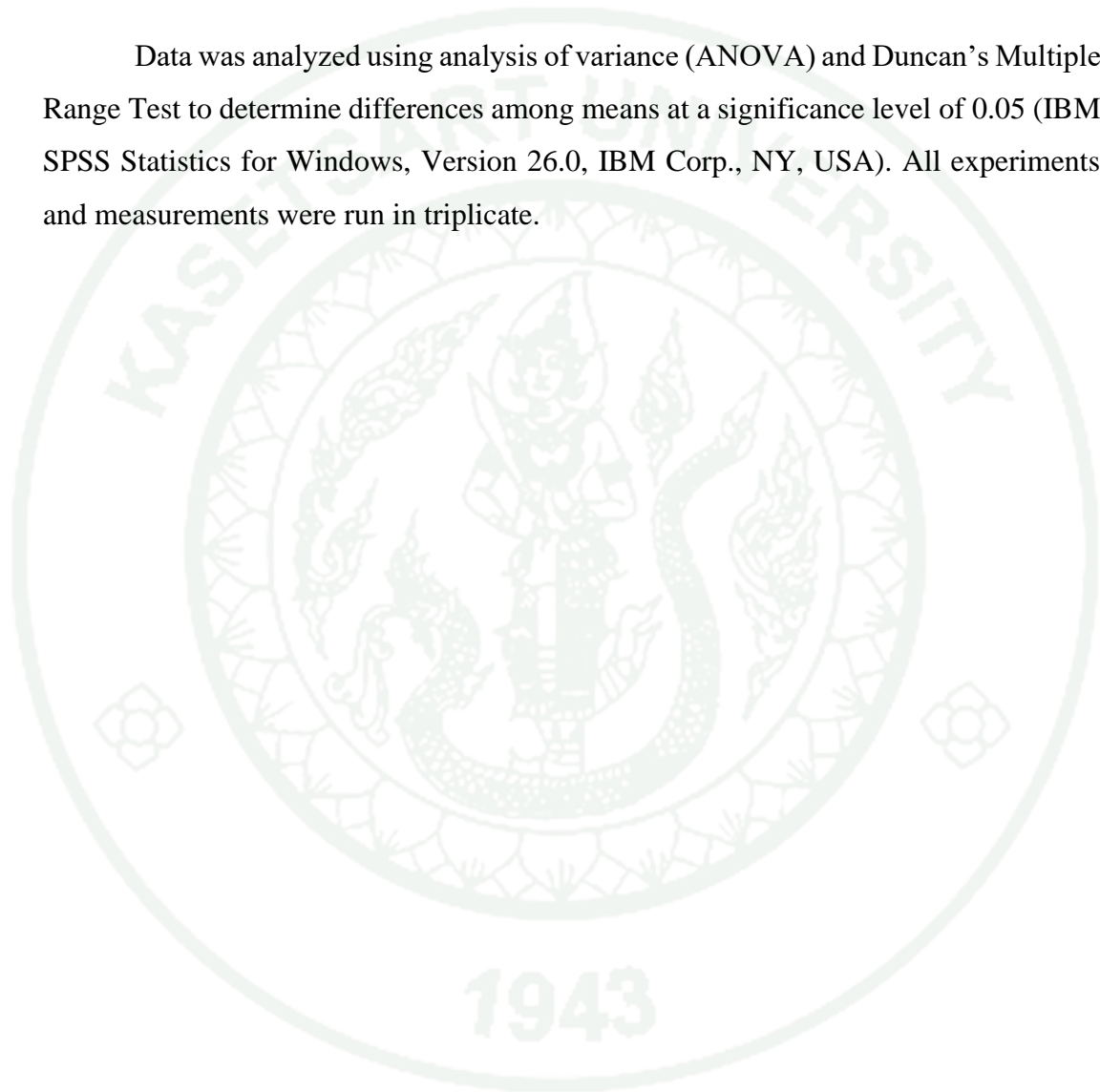
6. Oleogel formation and characterization

Oleogels were prepared using Pickering emulsions as a template, which were lyophilized using Freeze dryer (Salmenkipp, Breukelen, Netherlands) for 72h. The rheological properties of the oleogels were again measured using a stress-controlled

rheometer (MCR302, Anton Paar, Graz, Austria) using the same protocol as described in section 5.3.

7. Statistic analysis

Data was analyzed using analysis of variance (ANOVA) and Duncan's Multiple Range Test to determine differences among means at a significance level of 0.05 (IBM SPSS Statistics for Windows, Version 26.0, IBM Corp., NY, USA). All experiments and measurements were run in triplicate.



Part 4

Oleogel from Granular Cold Water Swelling-OSA with Polysaccharides and Its Application as Fat Mimetic

1. Granular cold-water soluble starch

Alcoholic-alkaline method was selected to prepare granular cold water swelling starch (GCWS) using method of Chen and Jane (1994). Native waxy rice starch (10 g) was suspended in absolute ethanol (70 g) at 35°C. The suspension was added with 3M NaOH (20g) and 80% ethanol (10 mL), stirred for 15 min, and filtered using a Büchner filter. The collected starch was added with 80 % ethanol (10 mL), stirred for 10 min, and adjusted pH to neutral with 3M HCl in absolute ethanol. The starch was washed with 95% ethanol, dehydrated with absolute ethanol, and air dried overnight. The starch was sieved into 100 mesh and stored in a tight plastic bag at room temperature.

2. OSA modification

Firstly, Starch (100 g) was dissolved in distilled water (200 mL), and adjusted pH to 7.4-7.8 using 1M NaOH. Then, OSA (Trigon Chemie, Schlüchtern, Germany) (3%, w/w of starch) was added into starch suspension as 4 portions, at 15 min interval. The pH was retained at pH closed to 7.6 using 1M NaOH with constant stirring until the pH was stable for at least 15 min. The suspension was centrifuged at 4000 rpm for 10 min and the supernatant was discarded. The precipitated starch was washed with distilled water, citric acid solution (pH 4.5-5), and distilled water for two times, and dried at 50°C for 2h (Saari *et al.*, 2019). The samples prepared in this way were labeled as high amylose starch-OSA (HS-OSA), waxy starch-OSA (WS-OSA), and granular cold water swelling starch-OSA (GCWS-OSA).

3. Pickering emulsion and oleogel formation

Pickering emulsion was prepared by dissolving HS-OSA, WS-OSA, and GCWS-OSA in water (200 mg/mL), mixed with medium chain triglyceride (MCT) oil at ratio 40:60, and homogenized using high-speed homogenizer (IKA Ultra-Turrax T25 homogenizer, Wiggins, Germany) at 13500 rpm for 2 min. The solution was then passed through a high-pressure homogenizer (HU 3.0, Delta Instruments lab homogenizer, Taipei, Taiwan) at 100 bar for 10 passes. Sodium azide (0.02 %) was added as a preservative. Pickering emulsion with polysaccharides was prepared by mixing HS-OSA, WS-OSA, and GCWS-OSA with 1% polysaccharide solution (200 mg/mL) and MCT oil at ratio 40:60. The solution was then pass through an emulsification process as ever mentioned. The polysaccharides used were pectin (CAS no 9000-69-5, galacturonic acid $\geq 74.0\%$), gum arabic (CAS no 9000-01-5), and xanthan gum (CAS no 11138-66-2). The Pickering emulsion was then lyophilized to obtain the OSA starch based oleogel which was stable at room temperature.

4. Degree of substitution

The degree of substitution was measured followed the method of Song *et al.* (2006). Starch sample (2.5 g, db) was added with a few drops of ethanol prior to the addition of 0.1M HCl (25 mL), stirred for 30 min, and centrifuged (4000 rpm) for 10 min. The precipitate was rinsed with 95% ethanol (25 mL) and washed twice with distilled water. The precipitate was dispersed in distilled water (150 mL) and heated in a water bath at 90°C for 10 min. The solution was rapidly cooled in an ice bath until 25°C, and the suspension was titrated while stirring with 0.1M NaOH until reached pH 8.3. The volume of NaOH was recorded to calculate the degree of substitution (DS) as in Eq (1):

5. Droplet size distribution

The emulsions were characterized for droplet size distribution using a Mastersizer 2000 (Malvern Instruments Ltd., Worcestershire, UK). The refractive index (RI) of MCT oil was 1.46 and starch was 1.43.

6. Rheological properties

The rheological measurement of both emulsion and oleogel was performed using Anton Paar Rheometer MCR302 (Anton Paar, Graz, Austria) with a 50 mm diameter stainless-steel parallel plate geometry, and 1 mm gap size. Emulsion sample (2 mL) was placed on the lower plate fixed on a Peltier element but oleogel sample (6 g) was directly put on plate. After positioning in the upper plate, the emulsion and oleogel were rested for 15 min at $20\pm 0.1^\circ\text{C}$ before analysis (Precha-Atsawan *et al.*, 2018). All samples were measured in triplicate.

6.1 Small amplitude oscillatory shear (SAOS)

Linear viscoelastic regime of emulsion and oleogel were determined using SAOS measurements. Frequency sweep tests were applied with angular frequency (ω) ranging from 0.1-100 rad/s, at a constant shear strain at 1.0 %. The amplitude sweep test was applied to determine the extent of the linear viscoelastic (LVE) regime at a shear strain (γ) range from 0.01 to 100% for emulsion and 0.001 to 100% for oleogel, using a ramp logarithmic mode with constant angular frequency (ω) at 1 rad/s at 20°C .

6.2 Large amplitude oscillatory shear (LAOS)

LAOS was used to perform viscoelastic properties in nonlinear regime. An amplitude sweep test was set from 0.1-100% for emulsion and 0.001-100% for oleogel with constant angular frequency (ω) at 1 rad/s at 20°C . The response viscoelasticity was analyzed by Lissajous plots. The intra-cycle strain stiffening behavior (S factor) and intra-cycle shear thickening behavior (T factor) were defined in Eq (2) and (3) (Ewoldt *et al.*, 2008).

7. Application of oleogel as fat mimetic in food model

An emulsion sausage was prepared followed the modified method of Pereira *et al.* (2019). The ingredients used were pork sirloin (65.2%), lard (16.3%), ice (16.3%),

salt (1.2%), sodium triphosphate (0.3%), tapioca flour (0.3%), sugar (0.2%), and pepper (0.2%). All ingredients were mixed in a commercial food processor and the temperature during mixing was kept at below 8°C. The meat emulsion was casing, cooked in water bath at 80°C for 30 min, and stored at 4°C. All OSA starch based oleogels with/without polysaccharide were substituted with lard at 75%.

8. Texture analysis

Texture profile analysis (TPA) was performed using texture analyzer TA-TX Plus (Stable Micro Systems Ltd., Godalming Surrey, UK), with load cell 50 kg (Pereira *et al.*, 2019). Cooked sausage was cut precisely (diameter 20 mm, thickness 15 mm) and measure for hardness, springiness, cohesiveness, and chewiness. The measurement was done in five replications.

9. Statistic analysis

The data was determined using analysis of variance (ANOVA) and Duncan multiple range test to find the difference between means at a significance level of 0.05 using SPSS software package version 26 (IBM company, Chicago, Illinois, USA.). All experiments and measurements were run in triplicate.

RESULTS AND DISCUSSION

Part 1

Inhibitory effect of polysaccharides on acrylamide formation in chemical and food model systems

1. Inhibitory effect of polysaccharides on acrylamide formation in chemical model

1.1 Acrylamide formation in a chemical model system

Conventional heating in a heating block resulted in acrylamide formation under all temperature conditions, with the highest levels recorded at 180 °C after 60 min of heating (27.88 µg/mL) (Figure 2). There was a marked increase in the rate of formation after 40 min of heating at 180°C. Gökmen and Şenyuva (2007) reported that high levels of acrylamide were generated at elevated heating temperature (180°C) and heating time (10 min), and decreased slightly after 10min until 60min, likely due to degradation of acrylamide into other compounds. This decrease was not observed in this study.

When the same reaction mixtures were subjected to microwave heating at a power of 800W, the results also showed an increase in acrylamide with increased temperature and time (Figure 2). There was a similar pattern of acrylamide formation between conventional and microwave heating, however it must be noted that the timescale in the microwave experiment is in seconds, while the timescale in the conventional heating system is in minutes. It is important to note that the microwave reactor is designed to prevent hotspots, and therefore we are confident that acrylamide formation was uniform in the solution. Microwaves cause fast temperature rises in the solvent due to their capacity to generate heat energy inside the system, without requiring any medium as vehicle for heat transfer. A low thermal conductivity product may quickly reach high temperatures (Campañone and Zaritzky, 2005). Moreover, microwaves cause molecular friction in alternating electrical and magnetic fields,

resulting in dipolar rotation of polar molecule (such as water) and rapid heat generation (Campañone and Zaritzky, 2005; Mudgett, 1989; Orzáez Villanueva *et al.*, 2000).

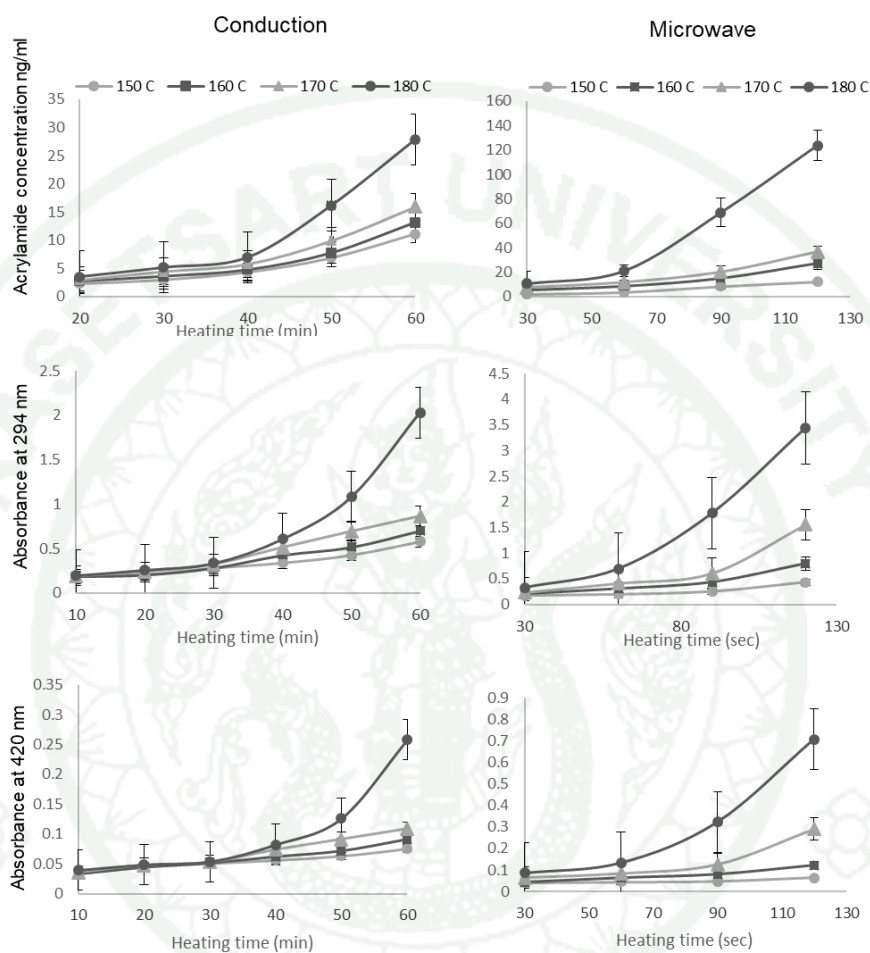


Figure 2 AA formation in the chemical model during heating mainly by conduction in a heating block (conventional) and microwave at various temperatures. The absorbance of the solutions was measured at 294 and 420 nm.

The formation of Maillard reaction intermediates was monitored with UV–Vis spectrometry at 294 nm and 420 nm (Figure 2). Absorbance values at 294 nm increased steadily with time at 150, 160 and 170°C, with a much steeper increase in absorbance values at 180°C after 40 min. These values correlate with acrylamide content in those conditions. Much smaller changes in absorbance values at 420 nm were

observed, suggesting that 294 nm is a better wavelength to monitor the reaction. Microwave heating showed similar patterns of absorbance change.

1.2 Kinetic parameters

Acrylamide concentrations formed at different time-temperature combinations were used to calculate the kinetic parameters. The concentration of acrylamide formed at various heating temperature was linear regressed against reaction time and indicated that the reaction followed a second-order reaction. This means that the reaction rate depends on the square of the concentration of one or more reactants. This is consistent with previous observations by BeMiller (2019b), but contrasts with the results from Gökmen and Şenyuva (2006). They used a fructose-asparagine mixture to study acrylamide formation at 120-200°C. Their results show that the reaction followed zero order and first order with respect to asparagine and fructose, respectively. As the concentration of asparagine increased, the rate of reaction remained constant. Activation energy (E_a) was calculated using the Arrhenius equation from rate constants at each temperature (Table 3). The apparent activation energy (E_a) was 17.85 ($r^2 = 0.884$) and 110.78 ($r^2 = 0.829$) kJ/mol for conventional and microwave, respectively. This indicates that a higher E_a is needed in the microwave heating conditions, but once activation energy is reached, the reaction progresses rapidly.

Table 3 Kinetic parameters of acrylamide formation in the chemical model under different heating conditions.

T °C	Conduction heating		Microwave heating	
	k (s ⁻¹)	R ²	k (s ⁻¹)	R ²
150	0.0302	0.9882	0.0204	0.92822
160	0.0385	0.9740	0.0180	0.9966
170	0.0421	0.9881	0.0176	0.9961
180	0.0529	0.9688	0.0151	0.9512

1.3 Inhibitory effect of polysaccharides on acrylamide formation

The inhibitory effect of sodium alginate, pectin and chitosan on acrylamide formation were investigated. Figure 3 shows that sodium alginate and pectin at 0.3% and 0.2% w/v reduced acrylamide formation significantly in both conventional and microwave heating conditions compared to control. At a concentration of 0.3% w/v, alginate and pectin reduced acrylamide formation by 64.9% and 55.9% respectively in conventional, and 35.9% and 30% respectively in microwave. Zeng *et al.* (2010) showed similar results with inhibitions >50% for pectin and alginic acid in conventional heating conditions, but with much higher solution concentration (2% w/w). However, very low concentration of alginate and pectin (0.1% w/v) did not show as good inhibition effect as higher concentration (0.2 - 0.3% w/v). The mechanisms behind sodium alginate inhibited acrylamide formation have been studied by previous studies. Gökmen and Şenyuva (2007) found that Na⁺ almost halved the acrylamide formation, because the cations prevented the formation of key intermediates. Lindsay and Jang (2005) also suggested that ionic associations involving the ions and charged groups on asparagine and related intermediates were likely to be involved. Pectin effectively inhibited acrylamide by lowering the pH without contributing to the reducing sugars content, and higher concentration of pectin (up to 5%) was found to be more efficient in inhibiting acrylamide formation (Passos *et al.*, 2018). Beside the ionic and pH effects, the presence of long polysaccharide chains is likely to prevent substrates coming together and slow down the motion of molecules in the chemical model system.

Chitosan did not inhibit acrylamide formation to the same extent as alginate and pectin. Only the highest concentration (0.3%) used slightly reduced (9.46%) acrylamide formation (Figure 3). Sung *et al.* (2018) found 1% chitosan reduced acrylamide formation by 46.8% and proposed that the amino groups of chitosan could compete with asparagine and react with the carbonyl groups of glucose in order to inhibit the formation of Maillard reaction products and acrylamide. Sansano *et al.* (2017) found that adding 0.5% of chitosan led to an inhibition of acrylamide formation by 52%, while 1% of chitosan could inhibit for 75% at 180 °C.

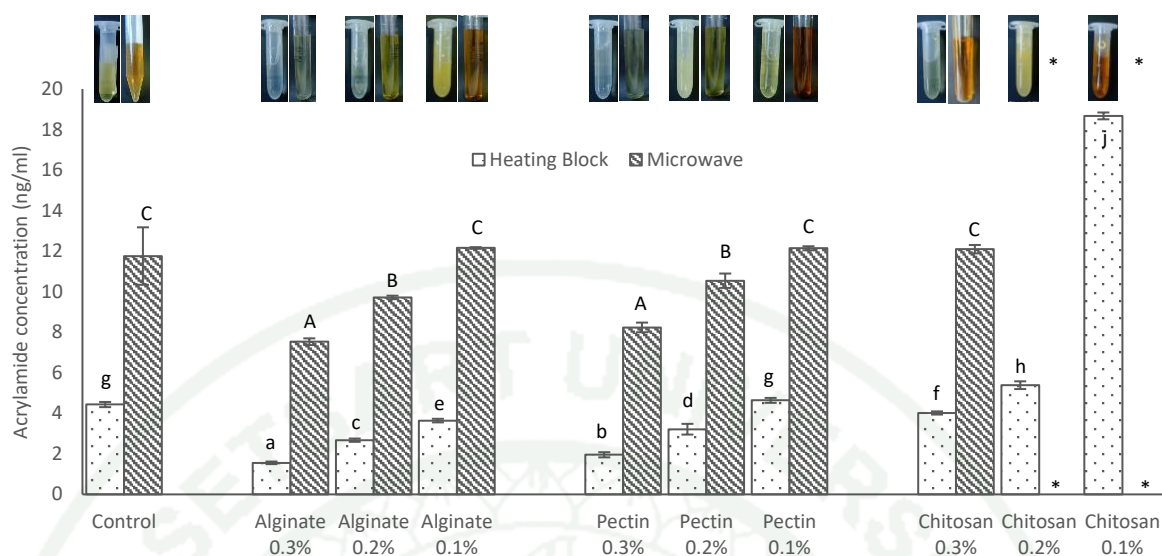


Figure 3 Acrylamide formation in conventional heating and microwave in the chemical model in the presence of various inhibitors. The conventional heating was carried out at 170 °C for 30 min. The microwave reaction was carried out at 800W microwave power for 60s. Data values are means \pm SD (n = 3).

Note: Different lowercase letters indicate significant difference at the 5% level for conventional heating, and uppercase letters for microwave.

*Samples containing low concentration of chitosan (0.2 and 0.1% w/v) carbonized in the microwave, hence acrylamide content could not be determined.

On the other hand, Figure 3 shows that low concentration (0.2 and 0.1% w/v) of chitosan promoted acrylamide formation in conventional heating, with 0.1 % chitosan increasing acrylamide by almost five-fold compared to control. Samples containing low concentration of chitosan (0.2 and 0.1% w/v) carbonized in the microwave, hence acrylamide content could not be determined, but suggesting the reaction was taking place at a very high speed. Therefore, the concentration of chitosan is a critical factor to determine whether it inhibits or promotes acrylamide formation. Previous studies also suggested that different properties of chitosan would significantly influence its potential to inhibit acrylamide formation, including molecular weight (Mw) (Chang *et al.*, 2016) and deacetylation degree (DD) (Sansano *et al.*, 2017; Tsai *et al.*, 2002). The chitosan used in this study had relatively low Mw (50-190 kDa) and

high DD (75-85%), both of these properties have been shown to be associated with lower acrylamide formation (Chang *et al.*, 2016; Sansano *et al.*, 2017). However, our study also shows chitosan concentration is critical to the inhibition effect.

2. Inhibitory effect of polysaccharides on acrylamide formation in a food model

To investigate the effect of polysaccharide inhibitors on acrylamide formation in a food model, potato chips were deep-fried or microwaved after dipping in polysaccharide solutions. Figure 4 shows the relative percentage of acrylamide in fried and microwave potatoes. Dipping in alginate, pectin and chitosan dramatically reduced acrylamide formation during frying by 53.5%, 51.2% and 40.9% respectively compared to control frying. Microwave cooking potato chips showed about a third less acrylamide formation compared to frying, and this was associated with less browning at the surface. It must be noted that the crips were cooked in a domestic microwave, not the microwave reactor used in the food model. Domestic microwaves have less homogeneous wave distribution, and it is therefore possible that hotspots were created within the potato chip. However, our replicate analysis shows good reproducibility between samples, indicating homogenous acrylamide formation. However for microwave cooking, only alginate and pectin significantly reduced acrylamide formation and only by 5.2% for both polysaccharides. Previous studies on the effect of microwave cooking on acrylamide formation have been contradictory (Michalak *et al.*, 2020). Some studies reported that microwave heating provides a favorable medium for the occurrence of acrylamide and promote the acrylamide formation (Michalak *et al.*, 2017; Yuan *et al.*, 2007; Zhang *et al.*, 2008), but other studies showed no acrylamide formation under microwave heating (Anese *et al.*, 2013; Barutcu *et al.*, 2009). Others suggest that microwave heating prior to frying may help to reduce acrylamide formation (Belgin Erdoğan *et al.*, 2007). The differences might be due to variations in microwave parameters such as power or heating time, as well as the chemical composition and water activity levels (Michalak *et al.*, 2020).

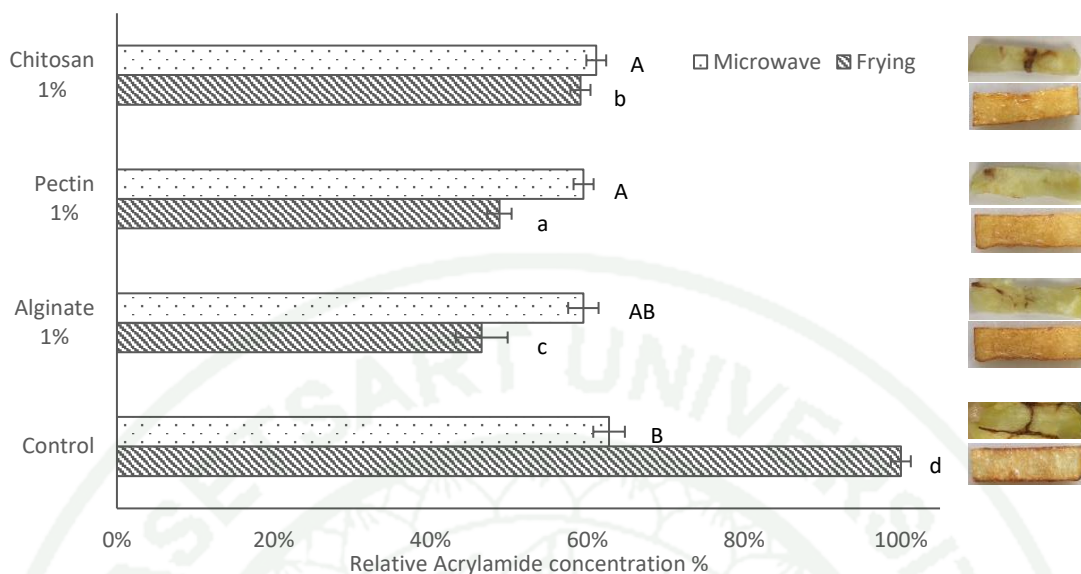
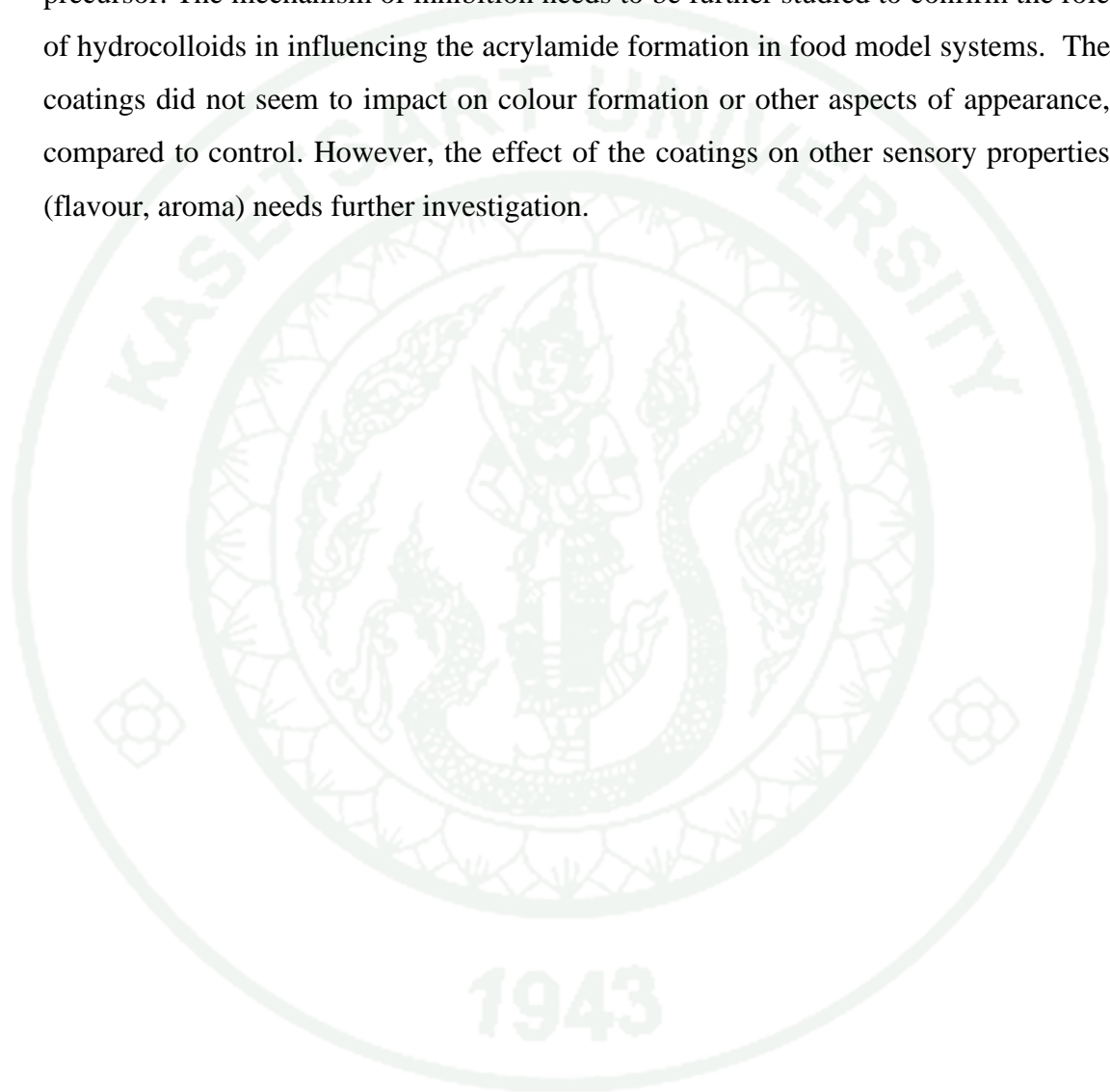


Figure 4 Acrylamide formation in the food model in the presence of various inhibitors relative to control (frying with no inhibitors). The microwave cooking was carried out at 800W power for 4 min. Frying was carried out at 170°C for 3min. Data values are means \pm SD (n = 3).

Note: Different lowercase letters indicate significant difference at 95% confidence level for frying, uppercase letters for microwave compared to the control.

Zeng *et al.* (2010) showed slightly different pattern for alginate and pectin in their food model compare to the current study. They found that 1% w/w alginic acid only lead to about 20% reduction of acrylamide, 1% pectin caused slightly elevated acrylamide contents and only efficiently inhibited acrylamide after 5h immersion (Zeng *et al.*, 2010). They suggest that duration of immersion played a predominant role in determining the final effect of the treatment (Zeng *et al.*, 2010). Sansano *et al.* (2016) found low concentration of chitosan (0.27% w/v) mitigated acrylamide formation by around 60% in batter system for frying, but did not inhibit when concentration increased to 0.54% w/v. Our results shows all three polysaccharides at 1% w/w efficiently reduced acrylamide formation, with alginate giving the best result followed by pectin and chitosan. Gaonkar (1991) explained that immersion of hydrocolloid solution would lower the food surface tension and thus facilitate the formation of a layer of coating on

the surface of the food products. Mousa (2018) confirmed that a rigid thermal gelation network formed during frying and prevent interaction between acrylamide precursors. Zeng *et al.* (2010) and Suyatma *et al.* (2015) also explained that pectin coating reduces heat penetration from the oil to the food during frying and interact with acrylamide precursor. The mechanism of inhibition needs to be further studied to confirm the role of hydrocolloids in influencing the acrylamide formation in food model systems. The coatings did not seem to impact on colour formation or other aspects of appearance, compared to control. However, the effect of the coatings on other sensory properties (flavour, aroma) needs further investigation.



Part 2

Acrylamide mitigation using zein–polysaccharide complex particles

1. Effect of zein on acrylamide inhibition

The inhibitory effect of zein on acrylamide was exerted in a dose- and temperature-dependent manner. The lowest and highest concentrations of zein which resulted in a substantial reduction of acrylamide formation were 0.17% (w/v) and 0.67% (w/v), respectively (Figure 5A). Zein contains hydrophobic amino acids, such as proline, glutamine, and asparagine (Elzoghby *et al.*, 2012). The acrylamide content was indicated by brown color formed after heating (Figure 5B). It has also been reported that acrylamide is generated from the Maillard reaction during heat treatment of amino acids and reducing sugar (Mottram *et al.*, 2002). However, the use of high concentrations of zein (>1%, w/v) exerted the opposite effect, resulting in higher acrylamide formation (6A). Glutamine (17.9–19.5%) and asparagine (4.6–5.2%) are the major amino acids found in zein (Gasteiger *et al.*, 2005). High amounts of these amino acids increased acrylamide formation. Reaction of glutamine with equimolar amounts of glucose at 180 °C was found to rapidly increase acrylamide formation (Stadler *et al.*, 2002) as the structure of glutamine is similar to that of asparagine (Claeys *et al.*, 2005) (Figure 5C). The addition of glutamine promoted acrylamide formation kinetics which studied in an asparagine-glucose model system (0.01 M, pH 6.0), and the solution was heated to 140°C–200 °C (Claeys *et al.*, 2005). However, reduction in acrylamide formation was reported after adding a small amount of glutamine (35 mM) in a food model (homogenized potato) and heating the solution in an oven at 180 °C for 25 min. Glutamine and glycine caused the highest reduction in the formation of acrylamide (76%), followed by lysine (43%), and alanine (14%) (Rydberg *et al.*, 2003).

Moreover, it has been reported that environmental factors, especially the pH, also affect acrylamide mitigation (Rydberg *et al.*, 2003). At pH 8.0, the α -amino group of asparagine exhibited a low pKa (8.9 at 25 °C), limiting its ability to protonate

compared with other amino acids. Therefore, it is more likely that asparagine reacts with the aldehyde groups of carbohydrates, resulting in the formation of Schiff base, which is the initial step in the process of acrylamide formation. The pH of the zein solution used in our study was 5.3–5.6 as it has been reported that acrylamide was rapidly degraded under acidic condition (Rydberg *et al.*, 2003).

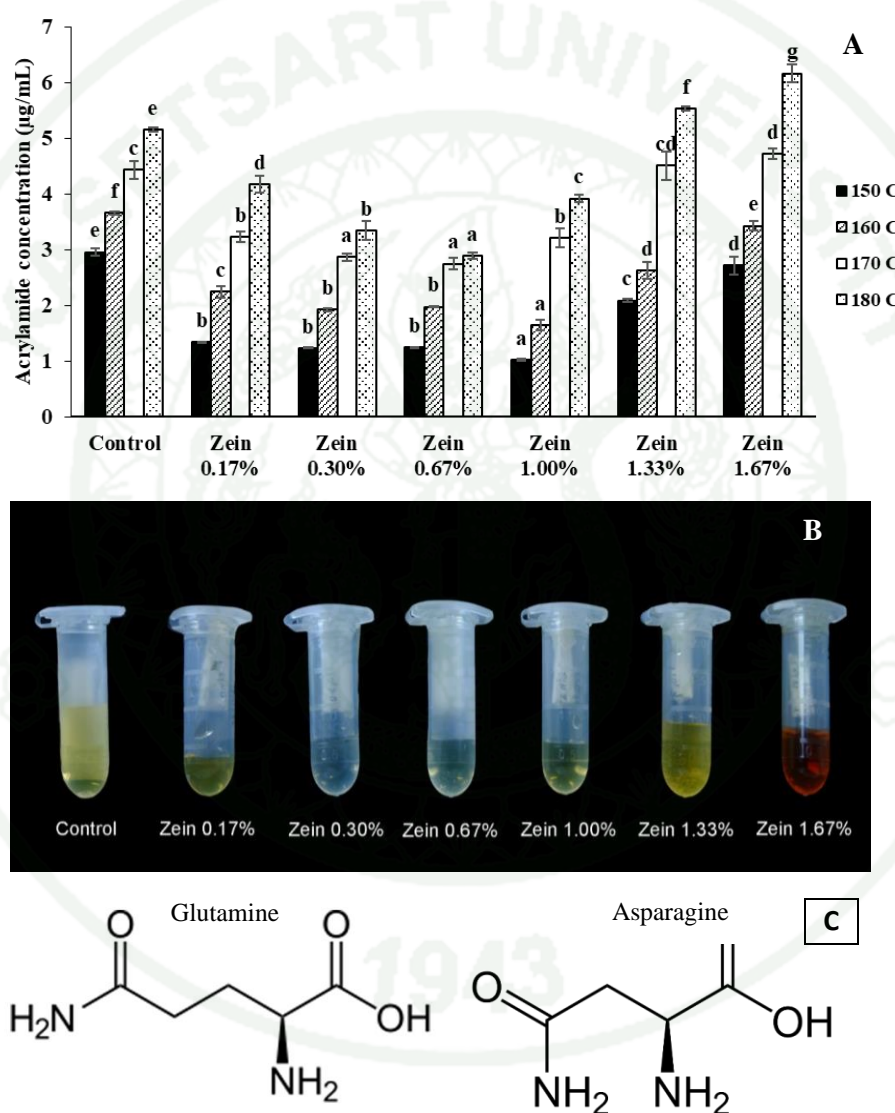


Figure 5 (A) The dose-dependent inhibitory effects of zein solutions heated in a heating block at 150 °C, 160 °C, 170 °C, and 180 °C for 30 min on acrylamide; (B) browning formation at various concentrations of zein heated in a heating block at 170 °C for 30 min; (C) structure of glutamine and asparagine.

Note: ^{a-g} mean \pm standard deviation with different lowercase letters in superscript indicating significant difference ($p \leq 0.05$) at the same temperature.

2. Effect of zein–polysaccharide complex particles on acrylamide inhibition

2.1 Formation and characterization of zein–polysaccharide complex particles

Zein was used to form complexes with chitosan, sodium alginate, and pectin. The colloidal zein–polysaccharide complex particle was prepared using the antisolvent precipitation method. This was achieved by mixing zein in ethanol solution (80%, v/v) with ionic polysaccharide solution (in water) and stirring at ambient temperature. Zein is miscible with an aqueous ethanol phase; however, water is a poor solvent for the dissolution of zein. Thus, the zein ethanol solution is sheared into the water phase and forms small droplets caused by the excellent miscibility of ethanol and water (Wang *et al.*, 2016). Zein–polysaccharide particles were precipitated after decreasing the concentration of ethanol in the dispersed phase through evaporation.

The zeta potential is used to estimate the surface charge of droplets in the dispersion medium, and it is an indicator of droplet stability. Values exceeding +30 mV and – 30 mV indicate good stability against coalescence (Kadu *et al.*, 2011). Following the formation of particles, the charge increased drastically, indicating markedly higher stability. The zeta potential of zein–sodium alginate (– 49.07 to – 57.20 mV) and zein–pectin (– 27.80 to – 31.57 mV) changed to a higher negative charge (Table 4). The zein solution had a positive charge (+25.93 mV), whereas the anionic polysaccharides (sodium alginate and pectin) had a negative charge at pH 4.0. The anionic polysaccharide molecules were absorbed by the cationic zein surface via electrostatic interaction (Hu and McClements, 2015). For zein–chitosan, the interaction between zein and chitosan was achieved by rapidly mixing the antisolvent into the original solvent, resulting in the formation of small droplets. When the concentration of ethanol decreased below the solubilization limit, zein precipitated and formed positively charged particles with chitosan. The self-assembly of zein and chitosan led to partial

complexation. The interaction between zein and chitosan via the antisolvent precipitation introduced the formation of hydrophobic moieties (Wang *et al.*, 2016).

Table 4 Average particle size, polydispersity index, and zeta potential of zein, polysaccharides, and zein-polysaccharide complex particles and non-particles

Sample	Z-avg (nm)	PDI	Zeta potential (mV)
Zein 2.0%	323.76 ± 32.67	0.32 ± 0.04	25.93 ± 0.25
CS 1.0%	1001.30 ± 69.04 ^e	0.54 ± 0.15 ^a	48.10 ± 0.66 ^h
CS 0.6%	671.80 ± 43.68 ^d	0.53 ± 0.14 ^a	47.33 ± 0.91 ^h
CS 0.3%	413.37 ± 27.66 ^{ab}	0.47 ± 0.07 ^a	44.07 ± 0.58 ^g
Alg 1.0%	490.20 ± 22.21 ^{bc}	0.31 ± 0.02 ^a	-47.33 ± 1.56 ^a
Alg 0.6%	520.30 ± 81.18 ^c	0.30 ± 0.02 ^a	-43.87 ± 1.90 ^b
Alg 0.3%	403.37 ± 10.90 ^a	0.40 ± 0.03 ^a	-40.20 ± 1.97 ^c
Pec 1.0%	388.27 ± 15.17 ^a	0.30 ± 0.02 ^a	-30.90 ± 1.14 ^d
Pec 0.6%	414.57 ± 33.47 ^{ab}	0.25 ± 0.02 ^a	-26.23 ± 0.35 ^e
Pec 0.3%	442.50 ± 48.77 ^{abc}	0.22 ± 0.01 ^a	-22.87 ± 0.81 ^f
Zein-polysaccharide complex particles			
Z:CS 1:0.50	2251.33 ± 26.10 ^c	0.17 ± 0.04 ^{aba}	61.30 ± 2.10 ^{ga}
Z:CS 1:0.30	1808.33 ± 5.69 ^c	0.23 ± 0.02 ^{abca}	56.20 ± 0.17 ^{fa}
Z:CS 1:0.15	1181.33 ± 4.86 ^{b*}	0.13 ± 0.06 ^{aa}	48.53 ± 0.87 ^e
Z:Alg 1:0.50	729.70 ± 7.63 ^{b*}	0.33 ± 0.03 ^c	-57.20 ± 0.44 ^{aa}
Z:Alg 1:0.30	706.73 ± 13.21 ^{ab*}	0.33 ± 0.03 ^{ca}	-56.57 ± 0.21 ^{aa}
Z:Alg 1:0.15	649.67 ± 12.91 ^{a*}	0.28 ± 0.01 ^{bca}	-49.07 ± 0.57 ^{ba}
Z:Pec 1:0.50	592.43 ± 9.33 ^{b*}	0.19 ± 0.03 ^{ab}	-31.57 ± 0.31 ^{ca}
Z:Pec 1:0.30	483.97 ± 3.12 ^a	0.16 ± 0.02 ^{aba}	-30.20 ± 0.27 ^{ca}
Z:Pec 1:0.15	401.73 ± 15.43 ^{aa}	0.17 ± 0.01 ^{aba}	-27.80 ± 0.35 ^{da}
Zein and polysaccharides (non-particles)			
Z:CS 1:0.50	2334.00 ± 9.54 ^c	0.49 ± 0.35 ^{ab}	47.70 ± 0.36 ^g
Z:CS 1:0.30	1855.66 ± 27.10 ^{bc}	0.54 ± 0.36 ^c	45.07 ± 0.06 ^f

Table 4 (Continued)

Sample	Z-avg (nm)	PDI	Zeta potential (mV)
Z:CS 1:0.15	1565.33 ± 31.66 ^b	0.47 ± 0.11 ^{ab}	43.17 ± 0.76 ^e
Z:Alg 1:0.50	646.33 ± 63.24 ^a	0.33 ± 0.17 ^{ab}	-46.50 ± 1.35 ^a
Z:Alg 1:0.30	658.63 ± 51.20 ^a	0.42 ± 0.09 ^{ab}	-46.77 ± 1.00 ^a
Z:Alg 1:0.15	527.50 ± 29.70 ^a	0.47 ± 0.07 ^{ab}	-42.80 ± 0.92 ^b
Z:Pec 1:0.50	574.57 ± 33.81 ^a	0.21 ± 0.03 ^a	-26.50 ± 0.40 ^c
Z:Pec 1:0.30	496.47 ± 36.63 ^a	0.24 ± 0.02 ^a	-25.53 ± 0.06 ^c
Z:Pec 1:0.15	440.00 ± 17.16 ^a	0.26 ± 0.03 ^a	-22.03 ± 0.45 ^d

Note: Abbreviations: Alg, alginate; CS, chitosan; Pec, pectin; Z, zein.

^{a-h} mean ± SD with different lowercase letters in superscripts indicates a significant difference ($p \leq 0.05$) in polysaccharides, zein–polysaccharide complex particles, and non-complex particles.

* Indicates a significant difference ($p \leq 0.05$) using t-test between complex particles and non-complex particles.

The average size of zein–polysaccharide complex particles was larger than that of zein or polysaccharides alone, indicating the formation of complex particles. Higher polysaccharide ratios were associated with larger average particles size and higher stability (Table 4). It has been reported that the complex particle abolishes its compact structure because the polysaccharide concentration is not adequate for stabilizing a high protein concentration in the core or low surface coverage, which induces bridging flocculation (Dickinson, 2017). Thus, an appropriate ratio of zein and polysaccharide for the complete coverage of zein particles could result in the formation of a perfect zein–polysaccharide core-shell structure. The highest particle stability was observed for zein–chitosan (48.5–61.3 mV), followed by zein–alginate (–49.1 to –57.2 mV) and zein–pectin (–27.0 to –31.6 mV); of note, the stability showed a negative correlation with the average particle size. The smallest average particle size was recorded for zein–pectin (401.7–592.4 nm), followed by zein–alginate (649.7–729.7 nm) and zein–chitosan (1181.3–2251.3 nm) (Table 4). The sample with higher PDI

would have a broader MW distribution. Generally, a PDI >0.4 indicated a broad distribution, whereas a PDI <0.1 denoted monodispersity of particle sizes (Mudalige *et al.*, 2019). After the formation of the complex particle, the PDI was drastically reduced. The PDI of the complex particles was the smallest (0.13), indicating more uniformity and monodispersity compared with zein (0.32), chitosan (0.47), alginate (0.31), pectin (0.22), and non-complex particles (0.21) (Table 4). Higher zeta potentials and lower PDI were indicative of increased formation and higher stability of protein–polysaccharide complex particles

To confirm the formation of complex particles, the particles were observed using confocal laser scanning microscopy at different wavelengths. The images showed particles of zein, colored green (Figure 6A); chitosan, sodium alginate, and pectin, colored red (Figure 6B1, 6B2, 6B3), and zein–polysaccharide complex particles of mixed colors, red and green (Figure 6C). All particles were noted at the same position. Orange colored complex particles were green zein particles mixed with red chitosan/polysaccharide particles. Imaging showed that zein–chitosan particles were much bigger (1181–2251 nm) than zein–alginate (650–730 nm), and zein–pectin particles (402–592 nm).

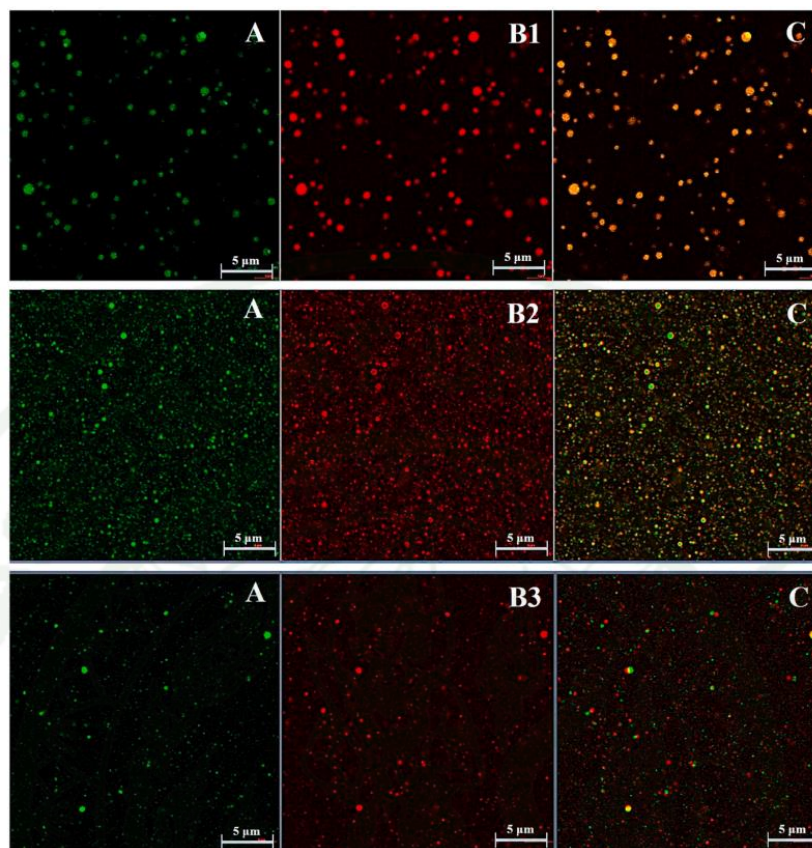


Figure 6 Confocal laser scanning microscope (CLSM) images ($63\times$) of zein–chitosan (top), zein–alginate (middle), and zein–pectin complex particles (bottom).

Note: The fluorescent dye for zein (A) was acridine orange, which showed emission at 543/565 nm; that for chitosan (B1) was rhodamine B, which showed emission at 271/ 520 nm; that for sodium alginate (B2) was fluoresceinamine, which showed emission at 490/520 nm; that for pectin (B3) was ruthenium red, which showed emission at 398/488 nm, and (C) the intersection between A and B showed particles complexed between zein and each polysaccharide.

2.2. Inhibition of acrylamide by zein–polysaccharide complex particles

The zein–polysaccharide complex particles successfully reduced the concentration of acrylamide in a heating block model (170 °C, 30 min). The most effective inhibitor of acrylamide was zein–alginate (1:0.50) ($1.45 \pm 0.17 \mu\text{g/mL}$),

followed by zein–pectin (1:0.50) ($2.25 \pm 0.04 \mu\text{g}/\text{mL}$), versus control ($4.43 \pm 0.17 \mu\text{g}/\text{mL}$). However, the use of zein–chitosan complex particles promoted acrylamide formation, particularly at lower concentrations of chitosan (Figure 7A). Chitosan could not inhibit acrylamide formation to the same extent as alginate and pectin owing to its lower emulsion stability. The zein–polysaccharide ratio was essential for complexation because the lack of a sufficient amount of polysaccharide available to stabilize high protein concentration in the core caused the complex particles to deteriorate (Dickinson, 2017). This finding was consistent with that of our previous study, which demonstrated that the optimum amount of sodium alginate (0.3%) and pectin (0.2%) could reduce acrylamide formation in both conventional and microwave heating (Champrasert *et al.*, 2021). The Na^+ in sodium alginate could inhibit acrylamide formation because the cations prevented the formation of asparagine and related intermediates (Gökmen and Şenyuva, 2007; Lindsay and Jang, 2005). Pectin could inhibit acrylamide by lowering the pH. Aside from the ion and pH effects, the presence of long chain polysaccharides could result in lower acrylamide formation by preventing the interaction of intermediates and slowing the motion of the molecules in the system (Passos *et al.*, 2018). The free amino group of zein could compete with asparagine to bind with the carbonyl group of glucose, resulting in reduced production of acrylamide (Anese *et al.*, 2009; Claeys *et al.*, 2005).

The effect of the formation of complex particles on acrylamide inhibition was also examined by comparison with the solution of zein and polysaccharides by skipping the antisolvent precipitation step, resulting in no particles being formed (non-complex particles). The zein–alginate and zein–pectin particles exhibited markedly higher efficiency in acrylamide mitigation ($1.45 \pm 0.05 \mu\text{g}/\text{mL}$ and $2.25 \pm 0.04 \mu\text{g}/\text{mL}$, respectively) than their non-complex counterparts ($6.26 \pm 0.01 \mu\text{g}/\text{mL}$ and $5.35 \pm 0.07 \mu\text{g}/\text{mL}$, respectively) (Figure 7A). The zein–polysaccharide complex particles showed less formation of brown color than the non-complex particles (Figure 7B).

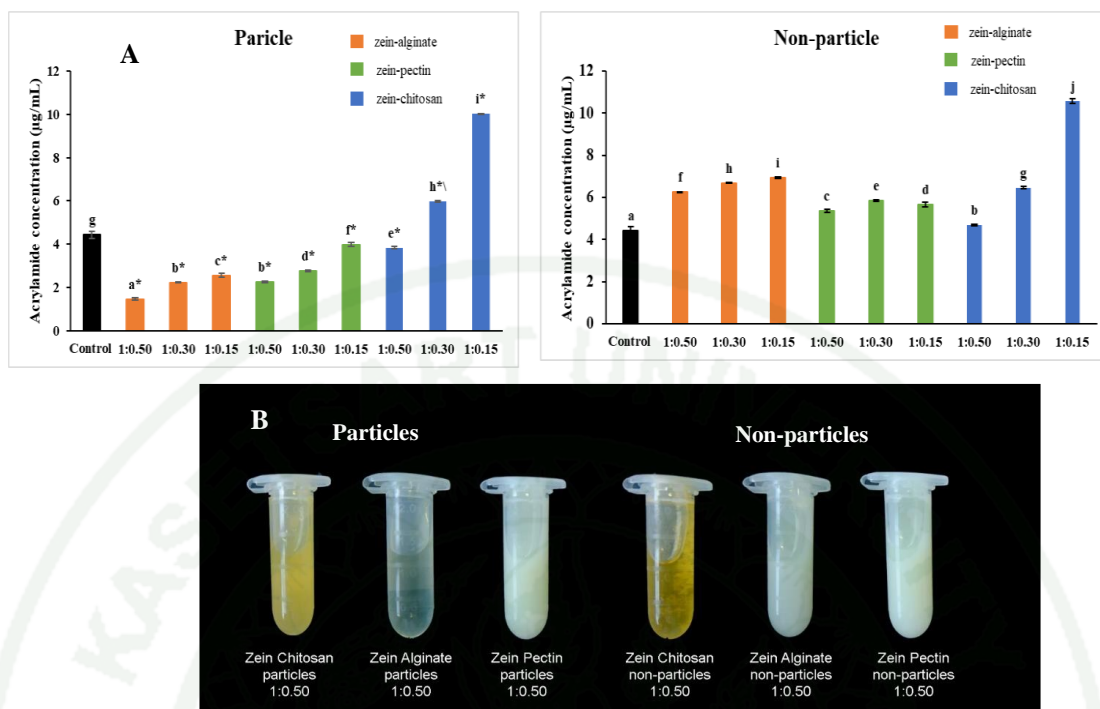


Figure 7 (A) Acrylamide formation after using protein–polysaccharide complexes as inhibitors in a heating block. (B) Effect of zein–polysaccharide complex particles and non-complex particles (1:0.50) on browning formation at 170 °C for 30 min in a heating block.

Note: Data are presented as the mean \pm standard deviation (n = 3).

^{a-j} different letters indicating statistically significant difference (p < 0.05).

* mean difference (t-test) between complex particles and non-complex particles.

Different polysaccharides have been reported to reduce acrylamide formation in chemical (heating block and microwave heating) and food models, (Champrasert *et al.*, 2021), but zein-polysaccharide complex particles of the same polysaccharides have been found to have stronger acrylamide inhibitory effects. A schematic image of the potential mechanism which these particles inhibit acrylamide formation is presented in Figure 8.

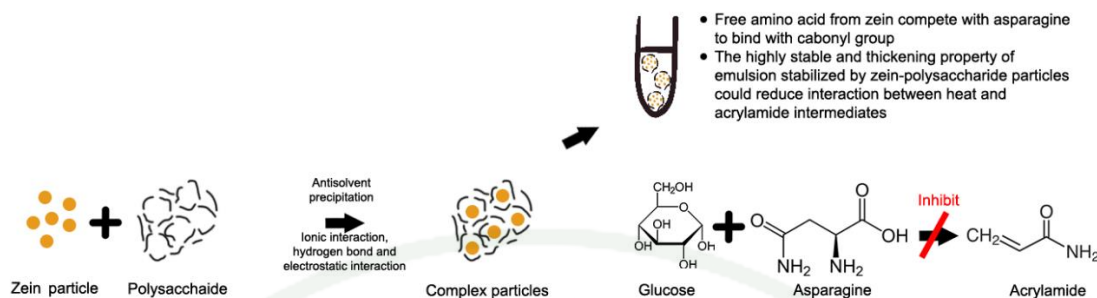


Figure 8 Schematic image of the potential mechanism by which zein-polysaccharide complex particles inhibit acrylamide formation.

3. Acrylamide inhibition in a food model

Fried potato chips were used as the food model because of their wide consumption and high acrylamide content (0.25–2.67 mg/kg) (Capuano and Fogliano, 2011). According to the World Health Organization (2005), the daily dietary intake of acrylamide should be in the range of 0.3–2.0 mg/kg body weight. The inhibition of acrylamide in deep-fried potato strips dipped in zein–pectin (1:0.5), zein–alginate (1:0.5), and zein–chitosan (1:0.5) compared with control was $31.16\% \pm 0.05\%$, $28.05\% \pm 0.09$, and $17.75\% \pm 2.24$, respectively (Figure 9). These results were similar to those obtained from the heating block model. The brown color of fried potato strips appeared to follow the formation of acrylamide. Maillard reactions involving asparagine produced acrylamide, and its concentration increased after cooking plant-derived foods (Mottram *et al.*, 2002). The immersion duration was crucial in acrylamide mitigation because it causes the food surface tension to decrease and leads to the formation of a coating on the food surface (Zeng *et al.*, 2010). The thermal gelation network of the coating could reduce heat penetration from the oil into the food during frying, thus reducing any interactions that may occur between heat and acrylamide intermediates (Mousa, 2018; Suyatma and Prangdimurti, 2015; Zeng *et al.*, 2010). The emulsions stabilized by protein-coated particles formed paste-like or gel-like networks (Hoffmann and Reger, 2013), which were stable and could thicken the system, thus facilitating the formation of a coating on the food surface and reducing the direct interaction between

heat and intermediates. However, the effect of the different interfacial rheology of these particles with the food surface on acrylamide inhibition requires further investigation. According to benchmark level of EU regulation, acrylamide concentration should not over 500 $\mu\text{g}/\text{kg}$. Acrylamide concentration of control sample was recorded at 16,000 $\mu\text{g}/\text{kg}$ which 32 times higher. However, deep-fried potato strips dipped in zein-pectin (1:0.5) and zein-alginate (1:0.5) were 11,000 $\mu\text{g}/\text{kg}$, the validation of acrylamide concentration must be needed to determine.

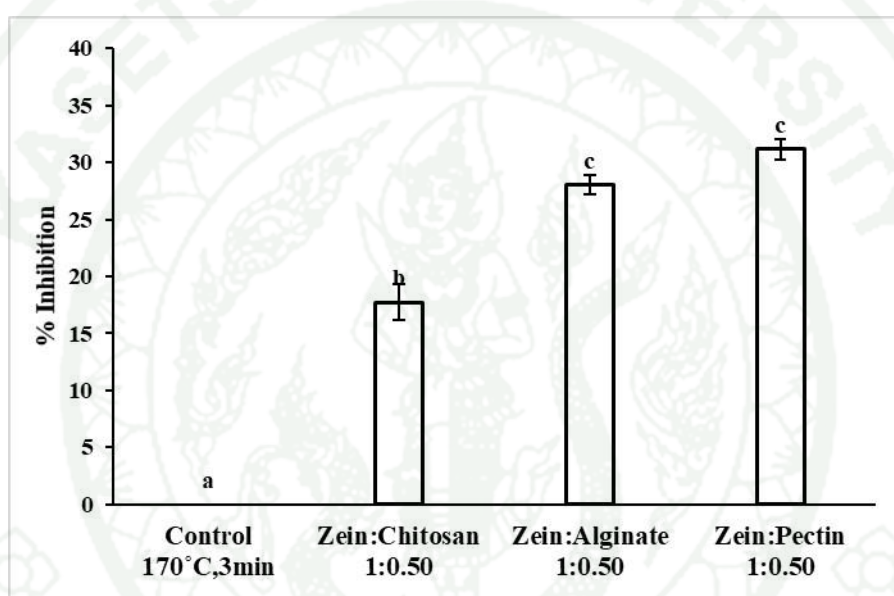


Figure 9 Inhibition of acrylamide (%) in potato strips soaked in various zein polysaccharides complex particles (1:0.5) for 30 min and deep fried at 170 °C for 3 min.

Note: ^{a-c} different letters indicating statistically significant difference ($p < 0.05$).

Part 3

Granular Cold-Water Swelling-Octenyl Succinic Anhydride Starch to Stabilize Pickering Emulsion and Use as a Template for Oleogelation

1. Formation and characterization of Pickering emulsions

The lipophilic octenyl succinic group of OSA was esterified with starch to increase hydrophobicity of the starches. The starch granule of GCWS-OSA was highly swollen indicated by the largest average particle size in both number length ($D[1,0]$) and surface area moment ($D[3, 2]$). In this study, the number length mean ($D[1,0]$) was used as it could give a precise average particle size because the absolute number of particles were known. The larger swollen granule of GCWS resulted in a highly amorphous structure which allowed its hydroxyl groups to be more exposed to OSA and promoted substitution efficiency. The surface area moment mean $D[3, 2]$ (Sauter mean diameter) was calculated using volume-to-surface ratio which indicated the surface activity of particles. The Sauter mean diameter agreed well with the esterification efficiency which was determined by degree of substitution (DS). Results in Table 5 showed that GCWS-OSA had the highest DS (0.0149) followed by WS-OSA (0.0098) and HS-OSA (0.0049). The wettability of the particles by the oil and water phase was measured to evaluate the potential of the particles to stabilize Pickering emulsions. The contact angle (θ) of OSA starch (73.3° - 80.4°) with the oil-water interface was significantly increased from native starch (50.6° - 55.0°), which indicated an increase in surface hydrophobicity (Table 5). The highest contact angle was found in GCWS-OSA (80.4°), followed by WS-OSA (76.2°), and HS-OSA (73.3°). Particles with a contact angle close to 90° are optimal for the fabrication of stable Pickering emulsions (Berton-Carabin & Schroen, 2015), since at that angle the desorption energy of the particles is at a maximum.

Table 5 Contact angle, degree of substitution, particle size of native and OSA starch

Sample	DS	Contact angle (°)	Average particle size of starch (µm)	
			Number weighted (D _[1,0])	Volume weighted (D _[3,2])
Native HS	-	50.60±2.42 ^d	4.23±0.01 ^b	22.67±0.42 ^c
Native WS	-	54.97±1.72 ^c	4.11±0.01 ^a	18.60±0.65 ^a
HS-OSA	0.0049±0.0006 ^c	73.33±2.51 ^b	4.35±0.01 ^c	20.95±1.09 ^b
WS-OSA	0.0098±0.0011 ^b	76.23±2.90 ^b	4.49±0.03 ^d	23.05±0.65 ^d
GCWS-OSA	0.0149±0.001 ^a	80.43±2.67 ^a	5.28±0.06 ^e	23.02±0.59 ^d

Note: Different lowercase letters indicate significant difference at 95% confidence level.

2. Particle size distribution and microstructure of Pickering emulsions

Pickering emulsions stabilized by GCWS-OSA had the smallest droplet size with a Sauter mean diameter (D_[3,2]) of 12.58 µm, followed by WS-OSA (22.83 µm) and HS-OSA (31.50 µm) (Figure 10). Particle size distribution of all emulsions exhibited a double peak. During OSA-starch preparation, the finished starch has been conceived to contain both bound (esterified) and free (non-esterified) starch (Yusoff and Murray, 2011). Some amylopectin branch chains were reported to remain unmodified which indicated a heterogeneously reaction occurred across all branch chains (Shogren *et al.*, 2000). As a result, the emulsified starch (esterified) caused smaller oil droplets size distribution. The larger size was the non-esterified starch that cause some coalescence of oil droplets. Moreover, the high energy used during

emulsification could produce some degradation of starch structure, altogether with the changes in shape and conformation of starch components which could impact emulsifying characteristics (Nilsson and Bergenstahl, 2006).

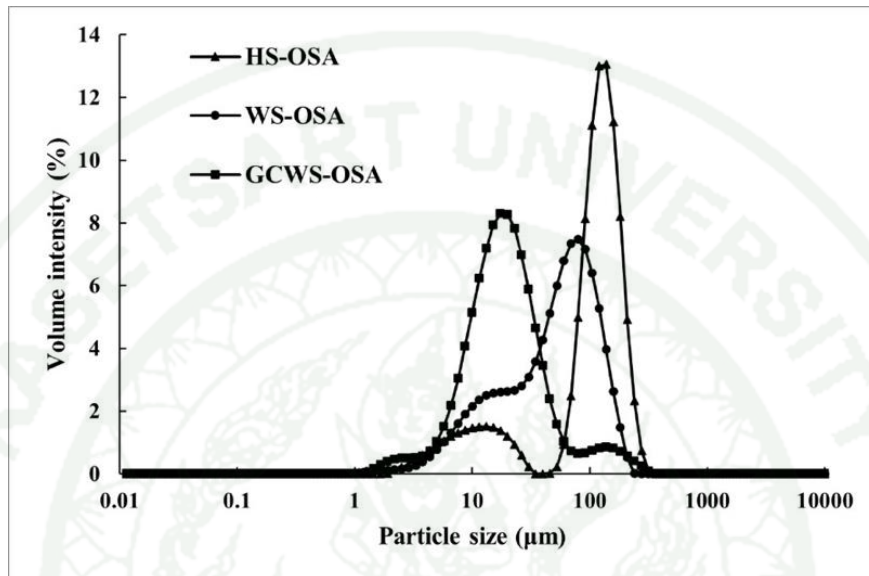


Figure 10 Particle size distribution of Pickering emulsion stabilized by starch particles

The main particle size peak shifted progressively in the direction of smaller droplet size as DS increased. Results for contact angle and droplet size correlated well with DS, since the higher DS and therefore higher wettability for the oil-water interface resulted in smaller droplet size. The increased DS could have resulted in increased surface coverage and this favors the formation of stable Pickering emulsion with smaller droplet sizes (Bello-Pérez *et al.*, 2015). In view of the droplet size versus the size of the starch particles, we expect that for GCWS-OSA only the smallest particles in the distribution ($\sim 1\ \mu\text{m}$ or less) will be adsorbed onto the interface.

The microstructure of the Pickering emulsion was imaged using light microscopy and confocal laser scanning microscopy, as shown in Figure 11.

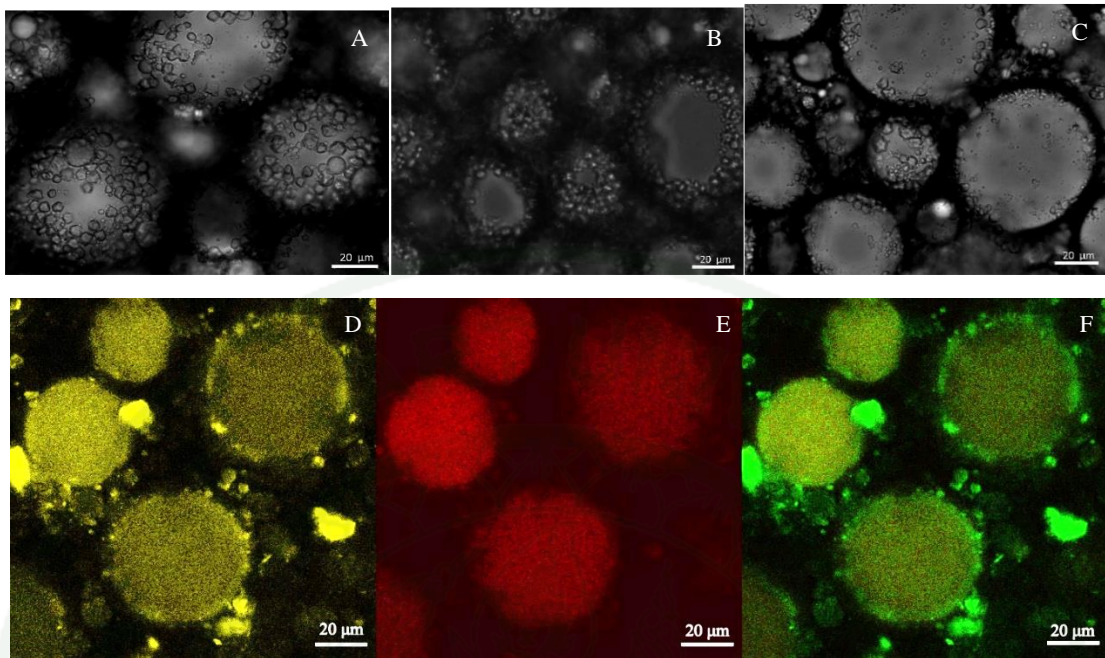


Figure 11 Microstructure images under light microscope (40x) of Pickering emulsion stabilized by starch-based particles from (A) HS-OSA (B) WS-OSA (C) GCWS-OSA. Confocal laser scanning microscope (CLSM) images of a 60% MCT oil Pickering emulsion stabilized by GCWS-OSA. (A) The starch was stained with Nile blue coded as yellow, (B) the oil phase was stained Nile Red and was coded red and (C) overlapping starch-rich and oil-rich regions appear green.

Nile red was used to stain the oil phase and is coded as a red color. Nile blue was used as a fluorescent marker for the starch granules, which coded yellow color in the images. The superimposed image of A and B appeared as green color showing an emulsion of oil droplets surrounded by starch. Starch particles were obviously seen to be attached at the oil-water interface of the oil droplets (Figure 11F). For the emulsion stabilized by GCWS-OSA the confocal images show that the interfaces are covered by a layer of starch particles, but some larger structures appear to have attached as well.

3. Rheology of Pickering emulsion stabilized by starch-based particles

3.1 Small amplitude oscillatory shear (SAOS)

To determine the linear viscoelastic properties of the HIPEs and the extent of the linear regime, the storage (G') and loss (G'') modulus were measured as a function of (1) frequency ($\omega = 0.1-150$ rad/s) at constant shear strain (1%) (Figure 12.1) and (2) amplitude ($\gamma = 0.01-100\%$) at fixed angular frequency (1 rad/s) (Figure 12.2). The amplitude was small enough to give a stress response in the linear regime. For all emulsions, the maximum linear strain was around 1%, and G' in the linear regime was about 100 Pa. All samples had G' higher than G'' over the entire range and showed a weak power law dependence of G' ($\sim\omega^n$), typical for a disordered solid (i.e. a gel or a jammed system). The loss tangent of all emulsions was in the order of 0.1 which means they all behaved as soft viscoelastic solids at the specified frequency.

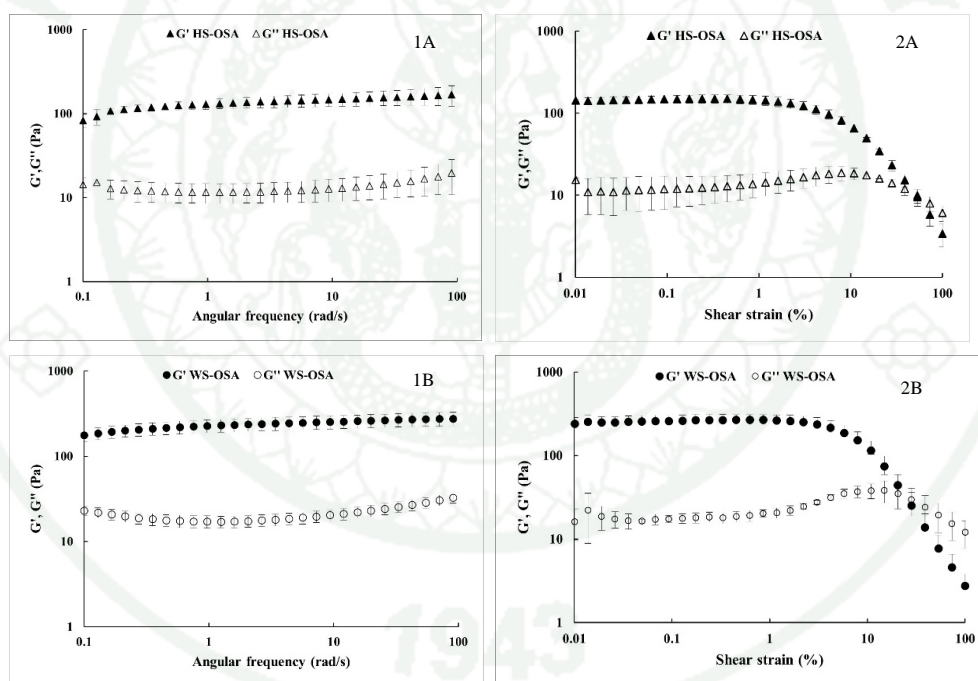


Figure 12 Small amplitude oscillatory shear test at 20°C for 1) frequency sweep test ($\omega = 0.1-150$ rad/s) and 2) amplitude sweep test ($\gamma = 0.01-100\%$) of Pickering emulsions stabilized by starch-based particles of (A) HS-OSA, (B) WS-OSA, (C) GCWS-OSA

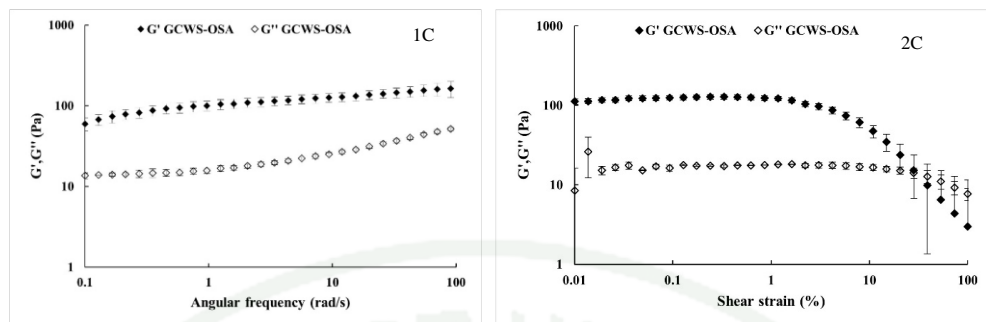


Figure 12 (Continued)

3.2 Large amplitude oscillatory shear (LAOS)

In practice, food products are often subjected to large and rapid deformation during processing, and the response to these is typically in the non-linear regime. At strains over 1%, G' decreased rapidly for all emulsions as the microstructure was gradually and progressively disrupted, until the flow point was reached, where G' equaled G'' (Liu *et al.*, 2021). The systems stabilized by HS-OSA and WS-OSA showed a weak strain overshoot in G'' , which is referred to type III nonlinear behavior. Type III behavior is a common feature in soft disordered materials such as concentrated emulsions (Bower *et al.*, 1999; Mason *et al.*, 1995). The overshoot in G'' is caused by the balance between formation and destruction of network links. It is thought to be related to the the rearrangement of unstable clusters during shearing, resulting in increased viscous dissipation (Raghavan and Khan, 1995). The overshoot was absent in the GCWS-OSA stabilized emulsion, which indicated a type I nonlinear behavior, in which both the elastic and viscous moduli decreased continuously with increasing amplitude. (Hyun *et al.*, 2011).

The viscoelastic moduli (G' and G'') are based only on the first harmonic contribution to the total stress, and to gain more structural insight in the behavior beyond linear viscoelasticity, we analyzed the response in the nonlinear regime using Lissajous plots (Figure 13). At 1.18% and 5.77% strain, all emulsions had Lissajous plots with an elliptical shape, which indicated linear viscoelastic behavior. The plots

gradually changed from an ellipse to a more rhomboidal shape when higher strain was imposed. At 14.9% strain, the emulsion stabilized by HS-OSA had the narrowest loop and showed a minor degree of strain hardening towards maximum intra-cycle deformation (evident from the slight up/down swing in the loop at those points). At 38.8% and 100% strain, the WS-OSA and GCWS-OSA had a near rhomboidal shape indicated a higher degree of plastic behavior than the HS-OSA emulsions. The slope of the curve for the elastic contribution to the total stress (the dashed lines within the loop) was close to zero around minimum strain, indicated a significant degree of disruption of the microstructure. Whereas the wider loop of the total stress indicated a relatively higher degree of dissipation (Figure 13.1). To investigate the viscous contribution to the total stress in more detail, intra-cycle plots of shear stress versus shear rate were plotted in Figure 13.2. All emulsions showed a gradual transition from a near circular plot (predominantly elastic behavior) to a sigmoidal shape, indicative of shear thinning behavior, and resulting from a gradual disruption of the structure of the emulsions. Consistent with the strain loops, the HS-OSA had the widest loop at the highest strain, again indicating there is relatively more residual elasticity in that sample.

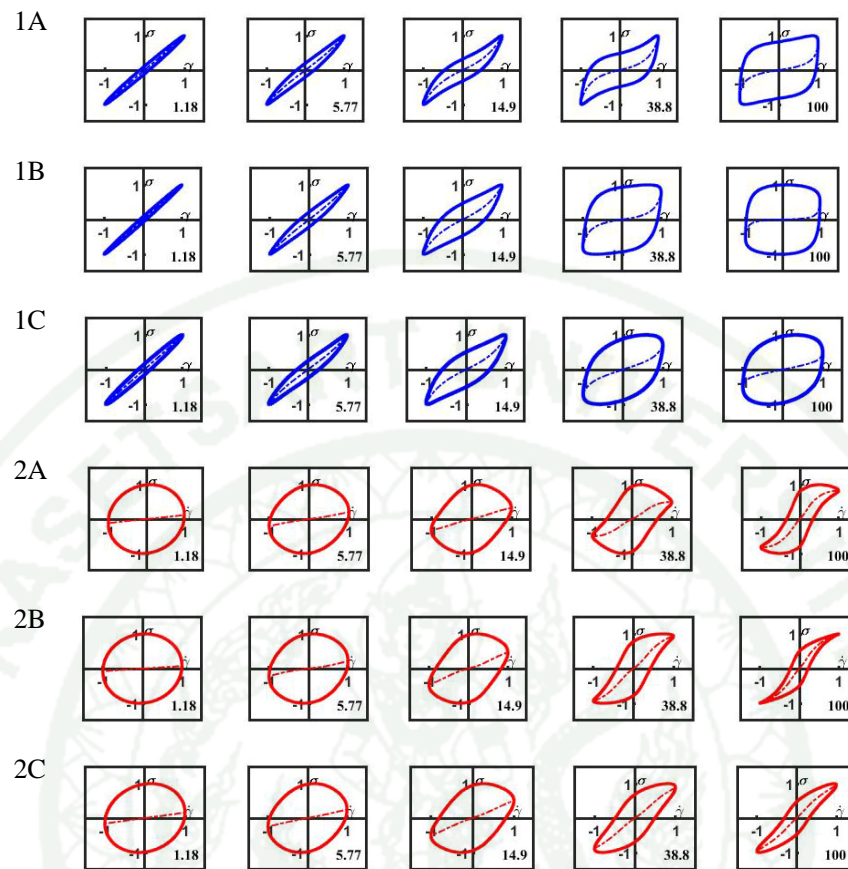


Figure 13 Normalized Lissajous curves of (1) shear stress (Pa) versus shear strain (%) and (2) shear stress (Pa) versus shear rate (1/s) at shear strain 1.18%, 5.77%, 14.9%, 38.8% and 100% at 20°C of Pickering emulsion stabilized by starch-based particles of (A) HS-OSA (B) WS-OSA (C) GCWS-OSA.

Note: Solid curve was the total stress, the dashed interior curve denoted the contribution of the elastic stress to the total stress

The shear stiffening (S factor) and the shear thickening (T factor) were calculated according to Eq (2) and Eq (3). All emulsions showed shear thickening behavior prior to the onset of thinning, as indicated by the increase in the T factor up to a shear rate of about 0.1/sec which corresponded to a strain amplitude of about 10%, and coincided with the location of the weak overshoot. The overshoot of GCWS-OSA was not visible in the strain sweep, which showed only strain thinning (Type I) behavior (Figure 14.1). Again, we need to consider the fact that the moduli in Figure 12 are based

on a first harmonic analysis, and the nonlinear effects present in the higher harmonics are not accounted for in this calculation

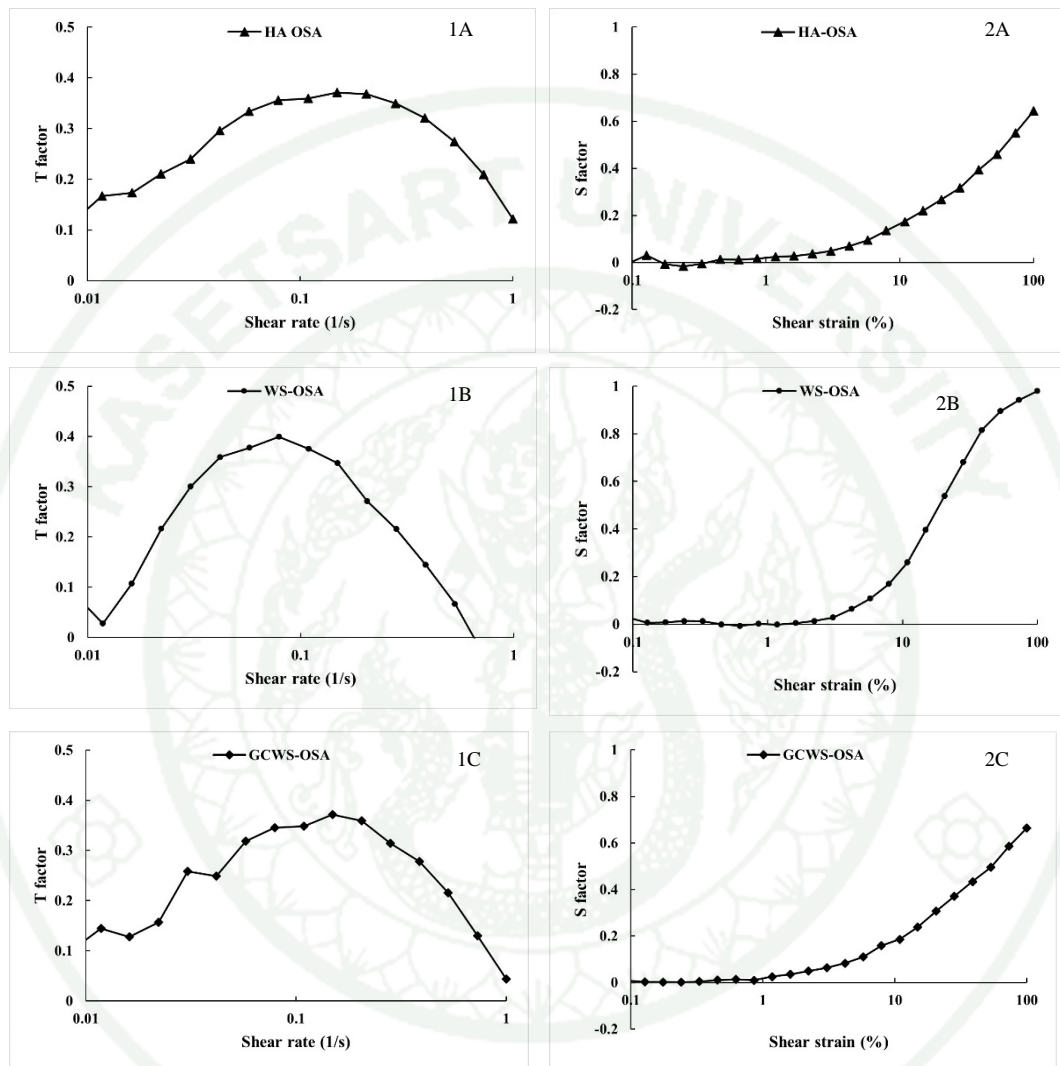


Figure 14 The (1) Shear thickening (T factor) and (2) shear stiffening (S factor) of Pickering emulsion stabilized by starch-based particles of (A) HS-OSA, (B) WS-OSA, and (C) GCWS-OSA

The modulus at minimum strain (G'_M) and at large strain (G'_L) where nearly equal up to a strain of a 1-2%, and as a result the S factor was zero at these strains (Figure 14.2). At higher strains S gradually increased. This is mostly *apparent* strain hardening, which results from the plastic behavior at high strains, as evident from the rhomboidal shape of the plots. For these plots, G'_M is near zero, while G'_L has a finite

value, which results in $S \approx 1$. The overall behavior at large strains is shear thinning, which is clearly visible in the shear rate plots (Figure 14) and the T-factor.

The degree of dissipation was quantitatively compared by calculating the dissipation ratio, which is defined by the ratio of the area of a single Lissajous cycle divided by the dissipation energy of a perfectly plastic material at the same strain and maximum stress (i.e. $\varphi = \pi G'' \gamma_0 / (4\sigma_{max})$). The dissipation ratio was plotted in Figure 15, the values range was 0 to 1, where the value of 1 implies perfectly plastic behavior. All emulsions had small dissipation ratios at low strain, which significantly increased after about 10% strain. The emulsions stabilized by GCWS-OSA had the highest initial dissipation ratio, of around 0.1. In combination with the results in Figure 12, we see that these emulsions are slightly less stiff and relatively more viscous in their response. But in contrast to the WS-OSA emulsion they are significantly less disrupted at a 100% strain. The HS-OSA emulsions start to be disrupted well below 1% deformation, and appear to be somewhat more brittle than the other two emulsions.

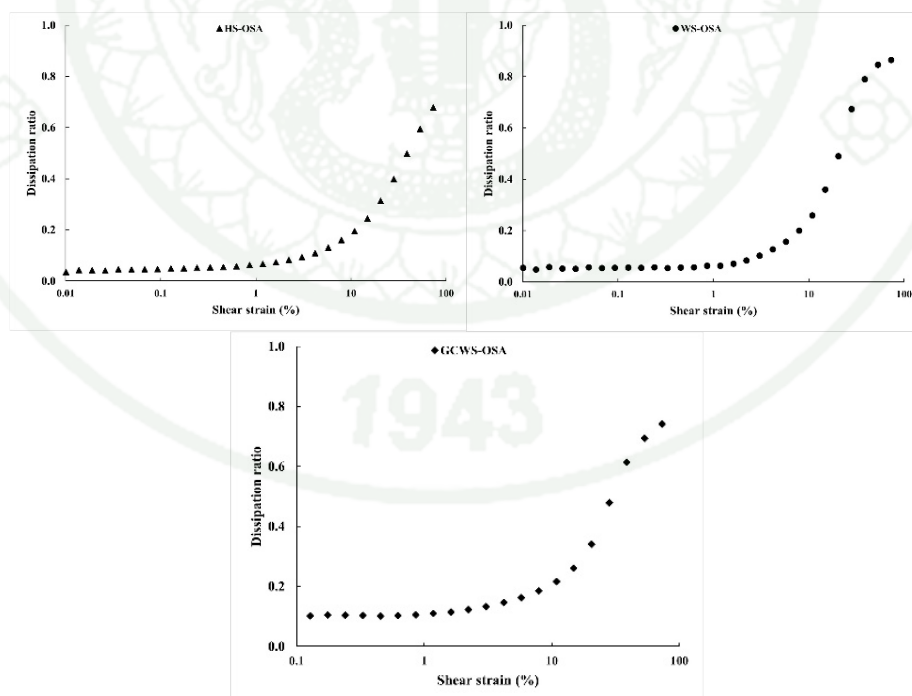


Figure 15 Dissipation ratio of oleogel using Pickering emulsion stabilized by starch-based particles of HS-OSA, WS-OSA, and GCWS-OSA

4. Rheological properties of oleogels

4.1 Small amplitude oscillatory shear (SAOS)

All starch based oleogels had G' greater than G'' ($\tan \delta \leq 0.1$), and both moduli were almost independent of frequency ranging from 0.1 to 150 rad/s, indicating all oleogels behaved as viscoelastic gels (Luo *et al.*, 2019; Patel *et al.*, 2014). All oleogels had lower maximum linear strain ($\sim 0.1\%$) and were considerably stiffer than their respective template emulsions (Figure 16).

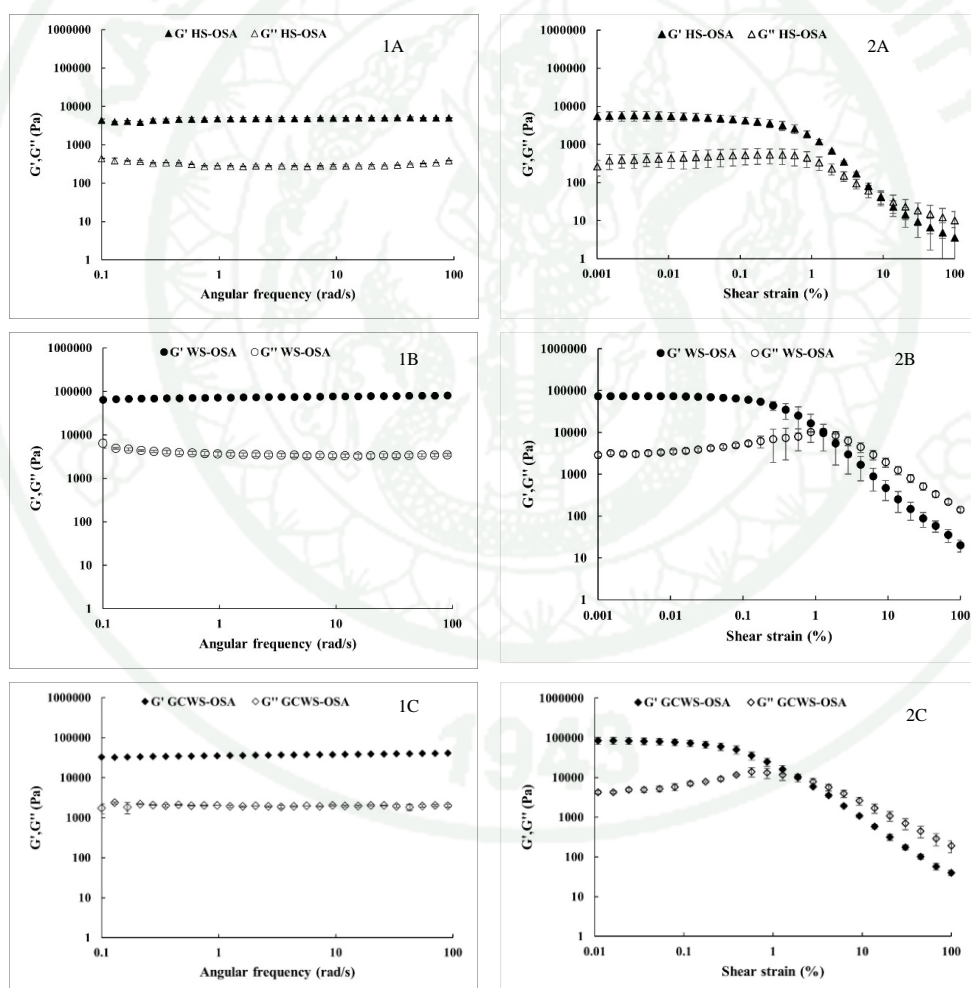


Figure 16 The (1) frequency sweep test ($\omega = 0.1$ -150 rad/s) and (2) amplitude sweep test ($\gamma = 0.01$ -100 %) of oleogel using Pickering emulsion stabilized by starch-based particles from (A) HS-OSA, (B) WS-OSA, (C) GCWS-OSA

According to the strain sweep tests, the highest gel strength was observed in WS-OSA and GCWS-OSA oleogels. The G' of oleogels from WS-OSA and GCWS-OSA was about 10 times higher ($\sim 10^5$ Pa) than the gels based on HS-OSA ($\sim 10^4$ Pa). WS-OSA and GCWS-OSA oleogels had a crossover point at about 1% which indicated a stiffer and more brittle material than the gels made with HS-OSA. The latter had a crossover point at a strain ($\sim 10\%$), indicative of a softer and more stretchable material. All oleogels had a pronounced overshoot in G'' and exhibited type III nonlinear behavior (Figure 16).

4.2 Large amplitude oscillatory shear (LAOS)

Elastic and viscous Lissajous curves were constructed by plotting the intracycle shear stress as a function of the applied shear strain and shear rate (Figure 17). At lower shear strain (0.024 and 0.261%), all oleogels exhibited a near linear viscoelastic solid-like behavior. At increased strain (0.857 and 1.900%), the Lissajous plot of WS-OSA and GCWS-OSA oleogels started to deviate from an ellipsoidal shape to a wider elliptical shape indicated a progressive disruption of the microstructure which resulted in an increase in viscous dissipation and a gradual shift from a predominantly elastic to a more viscous dominated behavior. But the HS-OSA oleogel was still displaying a near linear viscoelastic solid-like behavior (Figure 17.1). The slope of the elastic contribution to the total stress (dashed line) did not decrease to zero, as it did for WS-OSA and GCWS-OSA at 1.9% strain indicated that its structure did not undergo any considerable degree of disruption. At the highest strain of 20.5%, the Lissajous plots of WS-OSA and GCWS-OSA were rectangular showing perfect plastic behavior (i.e. $\phi = 1$). The dashed curve in the cycle for HS-OSA still had a finite slope, indicating there was still residual elasticity in the material, and its network structure had not yet been completely disrupted.

The normalized Lissajous curves of shear stress versus shear rate are shown in Figure 17.2. At low strain, all oleogels had wide elliptical shapes indicating a dominant elastic contribution to the total stress. For HS-OSA oleogel, this shape persisted until a strain of 1.9%, and became a sigmoidal shape after that. For WS-OSA

and GCWS-OSA oleogels, the curves transition to a rhomboidal shape at 1.9% strain, indicated a partial yielding of the gel structure, and an increase in viscous dissipation. At the highest strain, the curves transition to a very narrow S-shape with sharp edges, indicated strong shear thinning behavior.

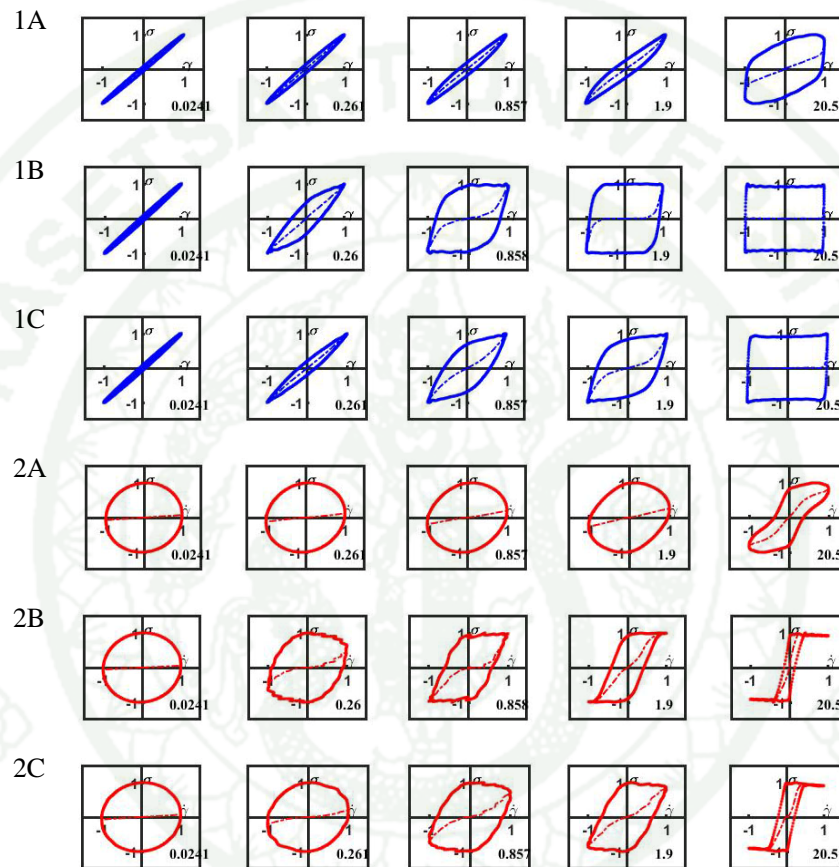


Figure 17 Normalized Lissajous curves of (1) shear stress (Pa) versus shear strain (%), (2) shear stress (Pa) versus shear rate (1/s) at 20°C of oleogel using Pickering emulsion stabilized by starch-based particles from (A) HS-OSA, (B) WS-OSA, and (C) GCWS-OSA at shear strain 0.0241%, 0.261%, 0.857%, 1.9%, and 20.5%

The S factor was near zero for most of the applied strain range, and started to increase to positive value at strain about 0.1% (Figure 18).

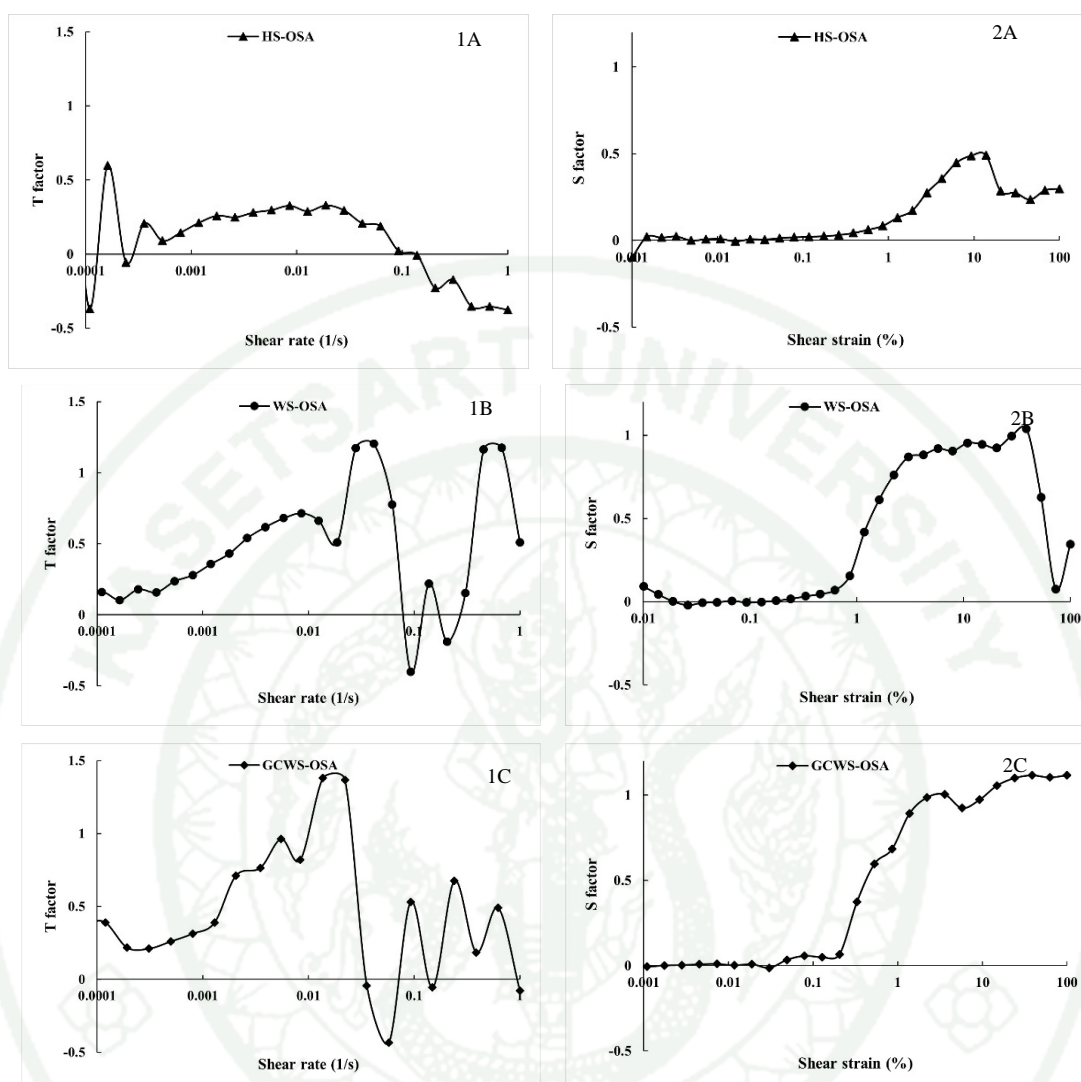


Figure 18 The (1) shear thickening (T factor) and (2) shear stiffening (S factor) of oleogels using Pickering emulsion stabilized by starch-based particles of (A) HS-OSA, (B) WS-OSA, and (C) GCWS-OSA

The positive S factor suggested strain hardening, but again this is clearly apparent strain hardening in WS-OSA and GCWS-OSA oleogels, as apparent from the near zero slope of the stress curve at strain zero. At larger strain, the viscous contribution was dominant and the overall behavior was strain softening. The T factor showed an increasing positive value at small strain (0.01/s) and the overshoot in G'' was also observed. Beyond this point, the T factor decreased, indicated a progressive

disruption of the structure. Beyond a shear rate of about 0.1/s and shear strain of about 50%, the signal became noisy and was no longer reliable.

The energy dissipation ratio was again calculated at low strain (up to 1% strain), all oleogels had dissipation ratio of approximately 0.1, which significantly increased to more plastic behavior after about 10% strain (Figure 19). At the maximum strain WS-OSA and GCWS-OSA levelled off at a ratio of close to 1, indicating almost perfectly plastic behavior. HS-OSA retained relatively more of its elasticity, with a value of the dissipation ratio at maximum strain just below 0.8.

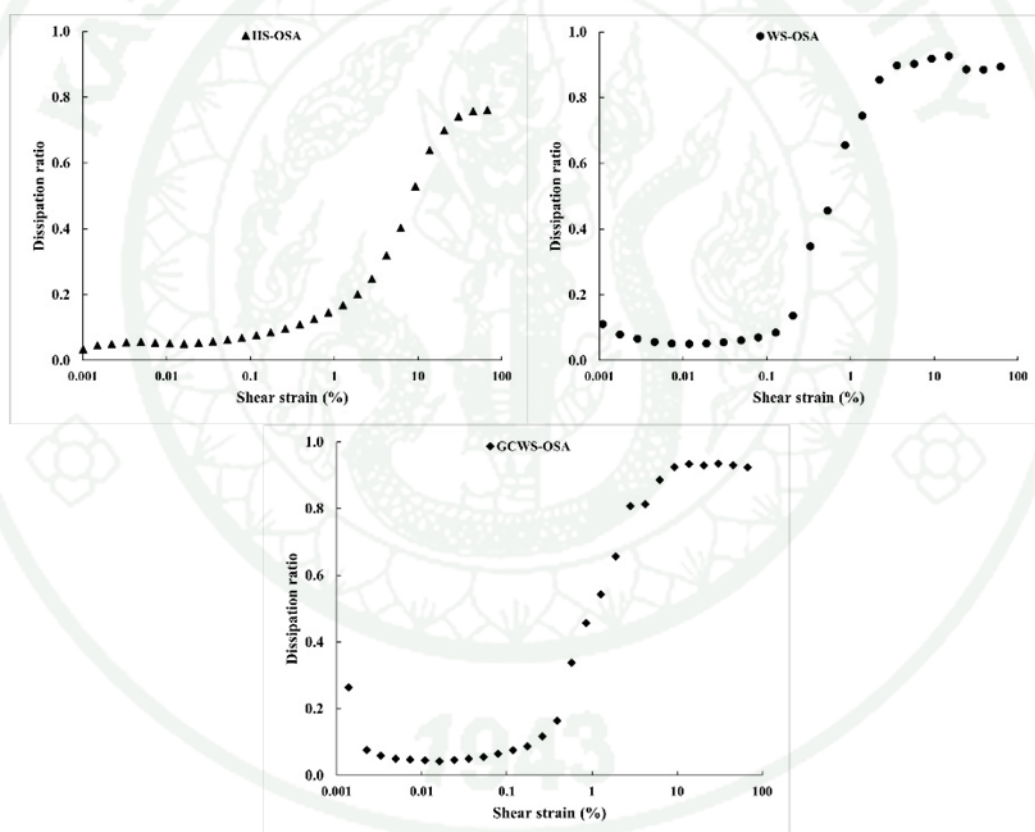


Figure 19 Dissipation ratio of oleogel using Pickering emulsion stabilized by starch-based particles of HS-OSA, WS-OSA, and GCWS-OSA

Part 4

Oleogel from Granular Cold Water Swelling-OSA with Polysaccharides and Its Application as Fat Mimetic

1. Formation and characterization of Pickering emulsion

Particle size distribution of oil droplets in Pickering emulsion stabilized by starch-based particle was presented in Table 6.

Table 6 Particle size distribution of Pickering emulsion stabilized by starch particles w/wo polysaccharides

Sample	Particle size (μm)	DS
HS-OSA	31.53 ± 1.23^g	0.0049 ± 0.0006^c
HS-OSA + pectin	18.80 ± 0.30^d	
HS-OSA + gum arabic	18.32 ± 0.75^d	
HS-OSA + xanthan	17.31 ± 0.17^c	
WS-OSA	22.85 ± 0.82^f	0.0098 ± 0.0011^b
WS-OSA + pectin	19.08 ± 0.40^d	
WS-OSA + gum arabic	20.87 ± 0.54^e	
WS-OSA + xanthan	21.55 ± 0.77^e	
GCWS-OSA	12.58 ± 0.16^b	0.0149 ± 0.001^a
GCWS-OSA + pectin	11.27 ± 0.24^a	
GCWS-OSA + gum arabic	13.34 ± 0.17^b	
GCWS-OSA + xanthan	13.56 ± 0.30^b	

Note: ^{a-g} mean \pm SD, the different lowercase superscript in the same column indicated significant difference ($p \leq 0.05$)

Emulsion stabilized with GCWS-OSA starch had the smallest particle size, followed by WS-OSA and HS-OSA. The Sauter mean diameter (D[3,2]) of oil droplets

ranged from 11-31 μm . The particle size distribution of oil droplets was shifted towards lower droplet size as degree of substitution (DS) increased. The surface hydrophobicity increased with DS, thus the higher DS the more stabilized emulsion. The smallest and homogeneous droplet size (11.27-13.56 μm) of emulsion stabilized with GCWS-OSA starch was observed in the system with/without polysaccharide. Polysaccharide concentration was reported to have no effect on droplet size distribution (Luo *et al.*, 2019; Patel *et al.*, 2014; Patel and Dewettinck, 2016).

2. Rheological properties of emulsion

2.1 Small amplitude oscillatory shear (SAOS)

Small amplitude oscillatory shear was measured in the linear viscoelastic regime. For the amplitude sweep test (Figure 20), storage modulus (G') and loss modulus (G'') were measured as a function of strain amplitude (0.1-100%) at fixed angular frequency (1 rad/s). At low strain (0.1-1%), all emulsions behaved as solid-like materials as G' was higher than G'' . In the linear regime, the structure of material was deformed reversibly without destruction. However, when strain was over 1%, G' and G'' were entered to a non-linear regime. G' was decreased rapidly as network structure and mechanical strength started to collapse irreversibly until reaching the flow point where G' equal to G'' (Liu *et al.*, 2021). For G'' , all emulsions were noticed an overshoot (maximum G'') at $\sim 40\%$ strain. The overshoot was regarded as a rising from the balance between the formation and the destruction of the network junction. The deformation amplitude at constant frequency of these response was a type III or weak strain overshoot. This was a remarkably feature of a soft glassy material such as concentrated emulsion (Bower *et al.*, 1995). The addition of polysaccharide increased the strength of emulsion and decreased the yield strain (crossover point G' equals G'') especially for GCWS-OSA emulsion. Hence, a better structure of Pickering emulsion was noticed with the presence of polysaccharide. G' and G'' was higher in emulsion with polysaccharide because of the stronger network structure by electrostatic interaction between different charges of OSA starch and polysaccharide (Yan *et al.*, 2019).

In the frequency sweep test (Figure 21), G' and G'' were measured as a function of angular frequency ($\omega = 0.1-100$ rad/s) at fixed strain amplitude (1%). All emulsions showed a low dependence of G' and G'' on frequency. Similarly to amplitude sweep test, G' was higher than G'' , and both G' and G'' were higher in emulsion with polysaccharide than without polysaccharide especially for the GCWS-OSA emulsion.

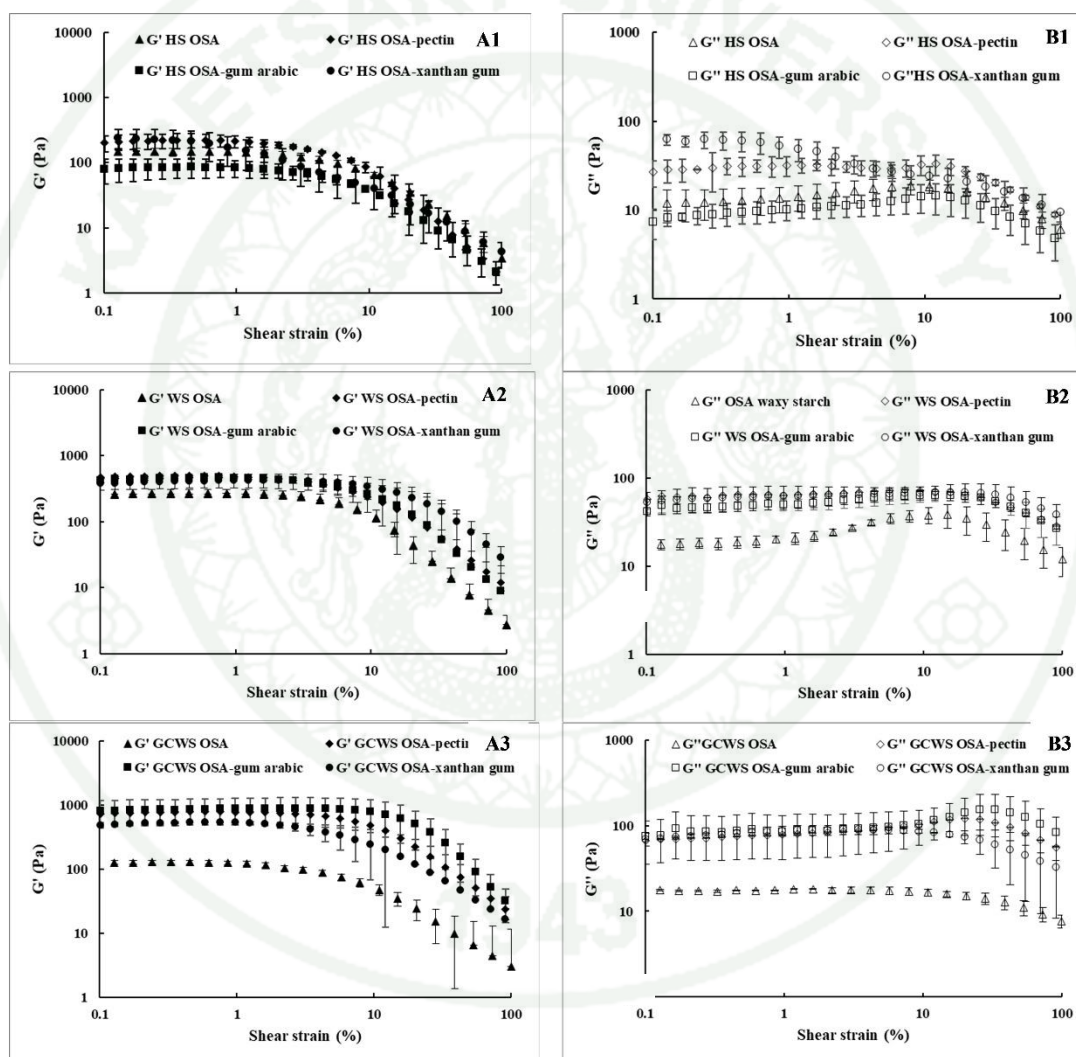


Figure 20 Amplitude sweep test ($\gamma = 0.1-100\%$) at 20°C showing (A) storage modulus and (B) loss modulus of Pickering emulsion stabilized by starch-based particles of (1) HS-OSA (2) WS-OSA (3) GCWS-OSA w/w/o polysaccharides.

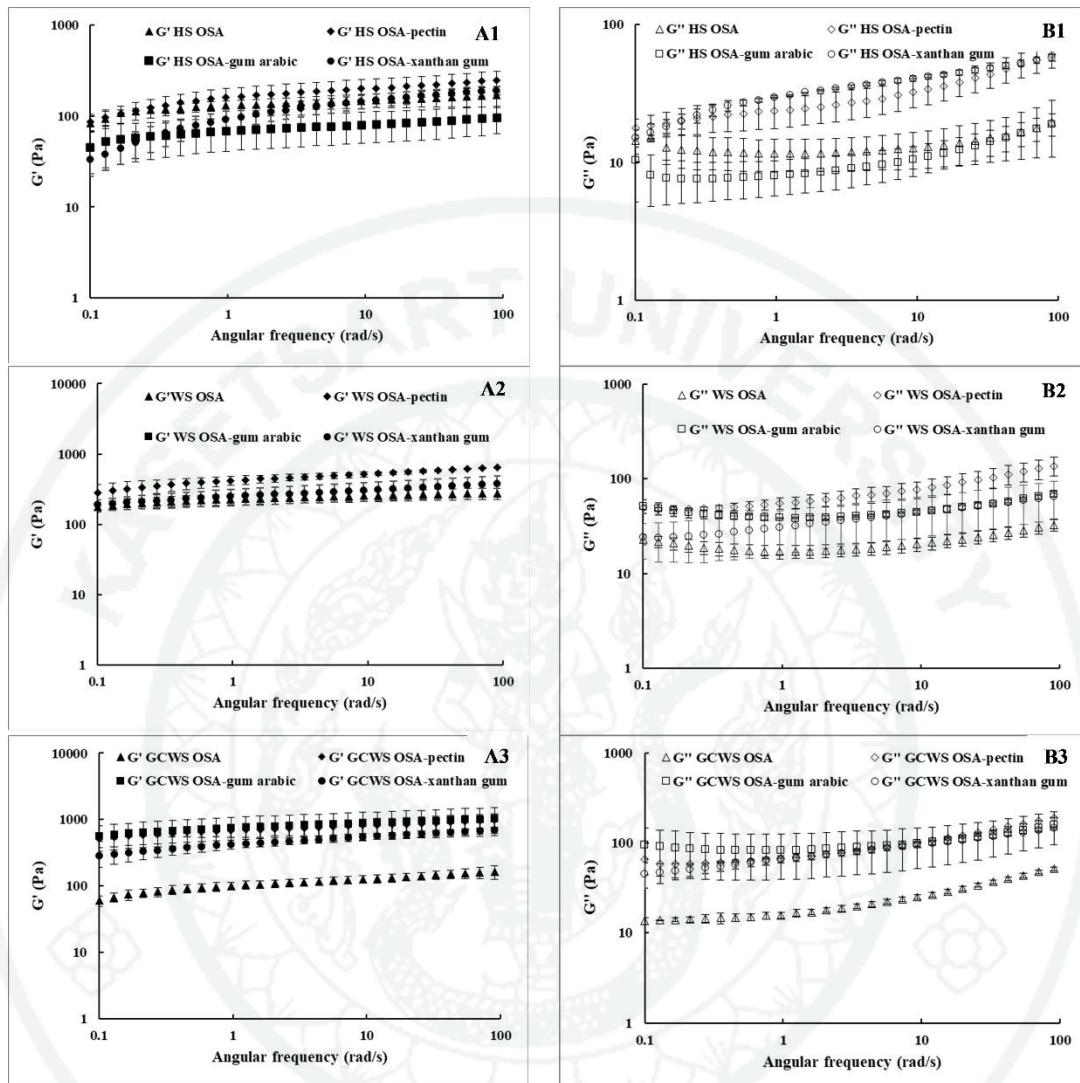


Figure 21 Frequency sweep test ($\omega = 0.1-100$ rad/s) at 20°C showing (A) storage modulus and (B) loss modulus of Pickering emulsion stabilized by starch-based particles of (1) HS-OSA (2) WS-OSA (3) GCWS-OSA w/wo polysaccharides.

2.2 Large amplitude oscillatory shear (LAOS)

2.2.1 Lissajous plot

G' and G'' were based only on the first harmonic contribution to the stress response which could have ambiguous physical meaning in the non-linear viscoelastic regime (NLVE). The non-linear and high harmonic contribution that induced a non-sinusoidal stress waveform were further investigated using LAOS. The elastic and viscous Lissajous plots demonstrated the intra-cycle stress of material as a function of applied strain and shear rate. These plots provided information on structural transition under large and rapid deformation of material which usually operated in food process. NLVE was observed when amplitude was increased from 5.77-100% and was demonstrated by Lissajous plot. The elastic contribution was plotted between shear stress (Pa) and shear strain (%) (Figure 22 left) and the viscous contribution was plotted between shear stress (Pa) and shear rate (1/s) (Figure 22 right) at five strains (1.18, 5.77, 14.90, 38.80, 100%). The dotted line indicated elastic stress and viscous stress, respectively (Ptaszek *et al.*, 2016).

At low strain (1.18%), all emulsions illustrated as elliptical shape or viscoelastic behavior and started to change to rhomboidal shape when imposed to higher strain (14.9-38.8%). At 5.77-100% strain, the secant modulus was higher than tangent modulus ($G'_L > G'_M$) indicated a nonlinear viscoelasticity with high harmonic contribution or a strain stiffening behavior. At higher strain, the Lissajous curve was distorted from elliptical to almost rectangular indicated a transition from elastic to viscous or plastic behavior.

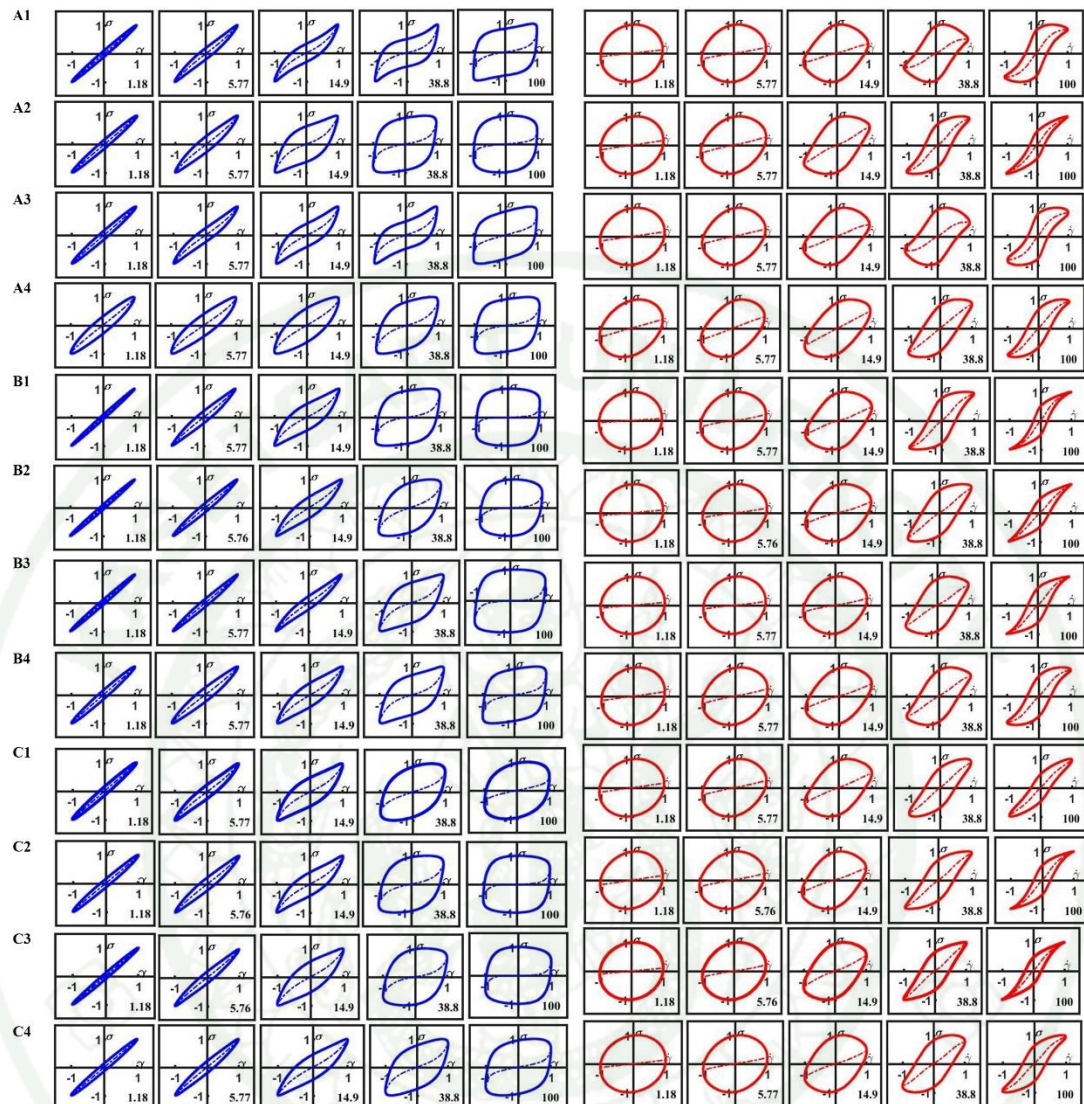


Figure 22 Normalized Lissajous plot of (left) shear stress (Pa) vs shear strain (%) and (right) shear stress (Pa) vs shear rate (1/s) of starch-based Pickering emulsion of (A) HS-OSA, (B) WS-OSA, (C) GCWS-OSA with (1) no hydrocolloid, (2) pectin, (3) gum arabic, and (4) xanthan gum

2.2.2 Strain-stiffening (S factor) and Shear-thickening (T factor)

The stiffening ratio (S factor) was predominantly positive over almost entire shear strain range indicated strain stiffening behavior and a transition from elastic to plastic behavior (Figure 23). The WS-OSA and GCWS-OSA emulsion of showed a

higher S factor than HS-OSA. Polysaccharide could increase S factor of the emulsions especially at high shear strain. The T factor represented shear thickening. It was calculated based on the ratio of the large rate (η'_L) and minimum rate (η'_M) dynamic viscosity (Eq.3). All emulsions had $\eta'_L > \eta'_M$ or shear thickening behavior (Figure 23). The T factor reached the maximum around 0.1% shear rate and dropped gradually. However, T factor was predominantly positive in all shear rate indicated an intra-cycle shear thickening in all samples. The OSA-starch emulsion without hydrocolloid had higher T factor than those with hydrocolloids.

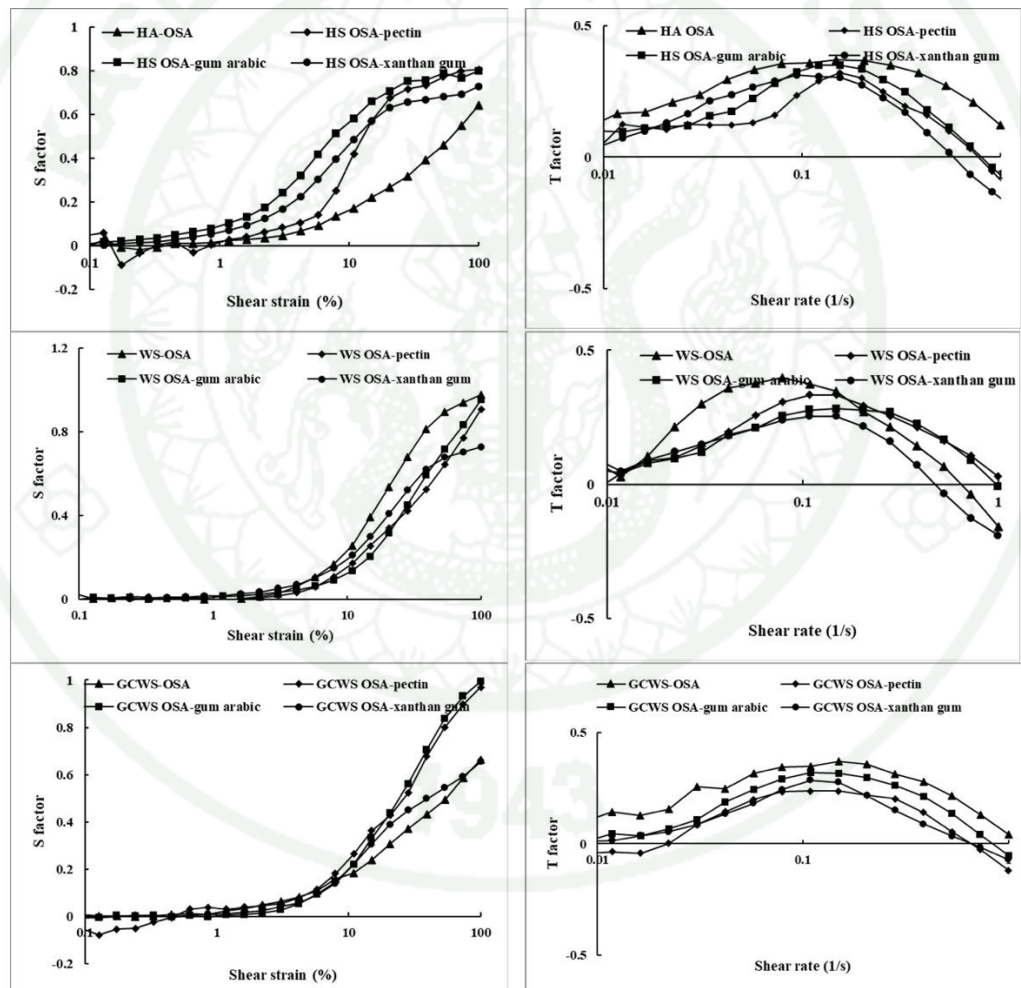


Figure 23 The S factor or ratio of shear stiffening and T factor or ratio of shear thickening of starch-based Pickering emulsion (60% oil), w/w hydrocolloids

3. Rheological properties of Oleogel

3.1 Small amplitude oscillatory shear (SAOS)

The G' of all oleogels was higher than G'' suggested the yielding of structure at higher stress. Oleogels from waxy starch (WS-OSA and GCWS-OSA) showed a higher G' and G'' than high amylose starch (HS-OSA) which demonstrated a stronger gel. The entanglement of the long-branched chain of waxy starch altogether with the higher DS of GCWS-OSA and WS-OSA could better stabilize emulsion and oleogel (Liu *et al.*, 2021; Luo *et al.*, 2019). G' and G'' of oleogels from WS-OSA and GCWS-OSA increased with the addition of gum arabic and xanthan gum, but decreased with pectin (Figure 24). The synergistic effect with polysaccharide promoted higher emulsion stability which led to stronger gel network in oleogel. The crossover point was noticed at 10% shear strain for HS-OSA oleogel and was delayed to 1% shear strain for GCWS-OSA and WS-OSA oleogel. The delayed crossover point of GCWS-OSA indicated a more difficult to break down and higher gel strength.

For frequency sweep test, all oleogels had solid-liked behavior as G' was much greater than G'' . G' and G'' were almost independent on frequencies ranging from 0.1-100 rad/s which indicated a well-structured gel system (Figure 25). The maximum G' was found in GCWS-OSA (10^6 Pa) which was much higher than WS-OSA (10^5 Pa) and HS-OSA (10^4 - 10^5 Pa) oleogel (Figure 25). There was no crossover point (G' equaled to G'') found in all oleogels even at higher frequency which indicated that the obtained oleogel did not transform into sol (Patel *et al.*, 2014).

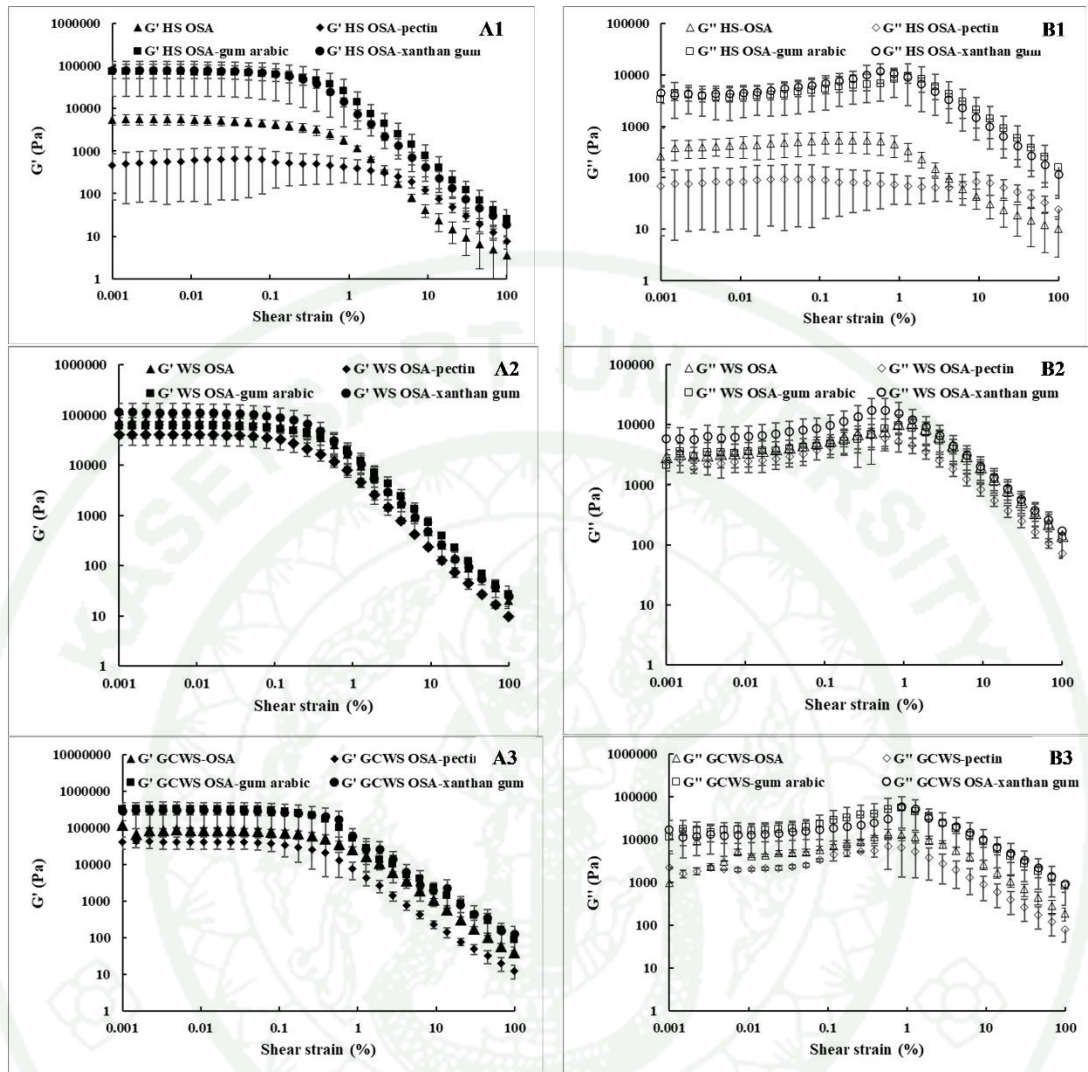


Figure 24 The amplitude sweep test ($\gamma = 0.1-100\%$) of oleogel from starch-based oleogel w/o polysaccharide showing storage modulus (G') and loss modulus (G'') at 20°C

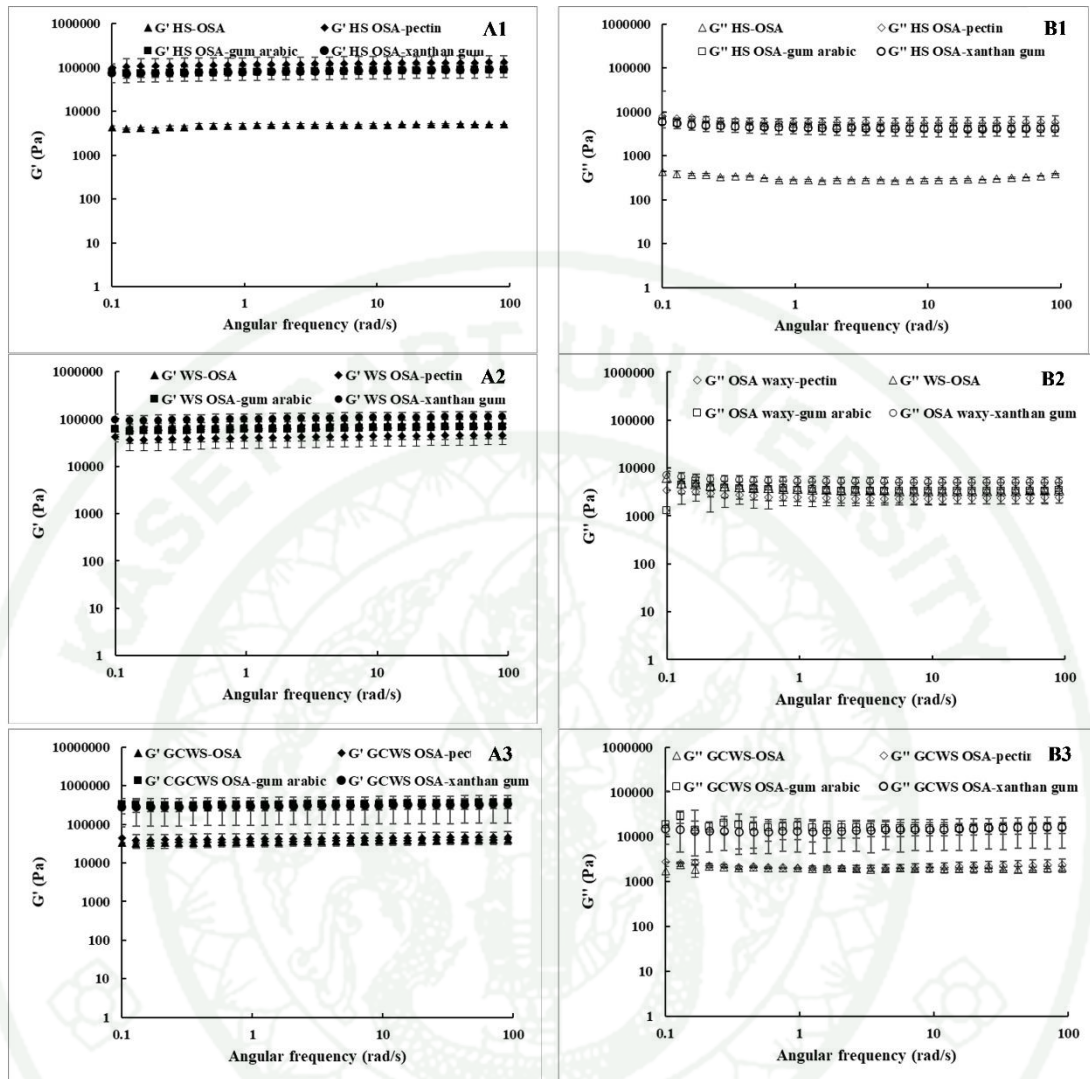


Figure 25 The frequency sweep test ($\omega = 0.1-100$ rad/s) of oleogel from starch-based oleogel w/wo polysaccharide showing storage modulus (G') and loss modulus (G'') at 20°C

3.2 Large amplitude oscillatory shear (LAOS)

3.2.1 Lissajous plot between shear stress and shear strain

At lower strain (0.0241% and 0.261%), the normalized Lissajous plot between shear stress and shear strain of all oleogels showed a sinusoidal shape with oscillatory stress response. The elastic and viscous contribution were in straight line

and elliptical shape, respectively, indicating a linear viscoelastic solid-like behavior (predominantly elastic). When strain was increased, the curve was distorted to the nonlinear regime or non-sinusoidal waveform. Change in Lissajous plot was related to microstructural attribute and structure response of material under large deformation (Li *et al.*, 2021). At larger strain (0.857%, 1.9%), all oleogels showed a wider elliptical shape which distorted to parallelogram form. The viscous dissipation increased during intracycle deformation and was shifted from elastic to viscous dominated behavior. At 20.5% strain, Lissajous curve was observed as rectangular shape or plastic behavior (Figure 26 left).

3.2.2 Lissajous plot between shear stress and shear strain

At small strain (0.0241% and 0.261%), the normalized Lissajous plot between shear stress and shear rate of all oleogels was observed as elliptical shape, suggesting a viscoelastic behavior. The viscous stress (dotted line inside the ellipse) was distorted slightly from the original shape, indicated a change from LVE to NLVE regime. At higher strain (0.857 %), Lissajous curve changed from an elliptical to sinusoidal shape, indicated a highly nonlinear viscoelastic behavior with strong shear-thickening. The viscous contribution began to emerge indicated by the slope of decomposed viscous stress (dotted line inside the loops) from ellipse to S-shape and the enclosed area expanded significantly which suggested a breakdown of structure. Lissajous plot of HS-OSA without hydrocolloids remained elliptical shape, indicating a LVE regime and remained highly viscous (Figure 26 right). Liu *et al.* (2021) proposed that OSA starch could provide emulsion with large G' (almost 10^3 Pa) with stronger network and more elastic gel-like emulsion. The oleogel from OSA starch had stable structure and high mechanical strength which was appropriate to be used as fat mimetic.

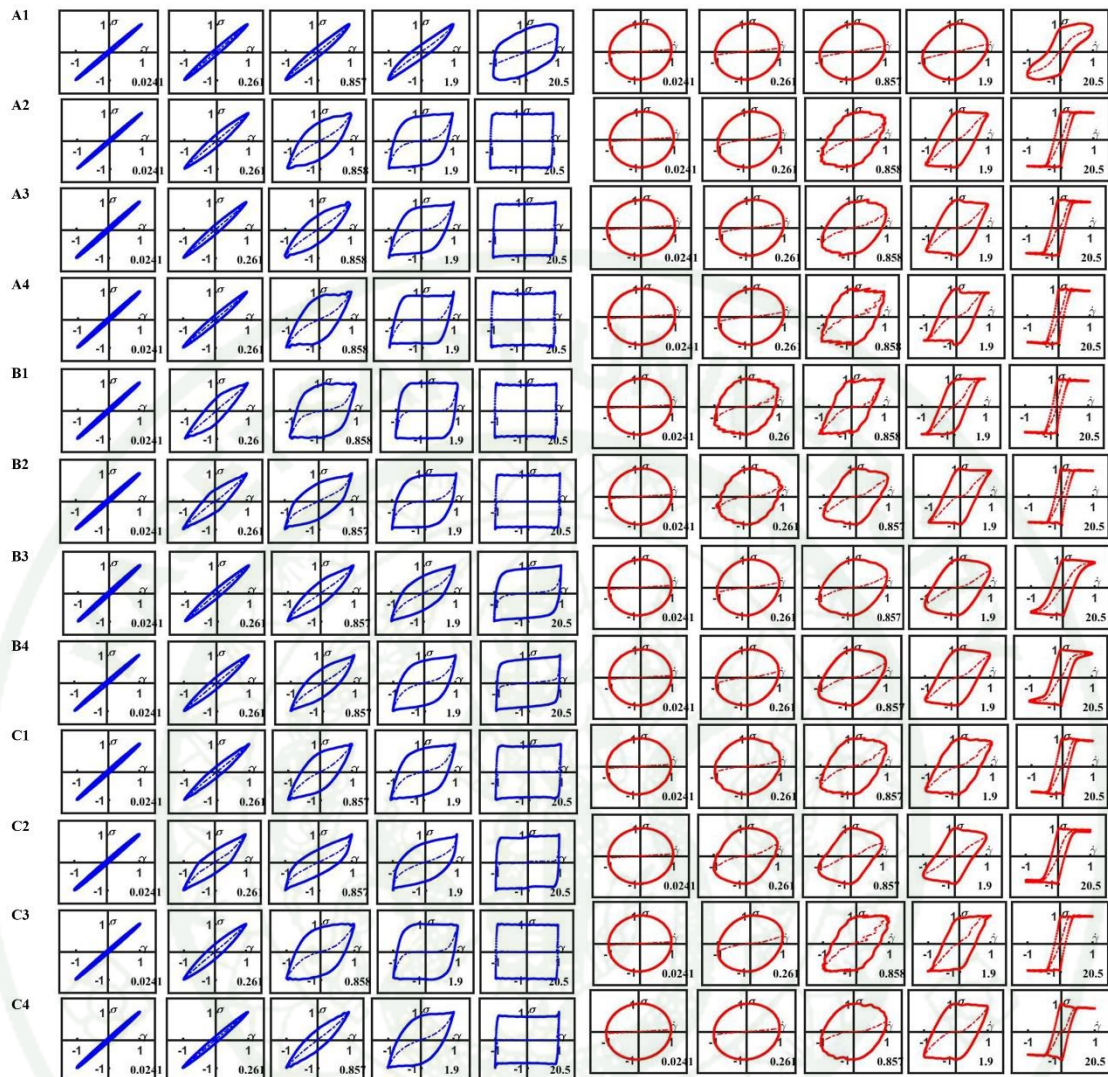


Figure 26 Normalized Lissajous plot of (left) shear stress (Pa) vs shear strain (%) and (right) shear stress (Pa) vs shear rate (1/s) of starch-based oleogel of (A) HS-OSA, (B) WS-OSA, (C) GCWS-OSA and (1) no hydrocolloid, (2) pectin, (3) gum arabic, and (4) xanthan gum

3.2.3 Strain-stiffening (S factor) and Shear-thickening (T factor)

The strain-stiffening (S factor) and shear-thickening (T factor) were used to determine the change in elastic modulus and instantaneous viscosity of material under shear (Figure 27). Strain-stiffening or hardening was imposed when S factor > 0 and strain softening or thinning was noticed when S factor < 0 . All oleogels had positive

S factors which increased at higher strain, indicating a strong shear-stiffening behavior. Furthermore, T factor of oleogels from GCWS-OSA and WS-OSA with polysaccharide increased drastically and then decreased, showing a shear-thickening behavior.

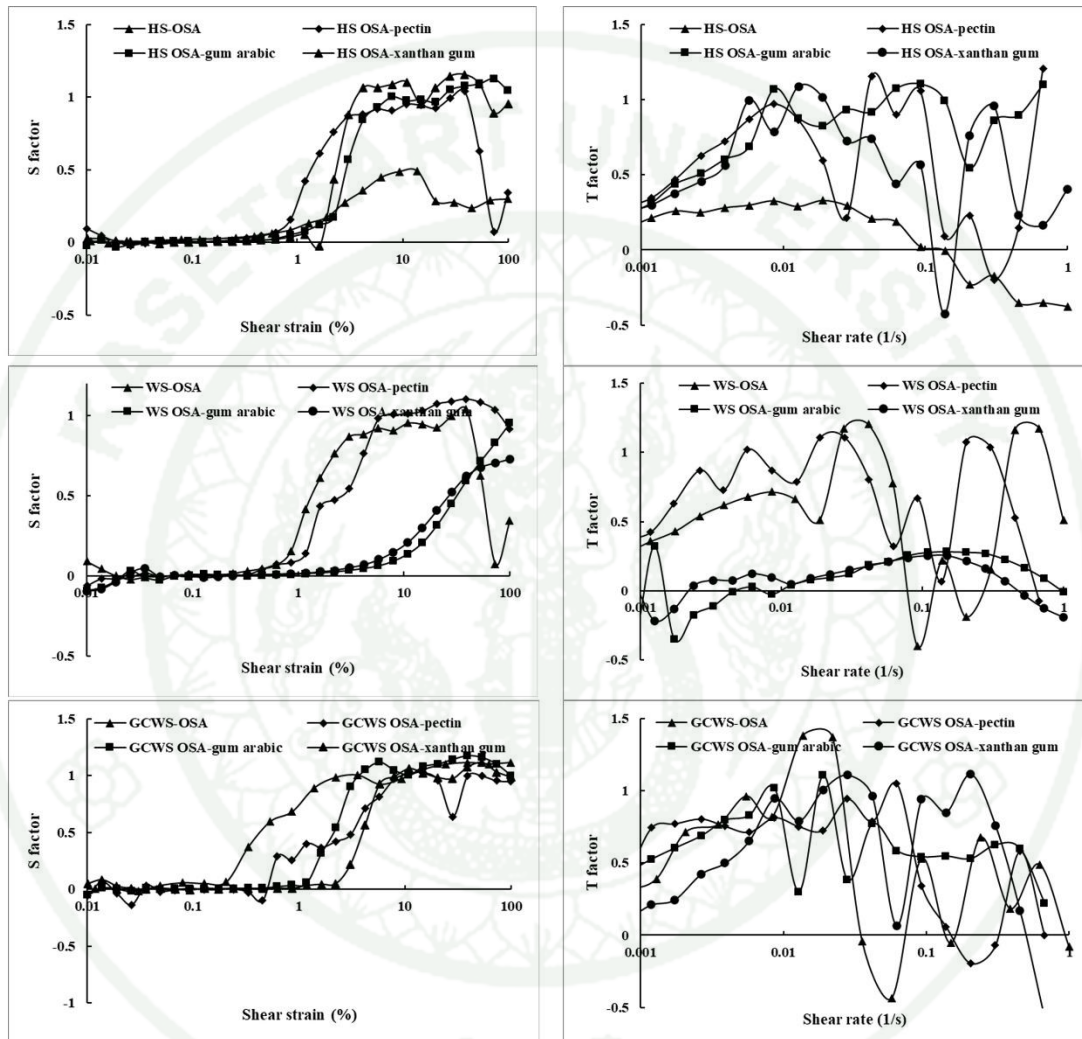


Figure 27 The S factor or shear stiffening and T factor or shear thickening of starch-based oleogel (60% oil), w/w/o polysaccharides

4. Oleogel as fat mimetic in food model

The emulsion type sausage was formulated using 75% oleogel substitution for lard. Result showed no significant differences in texture profile analysis of sample using

WS-OSA and GCWS-OSA oleogel comparing with control (100 % lard) ($p \leq 0.05$) (Figure 28).

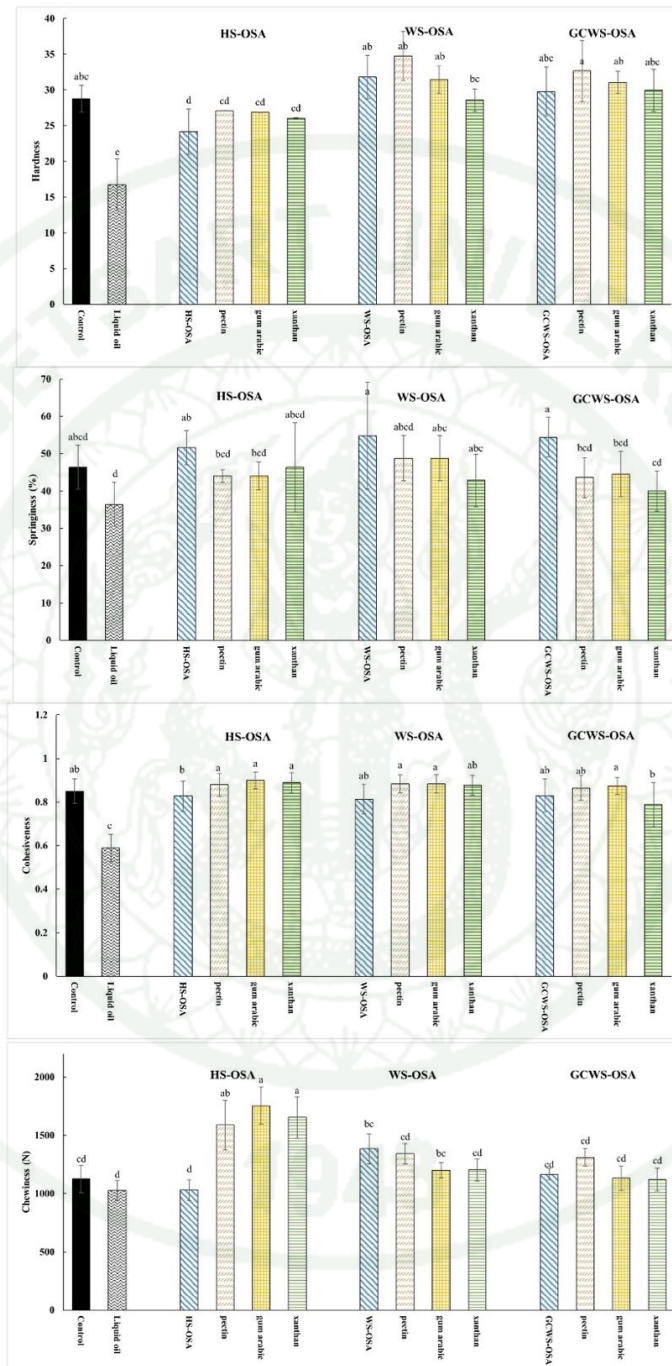


Figure 28 Texture profile analysis of emulsion type sausage from various types of oleogel (75% substitution) comparing with positive control (100% lard) and negative control (100% liquid oil)

Note: ^{a-e}mean±SD with different lowercase letter superscript indicated significant difference ($p\leq 0.05$)

Sample with HS-OSA oleogel had higher chewiness and lower hardness than control which agreed well with its low G' or soft gel characteristic oleogel. Sausage made with liquid oil was substantially different from control both textural properties and appearance (Figure 29). The result supports the possibility of OSA starch based oleogel to be used as a fat mimetic in foods.

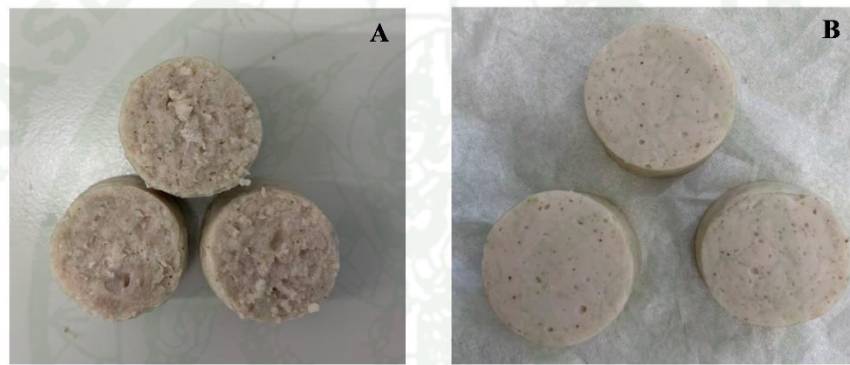


Figure 29 Emulsion-type sausage made from (A) 100% liquid oil (B) oleogel (75% substitution)

CONCLUSION

Low concentration of polysaccharides (0.2–0.3% w/v) successfully inhibited acrylamide formation in the chemical model, although chitosan was even increased acrylamide formation. In the food system, polysaccharides (1% w/v) reduced acrylamide by up to 53.5% during frying but much lower when microwaved (5.2%). Alginate was the most effective inhibitor of acrylamide formation in both chemical and food model, followed by pectin. The zein and polysaccharide complex could also reduce acrylamide at high temperature in chemical and food models. The mixture of zein and polysaccharide (non-complex particles) was less effective in acrylamide mitigation, emphasized the effect of complex particles. This study provided a new application of protein–polysaccharide complex particles for acrylamide mitigation.

GCWS-OSA had the highest degree of OSA substitution. The Pickering emulsion stabilized by this starch had the smallest average droplet size. In the linear viscoelastic regime, GCWS-OSA particles were soft and more easily deformable at the interface of the droplets. It was interesting to see that the template emulsion with the lowest stiffness (GCWS-OSA) gave the strongest oleogel. The smaller droplet size led to a more homogeneous network, with higher stiffness. Starch structure and degree of substitution were noticed as main parameter to stabilized emulsion and oleogel. GCWS had a loose internal structure, molecular chains break, and higher solubility which allowed more hydroxyl groups to expose with OSA resulted in an increase in substitution reaction. The emulsifying properties depend largely on the surface characteristics was increased with DS. As a result, oleogel from GCWS-OSA with gum Arabic and xanthan gum could produce oleogel of better rheological properties to be used as a fat mimetic in emulsion type sausage. These structured oil systems could be applied to formulate low saturated fat products.

LITERATURE CITED

- Abbasi, E., R. Amini Sarteshnizi, H. Ahmadi Gavlighi, M. Nikoo, M.H. Azizi and N. Sadeghinejad. 2019. Effect of partial replacement of fat with added water and tragacanth gum (*Astragalus gossypinus* and *Astragalus compactus*) on the /fat emulsion type sausage. **Meat Science** 147: 135-143.
- Alonso-Sande, M., M. Cuña, C. Remuñán-López, D. Tejeiro-Osorio, J.L. Alonso-Lebrero and M.J. Alonso. 2006. Formation of new glucomannan–chitosan nanoparticles and study of their ability to associate and deliver proteins. **Macromolecules** 39: 4152-4158.
- Anese, M., L. Manzocco, S. Calligaris and M.C. Nicoli. 2013. Industrially applicable strategies for mitigating acrylamide, furan, and 5-hydroxymethylfurfural in food. **Journal of Agricultural and Food Chemistry** 61: 10209-10214.
- _____, M. Suman and M.C. Nicoli. 2009. Technological strategies to reduce acrylamide levels in heated foods. **Food Engineering Reviews** 1: 169-179.
- Atashkar, M., M. Hojjatoleslami and L. Sedaghat Boroujeni. 2018. The influence of fat substitution with κ -carrageenan, konjac, and tragacanth on the textural properties of low-fat sausage. **Food science and nutrition** 6: 1015-1022.
- Barutcu, I., S. Sahin and G. Sumnu. 2009. Acrylamide formation in different batter formulations during microwave frying. **LWT - Food Science and Technology** 42: 17-22.
- Belgin Erdoğan, S., T.K. Palazoğlu, V. Gökmen, H.Z. Şenyuva and H.İ. Ekiz. 2007. Reduction of acrylamide formation in french fries by microwave pre-cooking of potato strips. **Journal of the Science of Food and Agriculture** 87: 133-137.

- Bello-Pérez, L.A., C.A. Bello-Flores, M.d.C. Nuñez-Santiago, C.P. Coronel-Aguilera and J. Alvarez-Ramirez. 2015. Effect of the degree of substitution of octenyl succinic anhydride-banana starch on emulsion stability. **Carbohydrate Polymers** 132: 17-24.
- BeMiller, J.N. 2019a. 17 - carbohydrate nutrition, dietary fiber, bulking agents, and fat mimetics, p. 323-350. *In* J. N. BeMiller, eds. **Carbohydrate chemistry for food scientists** (third edition). AACC International Press.
- _____. 2019b. 18 - nonenzymic browning and formation of acrylamide and caramel, p. 351-370. *In* J. N. BeMiller, eds. **Carbohydrate chemistry for food scientists** (third edition). AACC International Press.
- Berton-Carabin, C. C., and K. Schroen. 2015. Pickering emulsions for food applications: background, trends, and challenges. **Annual Review of Food Science and Technology** 6, 263-297.
- Biedermann, M., A. Noti, S. Beidermann-Brem, V. Mozzetti and K. Grob. 2002. Experiments on acrylamide formation and possibilities to decrease the potential of acrylamide formation in potatoes. **Mitteilungen aus Lebensmitteluntersuchung und Hygiene** 93: 668-687.
- Bos, M., A. and v.T. Vliet. 2001. Interfacial rheological properties of adsorbed protein layers and surfactants: A review. **Advances in Colloid and Interface Science** 91: 437-471.
- Bower, C., C. Gallegos, M.R. Mackley and J.M. Madiedo. 1999. The rheological and microstructural characterisation of the non-linear flow behaviour of concentrated oil-in-water emulsions. **Rheologica Acta** 38: 145-159.
- Campañone, L.A. and N.E. Zaritzky. 2005. Mathematical analysis of microwave heating process. **Journal of Food Engineering** 69: 359-368.

- Capuano, E. and V. Fogliano. 2011. Acrylamide and 5-hydroxymethylfurfural (hmf): A review on metabolism, toxicity, occurrence in food and mitigation strategies. **LWT - Food Science and Technology** 44: 793-810.
- Champrasert, O., J. Chu, Q. Meng, S. Viney, M. Holmes, P. Suwannaporn and C. Orfila. 2021. Inhibitory effect of polysaccharides on acrylamide formation in chemical and food model systems. **Food Chemistry** 363: 130213.
- Chang, C., T. Wang, Q. Hu, M. Zhou, J. Xue and Y. Luo. 2017. Pectin coating improves physicochemical properties of caseinate/zein nanoparticles as oral delivery vehicles for curcumin. **Food Hydrocolloids** 70: 143-151.
- Chang, Y.-W., W.-C. Sung and J.-Y. Chen. 2016. Effect of different molecular weight chitosans on the mitigation of acrylamide formation and the functional properties of the resultant Maillard reaction products. **Food Chemistry** 199: 581-589.
- Chen, J. and J.-L. Jane. 1994. Properties of granular cold-water-soluble starches prepared by alcoholic-alkaline treatments. **Cereal Chemistry** 71(6).
- Chen, H. and Q. Zhong. 2015. A novel method of preparing stable zein nanoparticle dispersions for encapsulation of peppermint oil. **Food Hydrocolloids** 43: 593-602.
- Chen, L., G.E. Remondetto and M. Subirade. 2006. Food protein-based materials as nutraceutical delivery systems. **Trends in Food Science & Technology** 17: 272-283.
- Cheng, K.W., X. Zeng, Y.S. Tang, J.J. Wu, Z. Liu, K.H. Sze, I.K. Chu, F. Chen and M. Wang. 2009. Inhibitory mechanism of naringenin against carcinogenic acrylamide formation and nonenzymatic browning in Maillard model reactions. **Chemical Research in Toxicology** 22: 1483-1489.

- Claeys, W.L., K. de Vleeschouwer and M.E. Hendrickx. 2005. Effect of amino acids on acrylamide formation and elimination kinetics. **Biotechnology Progress** 21: 1525-1530.
- Cooper, C.L., P.L. Dubin, A.B. Kayitmazer and S. Turksen. 2005. Polyelectrolyte–protein complexes. **Current Opinion in Colloid & Interface Science** 10: 52-78.
- Dai, L., C. Sun, Y. Wei, L. Mao and Y. Gao. 2018. Characterization of Pickering emulsion gels stabilized by zein/gum arabic complex colloidal nanoparticles. **Food Hydrocolloids** 74: 239-248.
- de Folter, J.W.J., M.W.M. van Ruijven and K.P. Velikov. 2012. Oil-in-water Pickering emulsions stabilized by colloidal particles from the water-insoluble protein zein. **Soft Matter** 8: 6807-6815.
- de Kruif, C.G. and R. Tuinier. 2001. Polysaccharide protein interactions. **Food Hydrocolloids** 15: 555-563.
- Dickinson, E. 2017. Biopolymer-based particles as stabilizing agents for emulsions and foams. **Food Hydrocolloids** 68: 219-231.
- Dissanayake, M. and T. Vasiljevic. 2009. Functional properties of whey proteins affected by heat treatment and hydrodynamic high-pressure shearing. **Journal of Dairy Science** 92: 1387-1397.
- Doublier, J.L., C. Garnier, D. Renard and C. Sanchez. 2000. Protein–polysaccharide interactions. **Current Opinion in Colloid & Interface Science** 5: 202-214.

- Duvarci, O.C., G. Yazar and J.L. Kokini. 2017. The comparison of LAOS behavior of structured food materials (suspensions, emulsions, and elastic networks). **Trends in Food Science and Technology**. 60: 2-11.
- Dybing, E. and T. Sanner. 2003. Risk assessment of acrylamide in foods. **Toxicological Sciences** 75: 7-15.
- Eastman, J. E. 1987. **Cold water swelling starch composition**. U. S. Patent 4,634,596.
- _____, and C. O. Moore. 1984. **Cold water soluble granular starch for gelled food compositions**. U. S. Patent 4,465,702.
- EFSA. 2009. Scientific report of EFSA prepared by data collection and exposure unit (datex) on monitoring of acrylamide levels in food. **The EFSA Scientific Report** 285: 1-26.
- Elzoghby, A.O., W.M. Samy and N.A. Elgindy. 2012. Protein-based nanocarriers as promising drug and gene delivery systems. **Journal of Controlled Release** 161: 38-49.
- Emerich, D.F. and C.G. Thanos. 2007. Targeted nanoparticle-based drug delivery and diagnosis. **Journal of Drug Targeting** 15: 163-183.
- Ewoldt, R.H., A.E. Hosoi and G.H. McKinley. 2008. New measures for characterizing nonlinear viscoelasticity in large amplitude oscillatory shear. **Journal of Rheology** 52: 1427-1458.
- Ewoldt, R.H., P. Winter, J. Maxey and G.H. McKinley. 2010. Large amplitude oscillatory shear of pseudoplastic and elastoviscoplastic materials. **Rheologica Acta**. 49: 191-212.

- Feng, Y. and Y. Lee. 2016. Surface modification of zein colloidal particles with sodium caseinate to stabilize oil-in-water Pickering emulsion. **Food Hydrocolloids** 56: 292-302.
- Galani, J.H.Y., N.J. Patel and J.G. Talati. 2017. Acrylamide-forming potential of cereals, legumes and roots and tubers analyzed by HPLC-UV. **Food and Chemical Toxicology** 108: 244-248.
- Gao, J.Y., P.L. Dubin and B.B. Muhoberac. 1997. Measurement of the binding of proteins to polyelectrolytes by frontal analysis continuous capillary electrophoresis. **Analytical Chemistry** 69: 2945-2951.
- Gao, Z.-M., X.-Q. Yang, N.-N. Wu, L.-J. Wang, J.-M. Wang, J. Guo and S.-W. Yin. 2014. Protein-based Pickering emulsion and oil gel prepared by complexes of zein colloidal particles and stearate. **Journal of Agricultural and Food Chemistry** 62: 2672-2678.
- Gaonkar, A.G. 1991. Surface and interfacial activities and emulsion characteristics of some food hydrocolloids. **Food Hydrocolloids** 5: 329-337.
- Gasteiger, E., C. Hoogland, A. Gattiker, S.e. Duvaud, M.R. Wilkins, R.D. Appel and A. Bairoch. 2005. Protein identification and analysis tools in the ExPASy server, p. 571-607. *In* J. M. Walker, eds. **The proteomics protocols handbook**. Humana Press, Totowa, NJ.
- Ge, S., L. Xiong, M. Li, J. Liu, J. Yang, R. Chang, C. Liang and Q. Sun. 2017. Characterizations of Pickering emulsions stabilized by starch nanoparticles: Influence of starch variety and particle size. **Food Chemistry** 234: 339-347.

- Ghosh, A., G. Chaudhary, J.G. Kang, P.V. Braun, R.H. Ewoldt and K.S. Schweizer. 2019. Linear and nonlinear rheology and structural relaxation in dense glassy and jammed soft repulsive pNIPAM microgel suspensions. **Soft Matter** 15: 1038-1052.
- Gibis, M., V. Schuh and J. Weiss. 2015. Effects of carboxymethyl cellulose (CMC) and microcrystalline cellulose (MCC) as fat replacers on the microstructure and sensory characteristics of fried beef patties. **Food Hydrocolloids** 45: 236-246.
- Girard, M., S.L. Turgeon and S.F. Gauthier. 2003. Quantification of interactions between β -lactoglobulin and pectin through capillary electrophoresis analysis. **Journal of Agricultural and Food Chemistry** 51(20): 6043-6049.
- Gertz, C. and S. Klostermann. 2002. Analysis of acrylamide and mechanisms of its formation in deep-fried products. **European Journal of Lipid Science and Technology** 104: 762-771.
- Gökmen, V. and H.Z. Şenyuva. 2006. A simplified approach for the kinetic characterization of acrylamide formation in fructose-asparagine model system. **Food Additives & Contaminants** 23: 348-354.
- Gökmen, V. and H.Z. Şenyuva. 2007. Acrylamide formation is prevented by divalent cations during the Maillard reaction. **Food Chemistry** 103: 196-203.
- Goldberg, M., R. Langer and X. Jia. 2007. Nanostructured materials for applications in drug delivery and tissue engineering. **Journal of Biomaterials Science, Polymer Edition** 18: 241-268.
- Granda, C., R.G. Moreira and S.E. Tichy. 2004. Reduction of acrylamide formation in potato chips by low-temperature vacuum frying. **Journal of Food Science** 6(69): E405-E411.

- Hoffmann, H. and M. Reger. 2013. Emulsions with unique properties from proteins as emulsifiers. **Advances in Colloid and Interface Science** 205: 95-104.
- Hogervorst, J.G., L.J. Schouten, E.J. Konings, R.A. Goldbohm and P.A. van den Brandt. 2007. A prospective study of dietary acrylamide intake and the risk of endometrial, ovarian, and breast cancer. **Cancer Epidemiology, Biomarkers & Prevention** 16: 2304-2313.
- Hu, K., X. Huang, Y. Gao, X. Huang, H. Xiao and D.J. McClements. 2015. Core-shell biopolymer nanoparticle delivery systems: Synthesis and characterization of curcumin fortified zein-pectin nanoparticles. **Food Chemistry** 182: 275-281.
- Hu, K. and D.J. McClements. 2015. Fabrication of biopolymer nanoparticles by antisolvent precipitation and electrostatic deposition: Zein-alginate core/shell nanoparticles. **Food Hydrocolloids** 44: 101-108.
- Hyun, K., M. Wilhelm, C.O. Klein, K.S. Cho, J.G. Nam, K.H. Ahn, S.J. Lee, R.H. Ewoldt and G.H. McKinley. 2011. A review of nonlinear oscillatory shear tests: Analysis and application of large amplitude oscillatory shear (LAOS). **Progress in Polymer Science** 36: 1697-1753.
- Jiang, Y., L. Liu, B. Wang, X. Sui, Y. Zhong, L. Zhang, Z. Mao and H. Xu. 2018. Cellulose-rich oleogels prepared with an emulsion-templated approach. **Food Hydrocolloids** 77: 460-464.
- Jones, O.G. and D.J. McClements. 2008. Stability of biopolymer particles formed by heat treatment of β -lactoglobulin/beet pectin electrostatic complexes. **Food Biophysics** 3: 191-197.
- Jones, O.G. and D.J. McClements. 2010. Biopolymer nanoparticles from heat-treated electrostatic protein-polysaccharide complexes: Factors affecting particle characteristics. **Journal of Food Science** 75: N36-43.

- Jones, O.G. and D.J. McClements. 2011. Recent progress in biopolymer nanoparticle and microparticle formation by heat-treating electrostatic protein-polysaccharide complexes. **Advances in Colloid and Interface Science** 167: 49-62.
- Jozinović, A., B. Šarkanj, Đ. Ačkar, J. Panak Balentić, D. Šubarić, T. Cvetković, J. Ranilović, S. Guberac and J. Babić. 2019. Simultaneous determination of acrylamide and hydroxymethylfurfural in extruded products by LC-MS/MS method. **Molecules** 24: 1971.
- Kadu, P.J., S.S. Kushare, D.D. Thacker and S.G. Gattani. 2011. Enhancement of oral bioavailability of atorvastatin calcium by self-emulsifying drug delivery systems (SEDDS). **Pharmaceutical Development and Technology** 16: 65-74.
- Keramat, J., A. LeBail, C. Prost and M.J.F. Jafari. 2011. Acrylamide in baking products: A review article. **Food and Bioprocess Technology** 4: 530-543.
- Kim, C.T., E.-S. Hwang and H.J. Lee. 2005. Reducing acrylamide in fried snack products by adding amino acids. **Journal of Food Science** 70: C354-C358.
- Krishnakumar, T. and R. Visvanathan. 2014. Acrylamide in food products: A review. **Journal of Food Processing & Technology** 05: 5-7.
- Kulkarni, G.T., K. Gowthamarajan, R.R. Dhobe, F. Yohanan and B. Suresh. 2005. Development of controlled release spheroids using natural polysaccharide as release modifier. **Drug Delivery** 12: 201-206.
- Lee, J.C.-W., L. Porcar and S.A. Rogers. 2019. Unveiling temporal nonlinear structure–rheology relationships under dynamic shearing. **Polymers** 1: 1189.

- Li, M.F., L. Chen, M.Z. Xu, J.L. Zhang, Q. Wang, Q.Z. Zeng, X.C. Wei and Y. Yuan. 2018. The formation of zein-chitosan complex coacervated particles: Relationship to encapsulation and controlled release properties. **International Journal of Biological Macromolecules** 116: 1232-1239.
- Li, Q., M. Xu, J. Xie, E. Su, Z. Wan, L.M.C. Sagis and X. Yang. 2021. Large amplitude oscillatory shear (LAOS) for nonlinear rheological behavior of heterogeneous emulsion gels made from natural supramolecular gelators. **Food Research International** 140: 110076.
- Li, H., D. Wang, C. Liu, J. Zhu, M. Fan, X. Sun, T. Wang, Y. Xu and Y. Cao. 2019. Fabrication of stable zein nanoparticles coated with soluble soybean polysaccharide for encapsulation of quercetin. **Food Hydrocolloids** 87: 342-351.
- Lindsay, R. and S. Jang. 2005. Chemical intervention strategies for substantial suppression of acrylamide formation in fried potato products. **Advances in Experimental Medicine and Biology** 561: 393-404.
- Linke, C. and S. Drusch. 2017. Pickering emulsions in foods - opportunities and limitations. **Critical Reviews in Food Science and Nutrition** 58(12):1971-1985.
- Liu, H., X.M. Xu and S.D. Guo. 2007. Rheological, texture and sensory properties of low-fat mayonnaise with different fat mimetics. **LWT - Food Science and Technology** 40: 946-954.
- Liu, S., Y. Xiao, M. Shen, X. Zhang, W. Wang and J. Xie. 2019. Effect of sodium carbonate on the gelation, rheology, texture and structural properties of maize starch-mesona chinensis polysaccharide gel. **Food Hydrocolloids** 87: 943-951.

- Liu, W., Y. Li, M. Chen, F. Xu and F. Zhong. 2018. Stabilizing oil-in-water emulsion with amorphous and granular octenyl succinic anhydride modified starches. **Journal of Agricultural and Food Chemistry** 66: 9301-9308.
- Liu, X., S. Ding, J. Wu, G. Liu, J. Wei, F. Yang and X. Liu. 2021. Molecular structures of octenyl succinic anhydride modified starches in relation to their ability to stabilize high internal phase emulsions and oleogels. **Food Hydrocolloids** 120: 106953.
- Luo, S.-Z., X.-F. Hu, Y.-J. Jia, L.-H. Pan, Z. Zheng, Y.-Y. Zhao, D.-D. Mu, X.-Y. Zhong and S.-T. Jiang. 2019. Camellia oil-based oleogels structuring with tea polyphenol-palmitate particles and citrus pectin by emulsion-templated method: Preparation, characterization and potential application. **Food Hydrocolloids** 95: 76-87.
- Luo, Y., Z. Teng and Q. Wang. 2012. Development of zein nanoparticles coated with carboxymethyl chitosan for encapsulation and controlled release of vitamin D3. **Journal of Agricultural and Food Chemistry** 60: 836-843.
- Luo, Y., B. Zhang, M. Whent, L.L. Yu and Q. Wang. 2011. Preparation and characterization of zein/chitosan complex for encapsulation of alpha-tocopherol, and its in vitro controlled release study. **Colloids and Surfaces B: Biointerfaces** 85: 145-152.
- Lv, P., D. Wang, L. Dai, X. Wu, Y. Gao and F. Yuan. 2020. Pickering emulsion gels stabilized by high hydrostatic pressure-induced whey protein isolate gel particles: Characterization and encapsulation of curcumin. **Food Research International** 132: 109032.
- Marangoni, A. G., and N. Garti. 2018. **Edible oleogels: Structure and health implications (2nd ed.)**. Urbana, Illinois: AOCS Press.

- Maskan, M. 2001. Kinetics of colour change of kiwifruits during hot air and microwave drying. **Journal of Food Engineering** 48: 169-175.
- Mason, T.G., J. Bibette and D.A. Weitz. 1995. Elasticity of compressed emulsions. **Physical Review Letters** 75: 2051-2054.
- Matulis, R.J., F.K. McKeith, J.W. Sutherland and M.S. Brewer. 1995. Sensory characteristics of frankfurters as affected by fat, salt, and pH. **Journal of Food Science** 60: 42-47.
- McClements, D.J., E.A. Decker and Y. Park. 2009. Controlling lipid bioavailability through physicochemical and structural approaches. **Critical Reviews in Food Science and Nutrition** 49: 48-67.
- Melito, H.S., C.R. Daubert and E.A. Foegeding. 2013. Relationships between nonlinear viscoelastic behavior and rheological, sensory and oral processing behavior of commercial cheese. **Journal of texture study** 44: 253-288.
- Michalak, J., M. Czarnowska-Kujawska, J. Klepacka and E. Gujska. 2020. Effect of microwave heating on the acrylamide formation in foods. **Molecules** 25: 4140.
- Michalak, J., E. Gujska, M. Czarnowska-Kujawska and F. Nowak. 2017. Effect of different home-cooking methods on acrylamide formation in pre-prepared croquettes. **Journal of Food Composition and Analysis** 56: 134-139.
- Modig, G., L. Nilsson, B. Bergenståhl and K.-G. Wahlund. 2006. Homogenization-induced degradation of hydrophobically modified starch determined by asymmetrical flow field-flow fractionation and multi-angle light scattering. **Food Hydrocolloids** 20: 1087-1095.

- Morales, G., M. Jimenez, O. Garcia, M.R. Mendoza and C.I. Beristain. 2014. Effect of natural extracts on the formation of acrylamide in fried potatoes. **LWT - Food Science and Technology** 58: 587-593.
- Mottram, D.S., B.L. Wedzicha and A.T. Dodson. 2002. Acrylamide is formed in the Maillard reaction. **Nature** 419: 448-449.
- Mousa, R.M.A. 2018. Simultaneous inhibition of acrylamide and oil uptake in deep fat fried potato strips using gum arabic-based coating incorporated with antioxidants extracted from spices. **Food Hydrocolloids** 83: 265-274.
- Mozaffarian, D. and R. Clarke. 2009. Quantitative effects on cardiovascular risk factors and coronary heart disease risk of replacing partially hydrogenated vegetable oils with other fats and oils. **European Journal of Clinical Nutrition**. 63: S22-S33.
- Mudalige, T., H. Qu, D. Van Haute, S.M. Ansar, A. Paredes and T. Ingle. 2019. Chapter 11 - characterization of nanomaterials: Tools and challenges, p. 313-353. *In* A. López Rubio, et al., eds. **Nanomaterials for food applications** Elsevier.
- Mudgett, R.E. 1989. Microwave food processing. **Food Technology** 43: 117.
- Nilsson, L. and B. Bergenståhl. 2006. Adsorption of hydrophobically modified starch at oil/water interfaces during emulsification. **Langmuir** 22: 8770-8776.
- Norton, I.T. and W.J. Frith. 2001. Microstructure design in mixed biopolymer composites. **Food Hydrocolloids** 15: 543-553.
- Oliveira, M.E.C. and A.S. Franca. 2002. Microwave heating of foodstuffs. **Journal of Food Engineering** 53: 347-359.

- Orzáez Villanueva, M.T., A. Díaz Marquina, E. Franco Vargas and G. Blázquez Abellán. 2000. Modification of vitamins B1 and B2 by culinary processes: Traditional systems and microwaves. **Food Chemistry** 71: 417-421.
- Ou, S., Q. Lin, Y. Zhang, C. Huang, X. Sun and L. Fu. 2008. Reduction of acrylamide formation by selected agents in fried potato crisps on industrial scale. **Innovative Food Science & Emerging Technologies** 9: 116-121.
- Park, J.J., I.F. Olawuyi and W.Y. Lee. 2020. Characteristics of low-fat mayonnaise using different modified arrowroot starches as fat replacer. **International Journal of Biological Macromolecules** 153: 215-223.
- Parzefall, W. 2008. Minireview on the toxicity of dietary acrylamide. **Food and Chemical Toxicology** 46: 1360-1364.
- Passos, C.P., S.S. Ferreira, A. Serôdio, E. Basil, L. Marková, K. Kukurová, Z. Ciesarová and M.A. Coimbra. 2018. Pectic polysaccharides as an acrylamide mitigation strategy – competition between reducing sugars and sugar acids. **Food Hydrocolloids** 81: 113-119.
- Patel, A.R., E.C. Bouwens and K.P. Velikov. 2010. Sodium caseinate stabilized zein colloidal particles. **Journal of Agricultural and Food Chemistry** 58: 12497-12503.
- Patel, A.R., N. Cludts, M.D.B. Sintang, A. Lesaffer and K. Dewettinck. 2014. Edible oleogels based on water soluble food polymers: Preparation, characterization and potential application. **Food and Function** 5: 2833-2841.
- Patel, A.R. and K. Dewettinck. 2016. Edible oil structuring: An overview and recent updates. **Food and Function** 7: 20-29.

- Pehlivanoglu, H., M. Demirci, O.S. Toker, N. Konar, S. Karasu and O. Sagdic. 2018. Oleogels, a promising structured oil for decreasing saturated fatty acid concentrations: Production and food-based applications. **Critical Review in Food Science and Nutrition** 58: 1330-1341.
- Pereira, J., H. Hu, L. Xing, W. Zhang and G. Zhou. 2019. Influence of rice flour, glutinous rice flour, and tapioca starch on the functional properties and quality of an emulsion-type cooked sausage. **Foods** 9(1): 9.
- Pietrasik, Z. and J.A.M. Janz. 2010. Utilization of pea flour, starch-rich and fiber-rich fractions in low fat bologna. **Food Research International** 43: 602-608.
- Pitchon, E., J. D. O'Rourke and T. H. Joseph. 1981. **Process for cooking or gelatinizing materials**. U. S. Patent 4,280,851.
- Precha-Atsawan, S., D. Uttapap and L.M.C. Sagis. 2018. Linear and nonlinear rheological behavior of native and debranched waxy rice starch gels. **Food Hydrocolloids** 85: 1-9.
- Ptaszek, P., M. Kabziński, A. Ptaszek, K. Kaczmarczyk, J. Kruk and A. Bieńczyk. 2016. The analysis of the influence of xanthan gum and apple pectins on egg white protein foams using the large amplitude oscillatory shear method. **Food Hydrocolloids** 54: 293-3.
- Rajagopalan, S. and P. A. Seib. 1991. **Process for the preparation of granular cold water-soluble starch**. U. S. Patent 5,037,929.
- Rajagopalan, S., and P. A. Seib. 1992. Granular cold-water soluble starches prepared at atmospheric pressure. **Journal of Cereal Science** 16:13-28.

- Raghavan, S.R. and S.A. Khan. 1995. Shear-induced microstructural changes in flocculated suspensions of fumed silica. **Journal of Rheology** 39(6): 1311-1325.
- Rather, S.A., F.A. Masoodi, R. Akhter, A. Gani, S.M. Wani and A.H. Malik. 2015a. Xanthan gum as a fat replacer in Goshtaba-a traditional meat product of India: Effects on quality and oxidative stability. **Journal of Food Science and Technology** 52: 8104-8112.
- Rather, S.A., F.A. Masoodi, R. Akhter, A. Gani, S.M. Wani and A.H. Malik. 2015b. Effects of guar-xanthan gum mixture as fat replacer on the physicochemical properties and oxidative stability of Goshtaba, a traditional Indian meat product. **Journal of Food Processing and Preservation** 39: 2935-2946
- Rice, J.M. 2005. The carcinogenicity of acrylamide. **Mutation Research/Genetic Toxicology and Environmental Mutagenesis** 580: 3-20.
- Rios, R., M. Pessanha, P. Almeida, C. Viana and S. Lannes. 2014. Application of fats in some food products. **Ciência e Tecnologia de Alimentos** 34: 3-15.
- Ruiz-Capillas, C., M. Triki, A.M. Herrero, L. Rodriguez-Salas and F. Jiménez-Colmenero. 2012. Konjac gel as pork backfat replacer in dry fermented sausages: Processing and quality characteristics. **Meat Science** 92: 144-150.
- Rydberg, P., S. Eriksson, E. Tareke, P. Karlsson, L. Ehrenberg and M. Törnqvist. 2003. Investigations of factors that influence the acrylamide content of heated foodstuffs. **Journal of Agricultural and Food Chemistry** 51: 7012-7018.
- Sansano, M., M.L. Castelló, A. Heredia and A. Andrés. 2016. Protective effect of chitosan on acrylamide formation in model and batter systems. **Food Hydrocolloids** 60: 1-6.

- Sansano, M., M.L. Castelló, A. Heredia and A. Andrés. 2017. Acrylamide formation and quality properties of chitosan-based batter formulations. **Food Hydrocolloids** 66: 1-7.
- Saari, H., M. Wahlgren, M. Rayner, M. Sjöo and M. Matos. 2019. A comparison of emulsion stability for different oxa-modified waxy maize emulsifiers: Granules, dissolved starch, and non-solvent precipitates. **PLoS One** 14: e0210690.
- Salcedo-Sandoval, L., S. Cofrades, C. Ruiz-Capillas Pérez, M.T. Solas and F. Jiménez-Colmenero. 2013. Healthier oils stabilized in konjac matrix as fat replacers in n-3 PUFA enriched frankfurters. **Meat Science** 93: 757-766.
- Schatz, C., A. Domard, C. Viton, C. Pichot and T. Delair. 2004. Versatile and efficient formation of colloids of biopolymer-based polyelectrolyte complexes. **Biomacromolecules** 5: 1882-1892.
- Seyrek, E., P. Dubin, C. Tribet and E. Gamble. 2003. Ionic strength dependence of protein-polyelectrolyte interactions. **Biomacromolecules**. 4: 273-282.
- Shogren, R.L., A. Viswanathan, F. Felker and R.A. Gross. 2000. Distribution of octenyl succinate groups in octenyl succinic anhydride modified waxy maize starch. **Starch - Stärke**. 52: (6-7).
- Soltani, S. and A. Madadlou. 2016. Two-step sequential cross-linking of sugar beet pectin for transforming zein nanoparticle-based Pickering emulsions to emulgels. **Carbohydrate Polymer** 136: 738-743.
- Song, X., G. He, H. Ruan and Q. Chen. 2006. Preparation and properties of octenyl succinic anhydride modified early Indica rice starch. **Starch – Stärke** 58: 109-117.

- Stadler, R.H., I. Blank, N. Varga, F. Robert, J. Hau, P.A. Guy, M.-C. Robert and S. Riediker. 2002. Acrylamide from Maillard reaction products. **Nature** 419: 449-450.
- Sun, C., Y. Gao and Q. Zhong. 2018. Properties of ternary biopolymer nanocomplexes of zein, sodium caseinate, and propylene glycol alginate and their functions of stabilizing high internal phase Pickering emulsions. **Langmuir** 34: 9215-9227.
- Sung, W.-C., Y.-W. Chang, Y.-H. Chou and H.-I. Hsiao. 2018. The functional properties of chitosan-glucose-asparagine Maillard reaction products and mitigation of acrylamide formation by chitosans. **Food Chemistry** 243: 141-144.
- Suyatma, N. and E. Prangdimurti. 2015. Effect of blanching and pectin coating as pre-frying treatments to reduce acrylamide formation in banana chips. **International Food Research Journal** 22: 936-942.
- Takatsuki, S., S. Nemoto, K. Sasaki and T. Maitani. 2003. Determination of acrylamide in processed foods by LC/MS using column switching. **Food Hygiene and Safety Science (Shokuhin Eiseigaku Zasshi)** 44: 89-95.
- Tamime, A.Y., M. Kalab, D. D Muir and B. Eduardo. 2007. The microstructure of set-style, natural yogurt made by substituting microparticulate whey protein for milk fat. **International Journal of Dairy Technology** 48: 107-111.
- Tardiff, R.G., M.L. Gargas, C.R. Kirman, M. Leigh Carson and L.M. Sweeney. 2010. Estimation of safe dietary intake levels of acrylamide for humans. **Food and Chemical Toxicology** 48: 658-667.
- Tareke, E., P. Rydberg, P. Karlsson, S. Eriksson and M. Törnqvist. 2002. Analysis of acrylamide, a carcinogen formed in heated foodstuffs. **Journal of Agricultural and Food Chemistry** 50: 4998-5006.

- Tolstoguzov, V. 2003. Some thermodynamic considerations in food formulation. **Food Hydrocolloids** 17: 1-23.
- Tsai, G.-J., W.-H. SU, H.-C. Chen and C.-L. Pan. 2002. Antimicrobial activity of shrimp chitin and chitosan from different treatments and applications of fish preservation. **Fisheries Science** 68: 170-177.
- Turgeon, S.L., C. Schmitt and C. Sanchez. 2007. Protein–polysaccharide complexes and coacervates. **Current Opinion in Colloid and Interface Science** 12: 166-178.
- Ubbink, J. and J. Krüger. 2006. Physical approaches for the delivery of active ingredients in foods. **Trends in Food Science and Technology** 17: 244-254.
- Vainio, H. 2003. Acrylamide in heat-processed foods--a carcinogen looking for human cancer? **European Journal of Epidemiology** 18: 1105-1106.
- Veneranda, M., Q. Hu, T. Wang, Y. Luo, K. Castro and J.M. Madariaga. 2018. Formation and characterization of zein-caseinate-pectin complex nanoparticles for encapsulation of eugenol. **Lwt** 89: 596-603.
- Wang, L.-J., S.-W. Yin, L.-Y. Wu, J.-R. Qi, J. Guo and X.-Q. Yang. 2016. Fabrication and characterization of Pickering emulsions and oil gels stabilized by highly charged zein/chitosan complex particles (ZCCPs). **Food Chemistry** 213: 462-469.
- Wang, L.J., Y.Q. Hu, S.W. Yin, X.Q. Yang, F.R. Lai and S.Q. Wang. 2015. Fabrication and characterization of antioxidant Pickering emulsions stabilized by zein/chitosan complex particles (ZCPs). **Journal of Agricultural and Food Chemistry** 63: 2514-2524.

- Yan, C., D.J. McClements, Y. Zhu, L. Zou, W. Zhou and W. Liu. 2019. Fabrication of OSA starch/chitosan polysaccharide-based high internal phase emulsion via altering interfacial behaviors. **Journal of Agricultural and Food Chemistry** 67: 10937-10946.
- Yasuhara, A., Y. Tanaka, M. Hengel and T. Shibamoto. 2003. Gas chromatographic investigation of acrylamide formation in browning model systems. **Journal of Agricultural and Food Chemistry** 51: 3999-4003.
- Yuan, Y., F. Chen, G.H. Zhao, J. Liu, H.X. Zhang and X.S. Hu. 2007. A comparative study of acrylamide formation induced by microwave and conventional heating methods. **Journal of Food Science** 72: C212-216.
- Zeng, X., K.-W. Cheng, Y. Du, R. Kong, C. Lo, I.K. Chu, F. Chen and M. Wang. 2010. Activities of hydrocolloids as inhibitors of acrylamide formation in model systems and fried potato strips. **Food Chemistry** 121: 424-428.
- Zhang, Y., H. Fang and Y. Zhang. 2008. Study on formation of acrylamide in asparagine–sugar microwave heating systems using UPLC-MS/MS analytical method. **Food Chemistry** 108: 542-550.
- Zhang, Y., G. Zhang and Y. Zhang. 2005. Occurrence and analytical methods of acrylamide in heat-treated foods: Review and recent developments. **Journal of Chromatography A** 1075: 1-21.
- Zhou, Y.Y., Y. Li and A.N. Yu. 2016. The effects of reactants ratios, reaction temperatures and times on Maillard reaction products of the L-ascorbic acid/L-glutamic acid system. **Food Science and Technology** 36: 268-274.
- Zhu, F. 2019. Starch based Pickering emulsions: Fabrication, properties, and applications. **Trends in Food Science and Technology** 85: 129-137.

Zielinska, A., F. Carreiro, A.M. Oliveira, A. Neves, B. Pires, D.N. Venkatesh, A. Durazzo, M. Lucarini, P. Eder, A.M. Silva, A. Santini and E.B. Souto. 2020. Polymeric nanoparticles: Production, characterization, toxicology and ecotoxicology. **Molecules** 25(16): 3731.





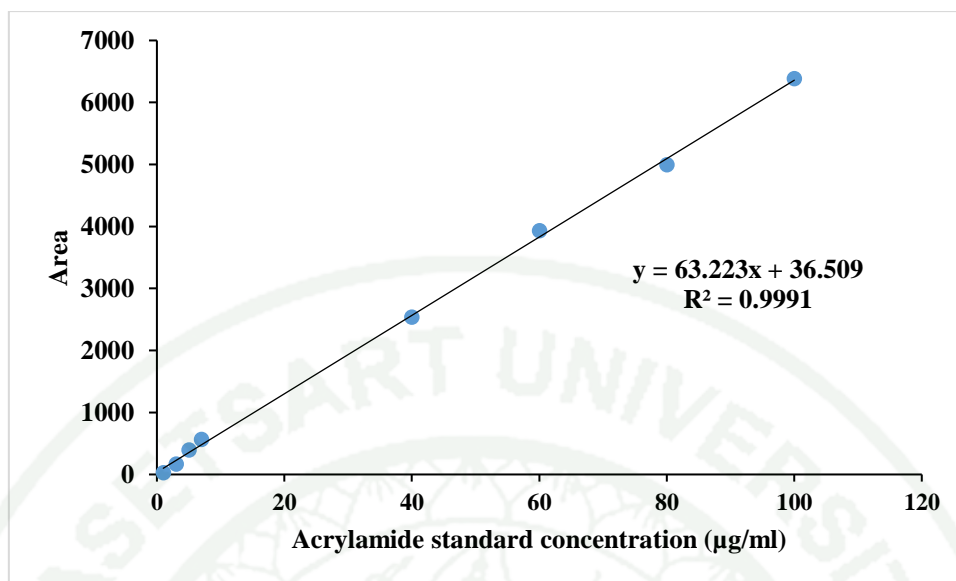
APPENDIX

Appendix Table 1 Benchmark level of acrylamide

Food	Benchmark level ($\mu\text{g}/\text{kg}$)
French fries (ready to eat)	500
Potato products from potato dough	750
Wheat base bread	50
Biscuit and wafers	350
Roast coffee	400
Instant coffee	850
Baby foods	40

Appendix Table 2 The various composition in chemical model system

Solution	Initial concentration	Final concentration
Glucose	1.5 M	0.5 M
Asparagine	1.5 M	0.5 M
Sodium	1.0 % (w/v)	0.33 % (w/v)
alginate/Chitosan/Pectin	0.6 % (w/v)	0.20 % (w/v)
	0.3 % (w/v)	0.1 % (w/v)



Appendix Figure 1 Acrylamide standard curve at concentration from 1 µg/mL to 100 µg/mL

Appendix Table 3 The series of different acrylamide concentrations (µg/mL) prepared from the stock solution (10 µg/mL) through dilution in water.

Acrylamide concentration (µg/mL)	Acrylamide solution 10 µg/ml (mL)	Milli Q water (ml)
1	1	9
3	3	7
5	5	5
7	7	3

Appendix Table 4 The series of different acrylamide concentrations ($\mu\text{g/mL}$) prepared from the stock solution ($100 \mu\text{g/mL}$) through dilution in water

Acrylamide concentration ($\mu\text{g/mL}$)	Acrylamide solution 100 $\mu\text{g/ml}$ (mL)	Milli Q water (ml)
10	1	9
20	4	6
40	5	5
60	6	4
80	8	2
100	10	0

CURRICULUM VITAE

NAME : Ms. Ornicha Champrasert

BIRTH DATE : June 9th, 1994

BIRTH PLACE : Bangkok, Thailand

EDUCATION	: YEAR	INSTITUTE	DEGREE/DIPLOMA
	2016	Chiang Mai Univ.	B.Sc. (Food Science and Technology)

SCHOLARSHIP/AWARDS : This study was supported by the Royal Golden Jubilee
PhD program (grant number PHD0052), year 2016
(Thailand Research Fund)